UNIVERSITÀ
DEGLI STUDI
DI PADOVA

Sede Amministrativa: Università degli Studi di Padova
Dipartimento di Scienze Chimiche

SCUOLA DI DOTTORATO DI RICERCA IN SCIENZE MOLECOLARI
INDIRIZZO: SCIENZE CHIMICHE

CICLO XVII

DYNAMIC NANOPROTEINS: SELF-ASSEMBLY OF PEPTIDES ON MONOLAYER PROTECTED GOLD NANOPARTICLES

Direttore della Scuola: Ch.mo Prof. Antonino Polimeno
Coordinatore d'indirizzo: Ch.mo Prof. Antonino Polimeno
Supervisore: Prof. Leonard J. Prins

Dottorando: Sergio Garcia Martin

Dedico este trabajo al progreso,
sin él no hay futuro

Dedico esta tesis a mi padre y a mi madre
por haber hecho de mí la persona que soy ahora

A mis abuelos,
este trabajo lleva la huella de vuestra eterna sabiduría

“Muchos años después, frente al pelotón de fusilamiento, el coronel Aureliano Buendía habría de recordar aquella tarde remota en la que su padre lo llevó a conocer el hielo. Primero llevaron el iman. Melquiades pregonaba: “Las cosas tienen vida propia, todo es cuestion de despertarles el anima”.[...] Esta vez llevaban un catalejo y una lupa del tamano de un tambor. “La ciencia ha eliminado las distancias”. [...] Dentro solo habia un enorme bloque transparente, con infinitas agujas internas en las cuales se despedazaba en estrellas de colores la claridad del crepúsculo. “Es el diamante más grande del mundo!” “No -corrigió el gitano- es hielo”. Jose Arcadio Buendía puso la mano sobre el hielo, y la mantuvo puesta por varios minutos, mientras el corazón se le hinchaba de temor y de júbilo al contacto del misterio. Con la mano puesta en el tempano, exclamó: “Este es el gran invento de nuestro tiempo”.”

Cien años de soledad , Gabriel García Márquez

Table of contents

Abbrevations

CHAPTER 1 1

1.1 PROTEIN-PROTEIN INTERACTIONS 1

1.2 MONOLAYER PROTECTED GOLD NANOPARTICLES 5

1.3 PEPTIDE-BASED GOLD NANOPARTICLES 6

1.3.1 Catalysis 7

1.3.2 Molecular recognition 9

1.4 SELF-ASSEMBLY OF DYNAMIC STRUCTURES 13

1.5 SCOPE OF THIS THESIS 18

CHAPTER 2: SELF-ASSEMBLY OF SMALL PEPTIDES ON MONOLAYER-PROTECTED GOLD NANOPARTICLES 21

2.1 SUMMARY 21

2.2 SMALL PEPTIDE FRAGMENTS AS RECOGNITION UNIT 21

2.3 PEPTIDE LIBRARY 27

2.4 A MULTIVALENT PROTEIN-LIKE SURFACE 32

2.5 CONCLUSIONS 33

2.6 EXPERIMENTAL SECTION 34

2.6.1 Instrumentation 34

2.6.2 Materials 35

2.6.3 Synthesis and characterization of Au NP 1[54] 36

2.6.4 Determination of the stock solution concentrations 40

2.6.5 Displacement experiments 42

2.6.6 Synthesis and purification of the peptides 42

2.6.7 Miscellaneous 45

CHAPTER 3: SELF-SELECTION OF PEPTIDES ON AU NPS 47

3.1 INTRODUCTION 47

3.2 METHODOLOGY FOR STUDYING THE SURFACE COMPOSITION 54

3.3 SELF-SELECTION EXPERIMENTS 58

3.4 CONCLUSIONS 62

3.5 EXPERIMENTAL SECTION 62

3.5.1 Instrumetation 62

3.5.2 Materials 62

3.5.3 Ultracentrifugation experiments 63

CHAPTER 4: MULTIVALENT DYNAMIC PEPTIDE SURFACES FOR PROTEIN RECOGNITION 69

4.1 INTRODUCTION 69

4.2 STABILITY STUDIES IN THE PRESENCE OF CHT 71

4.3 INFLUENCE OF AU NPS ON THE ACTIVITY OF CHT 74

4.4 SELF-SELECTION OF PEPTIDE SURFACES BY A TARGET PROTEIN 78

4.5 CONCLUSIONS 82

4.6 EXPERIMENTAL SECTION 83

4.6.1 Instrumentation 83

4.6.2 Materials 83

4.6.3 Stability studies 83

4.6.4 Binding studies in the presence of ChT 83

4.6.5 ChT assay: UHPL kinetics 84

4.6.6 Self-selection experiments 85

4.6.7 MANT-dADP binding assay 86

CHAPTER 5: AU NPS AS NANOZYMES FOR THE CLEAVAGE ON NON-ACTIVATED PHOSPHOMONOESTERS 87

5.1 INTRODUCTION 87

5.2 IMPACT OF AU NP 1 ON THE COMPOSITION OF A DYNAMIC PEPTIDE SYSTEMS 89

5.3 MECHANISTIC STUDIES 94

5.4 CONCLUSIONS 99

5.5 EXPERIMENTAL SECTION 99

5.5.1 Instrumentation 99

5.5.2 Materials 100

5.5.3 Impact of Au NP 1 on the composition of a dynamic peptide systems 100

5.5.4 Mechanistic studies 100

5.5.4 Miscellaneous 102

SUMMARY 105

SOMMARIO 109

ACKNOWLEDGEMENTS 113

This research project has been carried out within the framework of the Marie Curie ITN 'REaD' (289723).

Abbreviations

ADP	Adenosine diphosphate
Arg (R)	Arginine
Asn (N)	Asparagine
Asp (D)	Aspartic acid
ATP	Adenosine triphosphate
ATP	Adenosine triphosphate
ATP_F	2-Aminopurine riboside-5'-O-triphosphate
Au NPs	Gold nanoparticles
CCP	Cytochrom c peroxidase
ChT	α-Chymotrypsin
Cys (C)	Cystein
Cyt c	Cytochrom c
DCC	Dynamic combinatorial chemistry
DCL	Dynamic combinatorial library
DLS	Dynamic light scattering
ESI-MS	Electrospray Ionization-Mass Spectrum
Fmoc	Fluorenylmethyloxycarbonyl
Fmoc	Fluorenylmethyloxycarbonyl
Gly (G)	Glycine
His (H)	Histidine
HPNPP	2-hydroxypropyl-4-nitrophenyl
LC-MS	Liquid chromatography mass spectroscopy
Leu (L)	Leucine
Lys (K)	Lysine

MADLI-TOF	Matrix-Assisted Laser Desorption/Ionization-Time of Flight
MANT-dADP	2'-Deoxy-3'-O-(N'-methylanthraniloyl) adenosine-5'-O-diphosphate
PES	Polyethersulfone
Phe (F)	Phenylalanine
PPI	Protein-Protein interaction
PPIs	Protein-protein interactions
QD	Quantum dot
SAMs	Self-assembled monolayers
Ser (S)	Serine
Ser(H_2OP_3) S(p)	Phosphoserine
SIM	Selected-ion monitoring
SPNA	N-succinyl-L-phenylalanine p-nitroanilide
SPPS	Solid Phase Peptide Synthesis
SSC	Saturation concentration
TACN	Triazacyclononane
TEM	Transmission electroni microscopy
TGA	Thermogravimetric analysis
Trp (W)	Tryptophan
Tyr (Y)	Tyrosine
UHPLC	Ultrahigh pressure liquid chromatography

CHAPTER 1

1.1 Protein-protein interactions

Protein-protein interactions (PPIs) mediate a large number of important regulatory pathways and thus play a central role in many pathologies (see below). For that reason there is a strong interest in the development of pharmaceuticals able to inhibit PPIs[1,2]. Competitive inhibition of protein function is traditionally achieved using molecules that masquerade as enzyme substrates (Figure 1.1a)[3] or allosterically by binding to secondary sites indirectly effecting the active sites. Compared to the generally well-defined active site of an enzyme, it is much more challenging to develop inhibitors for PPIs. In terms of competitive inhibition, a small molecule must cover 800–1100 $Å^2$ of a protein surface and complement a poorly defined projection of hydrophobic and charged domains on a flat or moderately convex surface (Figure 1b).

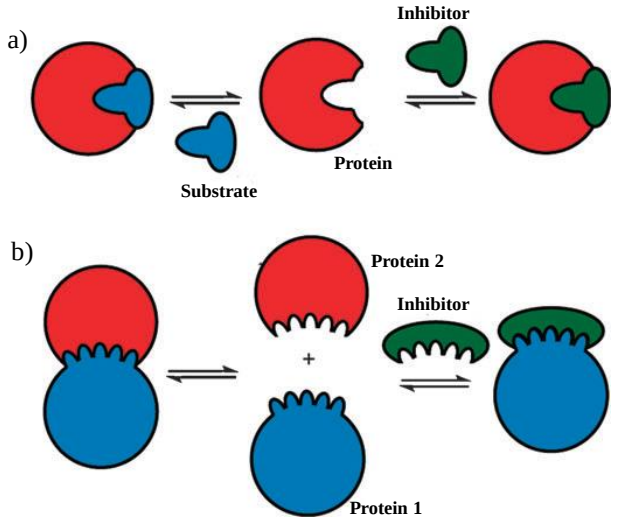

Figure 1.1. (a) Recognition and inhibition of enzyme
(b) recognition and inhibition of PPIs[4].

What makes PPIs such challenging targets for small-molecule intervention is the diverse variety of compositions at protein–protein interfaces[5]. One of the most important early discoveries was that whilst a PPI takes place over a large surface area, the dominant contributions to the free energy of binding typically originates

from a few key residues on the protein surface. Wells and Clackson identified this feature, known as a 'hot-spot', in the course of a mutagenesis study on the interaction of human growth hormone (hGH) with its receptor (hGHbp)[6].

The interaction between cytochrome c (Cyt c) and cytochrome c peroxidase (CCP) was one of the first PPIs to undergo crystallographic investigation[7]. The interaction involves the solvent exposed harm edge of cytochrome c surrounded by positively charged basic residues interacting with a complementary hydrophobic patch surrounded by negatively charged residues on the peroxidase (Figure 1.2a). Interestingly, calorimetric data[8] revealed that the interaction is entropy driven with a small favourable enthalpy of binding. This is consistent with a classical hydrophobic binding signature yet the data also revealed a small change in heat capacity which contrasts with that expected for hydrophobic binding. Binding is however dependent on ionic strength, which can be rationalised by assuming the desolvation of charged residues that form salt bridges upon development of the PPI.[4]

A more recently investigated PPI involves the interaction between the tumour suppressor p53 and the protein hDM2 (Figure 1.2b). Here, the transactivation domain of p53 binds in an α-helical conformation to a hydrophobic cleft on hDM2. Only three residues are key to binding, those found at the *i*, *i* + 4 and *i* + 7 positions of the p53 helix, *i.e.* F19, W23 and L26 all of which are hydrophobic in nature[9]. The thermodynamic data for binding of short p53 sequences reveal a favourable enthalpy and unfavourable entropy of binding. Again this is perhaps unexpected, although folding into the correct conformation is entropically unfavoured[10].

Stable isolated peptides with defined secondary structure would be ideal inhibitors of PPIs. However, since peptides with less than ≈15 amino acid residues rarely adopt a defined conformation in isolation, research on PPI inhibitors has so far been stronglys focused on constrained peptide secondary structures and the development of peptide mimics.

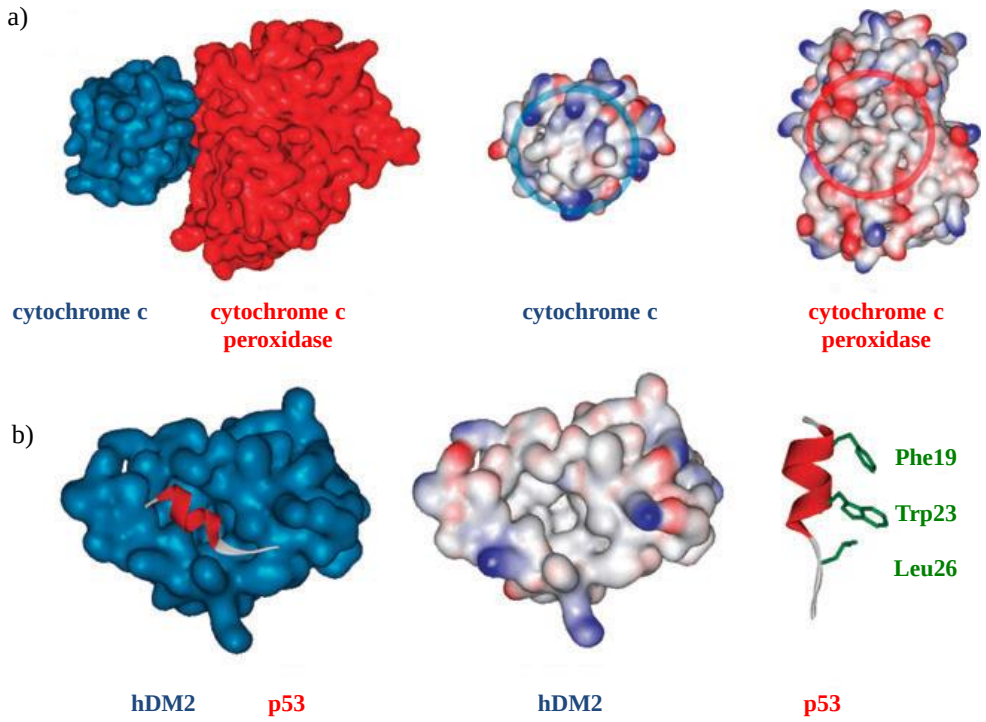

Figure 1.2. (a) Cytochrome c–cytochrome c peroxidase PPI with recognition domains highlighted by circles (PDB ID: 2PCB). (b) hDM2–p53 PPI with key side chains highlighted (PDB ID: 1YCR)[9].

One of these approaches is based on constraining α-helix and β-sheets secondary structures in small peptide sequences. α-Helices form fundamental recognition elements in many naturally occurring PPIs, such as assembly in the HIV gp41 fusion complex[4] and hDM2–p53[7].

Covalent linkages between adjacent residues in peptides can impart stabilization of the helical conformation. Verdine, Korsemeyer and co-workers have shown that cell apoptosis can be induced using peptides that are covalently constrained using hydrocarbon stapling (Figure 1.3a)[11]. It consists of covalently constraining (olefin metathesis) the peptide to adapt a certain 3D strucutre. Arora *et al.* have similarly employed the hydrogen-bond surrogate approach to identify metabolically stable artificial helices by substituting intra-helical hydrogen bonds with covalent bonds (Figure 1.3b)[12].

Another small molecule approach is the use of easily accessible synthetic non-peptide molecules to mimic the secondary structural features of peptide fragments. Hirschmann and Smith at the University of Pennsylvania made the first significant contributions to the field of nonpeptidyl peptidomimetics. A mimetic for

the cyclic peptide somatostatin was reported using a D-glucose scaffold (Figure 1.4a)[13].

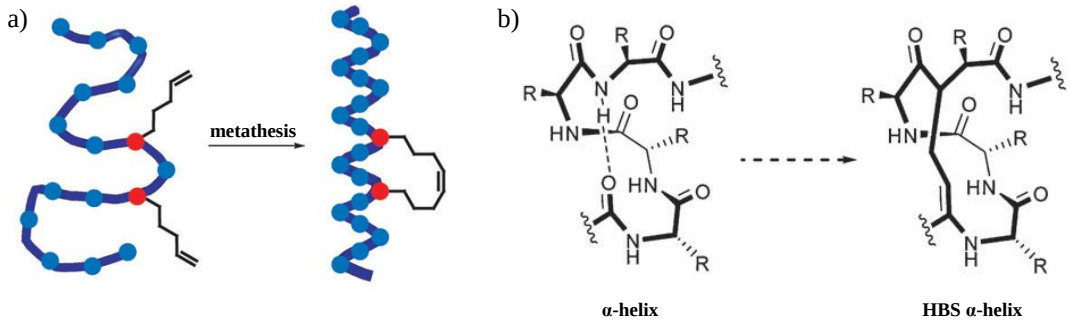

Figure 1.3. Approaches for stabilisation of helix conformation: (a) hydrocarbon stapling; (b) hydrogen-bond surrogate.

It was proposed by the Hamilton's group that terphenyl scaffold could reasonably mimic the surface of an α-helical peptide. In this scaffold the *ortho*-substituents on the phenyl ring have a similar spatial orientation as those in the α-helix (Figure 1.4b)[14]. A series of alternative α-helix mimetic scaffolds based on oligoamides, terephthalamides, oligoureas and benzoylurea amongst others have subsequently been elaborated by the Hamilton group and shown to inhibit the Bcl-xL–BAK interaction.

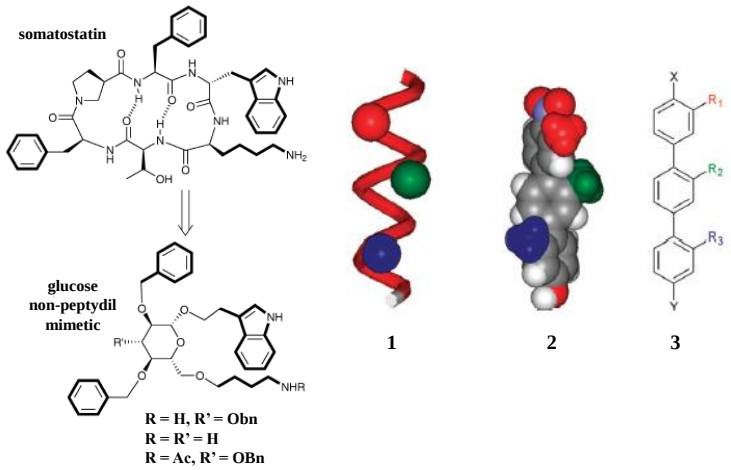

Figure 1.4. (a) Transfer of pharmacophores onto a non-peptidyl glucose derived scaffold.(b) (**1**) α-Helix showing key side chains often found to play a key role in a PPI; (**2**) crystal structure of a terphenyl illustrating how ortho side chains recapitulate the 3D presentation of key side chains in an α-helix; (**3**) Core structure of a terphenyl scaffold.

These examples show that it is possible to develop small molecules capable of recognizing solvent exposed surfaces and inhibiting PPIs. However, PPIs take

place between relatively large entities[15]. This size issue, when combined with the wide nature of many protein-protein interfaces, as well as the difficulty in the synthesis in some cases make the development of PPI inhibitors using small molecules very difficult. Thus, with regard to PPI inhibitors, there is room here for alternative solutions. Among many possibilities such as dendrimers, polymers, monolayer protected gold nanoparticles in the past years have turned out to be very attractive.

1.2 Monolayer protected gold nanoparticles

Over the past decaded, monolayer protected gold nanoparticles (Au NPs) have gained increasing importance because of the emergence of the fields of nanoscience and nanotechnology[16]. Gold nanoparticles are attractive because of their interesting physical and chemical attributes[17]. They possess unique optoelectronic properties such as surface plasmon resonance absortion[18], conductivity and redox[19] (Figure 1.5) that make them excellent scaffolds for the application in biosensing[20] and nanomedicine[21], for example. Indeed, the ability of Au NPs to quench the fluorescence[22,23] of bound fluorophores has been heavily exploited for sensing and imaging.

From a chemical point of view, Au NPs can be synthesized in a straightforward manner and can be made highly stable by covering the gold nuclei with an organic monolayer of thiols. Brust and Schiffrin reported a two-phase synthetic strategy, utilizing strong thiol-gold interactions to protect Au NPs with thiol ligands[24]. In 2008, Scrimin *et al.*[25] reported the synthesis of water-soluble thiol-protected Au NPs. In this way, many different thiols can be synthesized and attached to the gold nucleus in order to create a large variety of Au NPs. Likewise, their properties (size and the surrounding chemical environment) can be readily tuned. Hence, since their ease of modification Au NPs offer a suitable platform for developing multifunctionalised nanosystems with a wide range of synthetic or biological ligands suitable for the selective binding and detection of small molecules and biological targets such as proteins.

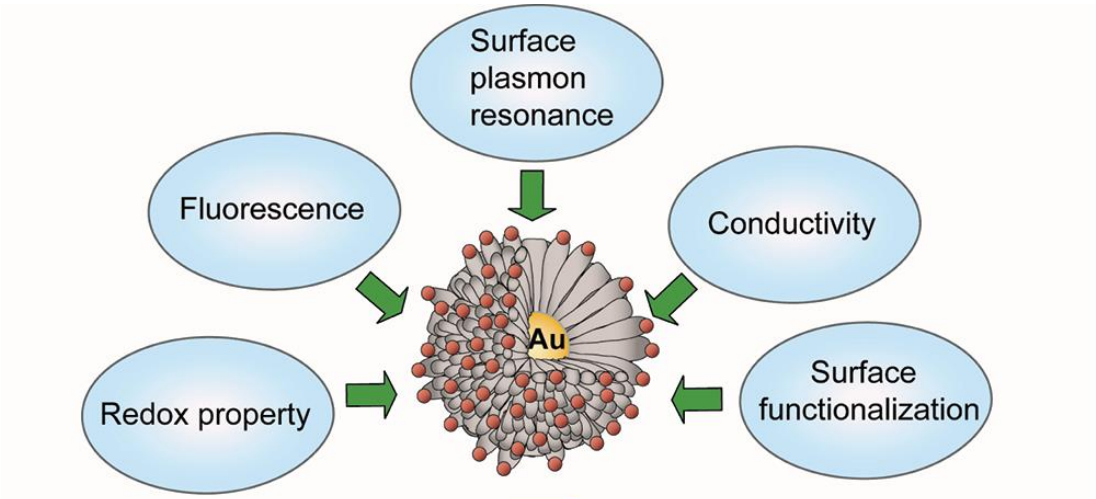

Figure 1.5. Physical and chemical properties of Au NPs.

1.3 Peptide-based gold nanoparticles

Of particular interest in the context of synthetic proteins are Au NPs functionalized with peptide fragments. These type of nanoparticles are composed of an Au-core and an organic monolayer formed by peptides. It has indeed been shown that these constructs can display protein-like properties such as molecular recognition and also catalysis. The large variety of functional peptides opens up new possibilities for the bottom-up assembly of devices[26], for catalysis[27], for crossing the cell-membrane barrier by using cell-penetrating peptides[28,29] and for biomolecular recognition. Multivalency[30], which is at the basis of the amplification of the binding events with functional nanoparticles, has been exploited for the molecular recognition of proteins but also for the preparation of catalytic systems in which a cluster of functional groups led to catalytic activity which was not just the sum of the individual contributions[31]. In the following section some key examples of functional peptide-gold nanoparticle conjugates will be discussed.

1.3.1 Catalysis

Scrimin *et al.* have reported some examples in which peptide-modified gold nanoparticles[32] have been used as catalyst. In a first example, a thiol-functionalized dipeptide by *N*-acylation of His-Phe was prepared[33] (Figure 1.6a). This was the first example of peptide-functionalized gold nanoparticles hydrolytically active against carboxylic esters. The interesting feature was that the confinement of the catalytic units in the monolayer covering the nanoparticles triggers a cooperative hydrolytic mechanism operative at pH < 7 in which a carboxylate and an imidazolium ion act as general base and general acid, respectively. However, nanoparticles functionalized with these peptides not only gave positive proof of cooperativity but showed that within the monolayer, hydrolytic mechanisms not available for similar monomeric catalysts are activated[34]. The monomeric catalyst behaved as a system in which a catalytically relevant nucleophile is generated with pK$_a$ 6.6, which is consistent with the basicity of the imidazole. On the other hand, the profile observed for the nanoparticle system indicated the formation of first nucleophilic species with pK$_a$ 4.2 and a second one with pK$_a$ 8.1, which are the carboxylic acid and imidazolium, respectively. The reason for the higher value of the pK$_a$ of the imidazolium in the nanoparticle is due to the anionic nature of the nanoparticle that disfavors the deprotonation of the imidazolium cation[35]. This difference resulted a in a 300-fold rate acceleration at acidic pH for the nanoparticle based catalyst (Figure 1.6b).

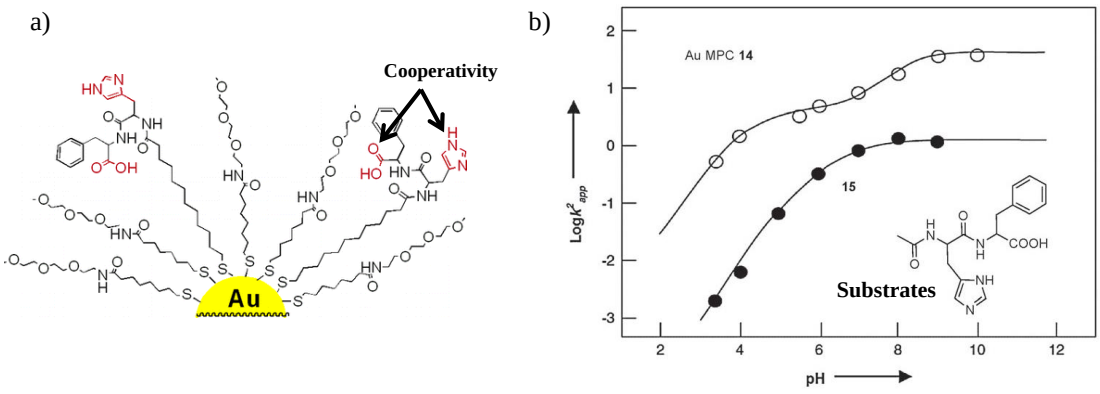

Figure 1.6. Schematic representation of (a) the thiol-functionalized dipeptide by *N*-acylation of His-Phe, (b) Logarithm of the apparent second-order rate constants as a function of pH[33].

Finally, it was shown that these systems can be developed into hybrid organic–inorganic structures of higher complexity by grafting catalytic

dodecapeptides on the surface of Au NP[36]. The observed catalytic activity of this system illustrates that this kind of system may in fact yield synthetic catalytic systems that can match up to the complexity of enzymes.

An application of peptide-based Au NP catalysts for a different kind of chemistry was reported by Malkov, Cooke, Kočovský *et al*[37]. They immobilized valine-derived formamide on gold nanoparticles to generate a catalytic system for the asymmetric reduction of imines with trichlorosilane (Figure 1.7). Valine-derived-functionalized Au NP were obtained by place-exchange with either C_4 or C_8-chain. The system gave excellent performances exhibiting a yield > 90% with an enantioselectivity up to 84% ee. From a structural point of view, the presence of a short C4-chain in the surrounding thiols gave better results compared to the C8-chains (88%, 70% ee). The highest level of catalytic activity was of 90% and enantioselectivity of ≤84% ee. From a structural point of view, the presence of a short C4-chain in the surrounding thiols gave better results compared to the C8-chains (88%, 70% ee).

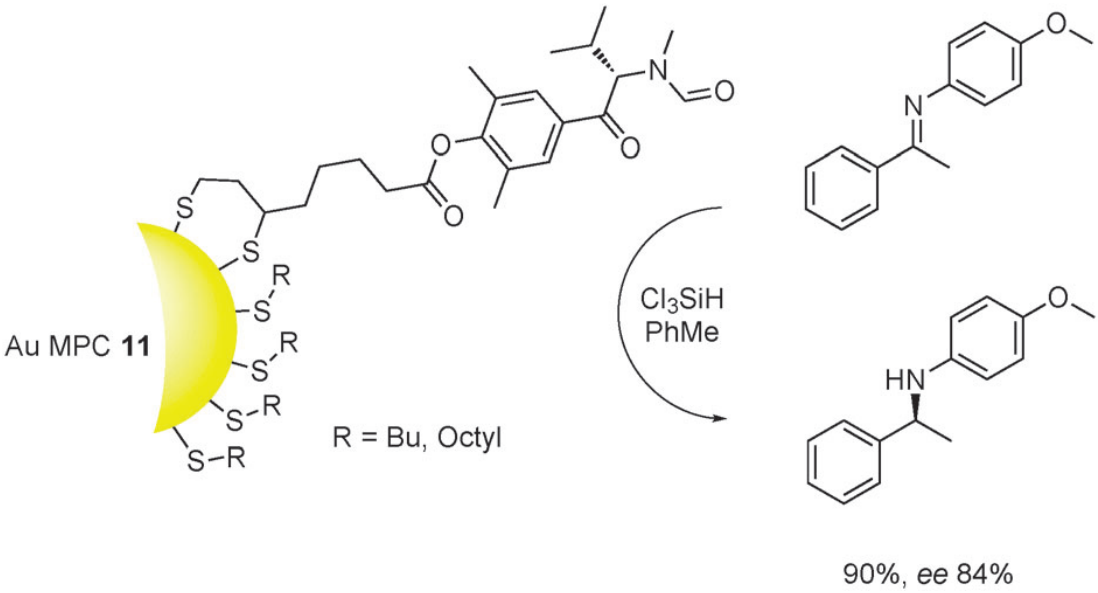

Figure 1.7. Representation of valine-derived-functionalized Au NP[35].

1.3.2 Molecular recognition

Protein surface recognition provides a powerful tool for the regulation of protein-protein interactions central to a number of cellular processes, such as cellular signal transduction, DNA transcription, and protein antigen/antibody recognition[38,39] (see section 1.1). Multivalent interactions are frequently used in biology to enhance the affinity and specificity of binding[40]. Peptide monolayers on Au NPs can be designed to incorporate one or several molecular-recognition groups[41]. Several examples are found in literature of peptide-functionalized gold nanoparticles that can recognize biomolecules.

Boram Kim and Yong-beom Lim recently reported a strategy to stabilize the α-helical secondary structures of peptides upon binding to gold nanoparticles [42]. The α-helix is one of the essential secondary structures in proteins and plays an important role in biomacromolecular interactions, among which protein-protein (see section 1.1) and protein-nucleic acid interactions[43]. α-Helices tend to be unstructured when isolated from the protein as monomeric peptides because of their inherent thermodynamic instability. Kim and Lim found that the elf-assembly of α-helical peptides on Au NPs resulted in a stabilization of the secondary structure for molecular recognition (Figure 1.3). The peptide scaffold was designed to be cyclic in order to constrain the peptide. The cysteine-rich segment had multiple cysteine residues and was used to facilitate the formation of multiple gold–thiolate bonds. A linker segment (Ebes) was inserted to connect the cysteine-rich and the helical segments. The helical segment was derived from the transactivation domain of the p53 tumor suppressor protein (see section 1.1). MDM2 was expressed with a hexa histidine-tag (His-tag), and Au NPs derivatized with Ni(II)–NTA. Colorimetric assay based on recognition between differently functionalized Au NPs revealed multiple interactions between p53 peptides and MDM2 promoting the formation of Au NP aggregates. The color of the suspension darkened, and a precipitate formed as well as shift in the plasmon bands from 545 nm (mixture 2) to 560 nm (mixture 1) by UV/Vis demonstrated the Au NP aggregation.

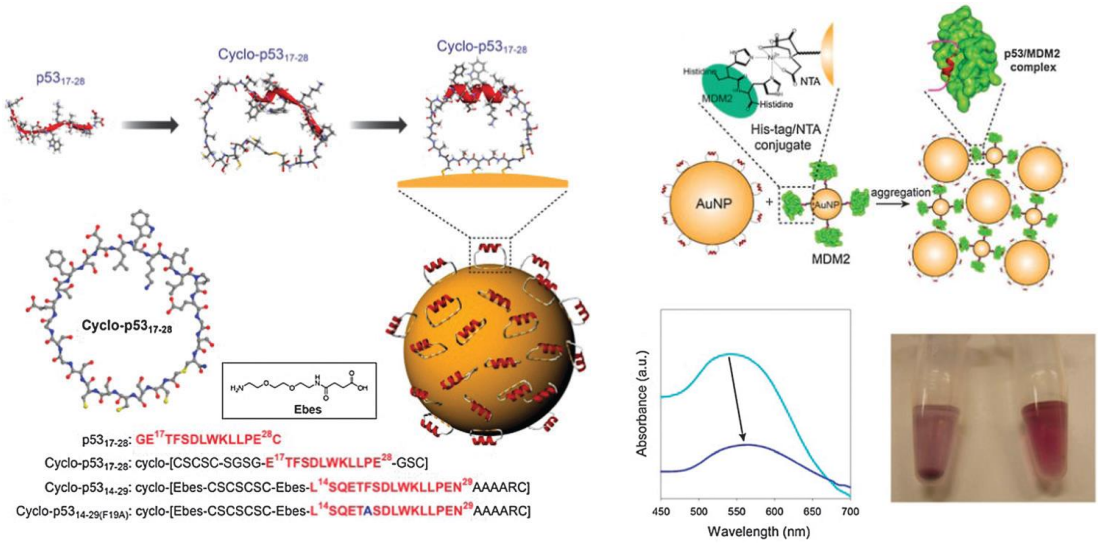

Figure 1.3. (a) Macrocyclic strategy to construct bioactive α-helix-decorated Au NP biohybrids; scheme depicting the colorimetric assay; UV/Vis absorption spectra

Rotello *et al.*[44] developed water-soluble gold nanoparticles bearing diverse L-amino acid terminals for the inhibition of α-chymotrypsin. (Figure 1.4a). They demonstrated that by incorporating simple L-amino acids in the monolayer, Au NPs exhibited different inhibition activity of ChT. Au NPs were capped with a series of amino acids that provide different effects: hydrophobic groups (e.g., Leu, Val), anionic groups (e.g., Asp, Glu), cationic groups (e.g., Arg), and hydrogen-bonding functionalities (e.g., Asn, Gln). Amino acid-functionalized Au NPs were obtained by subjecting amino acid-functionalized alkanethiols to ligand exchange reaction with 1-pentanethiol-coated Au NP. ChT-catalyzed hydrolysis of *N*-succinyl-L-phenylalanine *p*-nitroanilide (SPNA) was first investigated to probe the interaction between ChT and the amino acid-terminated Au NP. The results showed that the nanoparticles inhibited the activity of ChT except for **NP_L-Arg** that presented a slightly superactivity (x 1.15) (Figure 1.4b).

It was found that the inhibition of ChT activity depended essentially on the side chain properties of nanoparticles. The nanoparticles with polar side chains, for example, **NP_L-Asp**, **NP_L-Asn**, and **NP_L-Glu**, showed the strongest inhibitory potency with around 80% ChT activity suppression, while the nanoparticles with hydrophobic side chains exhibited less pronounced inhibition. **NP_L-Met** and **NP_L-Ala**, for instance, showed only 60% inhibition on ChT activity. The activity assay results were further analyzed to evaluate the association strength between ChT

and nanoparticles. For nanoparticles with hydrophilic amino acid side chains, that is, **NP_L-Asp**, **NP_L-Glu**, **NP_L-Asn**, and **NP_L-Gln**, the binding constants were around 3 x 10^6 M^{-1}. **NP_L-Met** presented the highest binding constant of 1.3 x 10^7. For nanoparticles with hydrophobic amino acid side chains, considerably enhanced binding affinity was observed (6 x 10^6 - 8 x 10^6 M^{-1}). These suggested that the hydrophobic side chain aids the interaction between nanoparticles and ChT (Figure 1.4.c).

The conformation of ChT after the influence of the amino acid-functionalized Au NP was investigated by CD. The studies showed that the CD signals of ChT were little influenced by the presence of nanoparticles bearing hydrophobic amino acid side chains while ChT experiences conformational changes in the presence of nanoparticles bearing polar amino acid side chains.

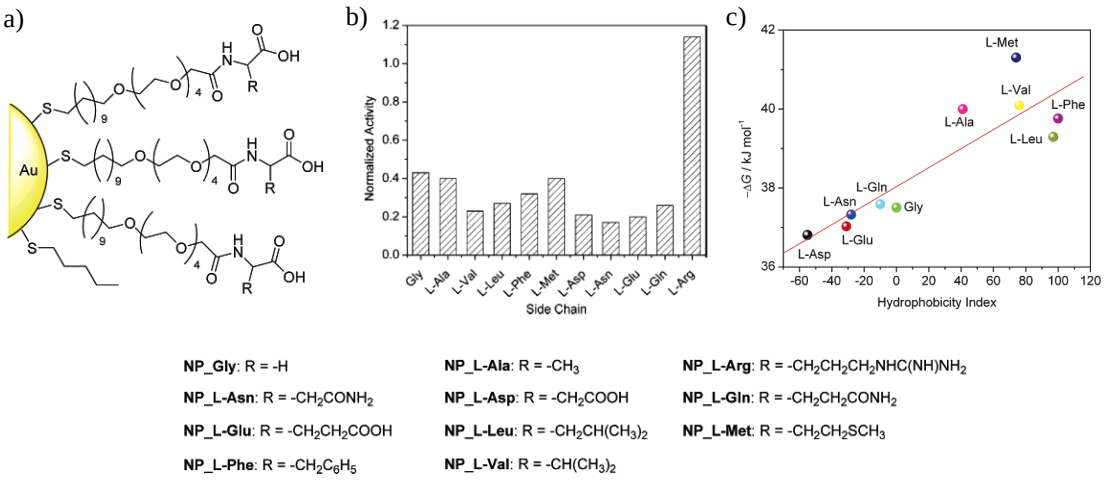

Figure 1.4. (a) Representation of amino acid-functionalized Au NP (b) Normalized activity of ChT with acid-functionalized Au NP (c) Correlation between Gibbs free energy changes and hydrophobicity index of amino acid side chains;

The kinetics in the denaturation process of ChT in the presence of nanoparticles were also followed by fluorescence. After 24 h incubation, hydrophilic **NP_L-Asp** and **NP_L-Asn** induced about 90% and 40% denaturation of ChT, respectively, while hydrophobic **NP_L-Phe** and **NP_L-Leu** induced only 10% and 20% denaturation (considering total denaturation at 356 nm, i.e., L-Trp in water).

To show the versatility of Au NPs, Rotello and coworkers demonstrated that mixed-monolayer protected colloids (MMPCs) containing different biocompatible TEG head groups could be also used to effectively recognize different proteins

(Figure 1.5). These MMPCs were commensurate in size with proteins, biocompatible, and possessed surfaces that could be easily imparted with functional groups[45]. Surface-functionalized MMPCs with gold cores (2 nm) were prepared utilizing thiolates with biocompatible TEG groups terminated with alcohol (**Au-TOH**), carboxylate (**Au-TCOOH**), or trimethylamine (**Au-TTMA**) functionalities. Cyt c binding to CCP (see Chapter 1) involves a single moderate-affinity site (K_D ~ 10 μM)[46,7]. Indeed, steady-state kinetics indicate that the 1 : 1 adduct is relevant for the reaction of Cyt c with CCP[47]. The moderate-affinity site is defined by salt bridges between the basic Cyt c (pI = 10.3)[48] and acidic CCP (pI =5.3)[49]. Specifically, the CCP residues Asn38, Glu35, and Glu290 present a negative area on the surface of CCP involved in the electron transfers with Cyt c. The surface of Cyt c is rich in basic residues, with Lys72, Lys73, and Lys8 found at the electron-transfer interface. Thus, these charged surfaces were ideal to be selectively and competitively recognized by the MMPCs mentioned before.

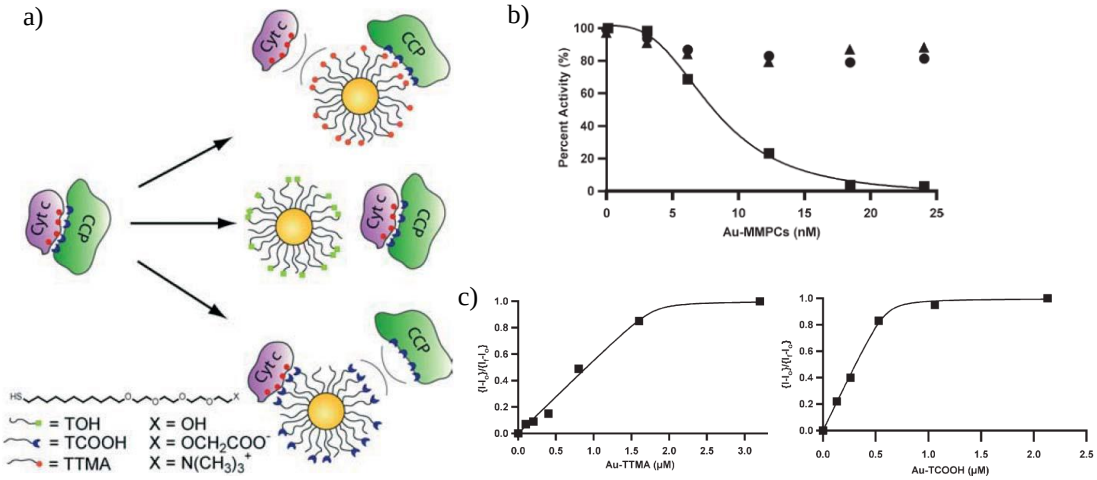

Figure 1.5. (a) Protein surface recognition by CCP, Cyt c, and MMPCs (b) Inhibition of CCP by **Au-TTMA** (squares); and lack of interaction with **Au-TCOOH** (circles), and **Au-TOH** (triangles) (c) Binding isotherms by CD.

Native gels experiments demonstrated that **Au-TTMA** selectively bound to CCP, disrupting the CCP–Cyt c adduct. Indeed, **Au-TCOOH** bound selectively to Cyt c whereas **Au-TOH** had no effect. This indicated that the K_D for MMPC–protein binding was lower than the K_D for Cyt c–CCP (K_D , 10 μM). The ability of **Au-TTMA** and **Au-TCOOH** to act as enzyme inhibitor by titrating increasing amounts of MMPCs showed how **Au-TTMA** inhibited CCP but **Au-TCOOH** and **Au-TOH** did not (Figure 1.5b). The inhibition with **Au-TTMA** was fitted showing that Au-

TTMA was a potent inhibitor of CCP, IC_{50} = 13 nm (concentration of inhibitor causing 50% inhibition). The binding stoichiometry for the **Au-TTMA–**CCP and **Au-TCOOH–**Cyt c adducts were determined by circular dichroism (Figure 1.5c). The binding of CCP to **Au-TTMA** was fit with n =2.1 ± 0.1 and K_D =25 ± 30 nM. The binding ratio and K_D of **Au- TCOOH**–Cyt c was calculated as 4.0 ± 0.2 and 40 ± 31 nM respectively. Hence, surface functionalized MMPCs selectively interacted with CCP and Cyt C based upon charge complementarity and, the proteins retained their native structure upon binding MMPC. Indeed, both the **Au-TTMA**–CCP and **Au-TCOOH**–Cyt c adducts bound with about 3 orders of magnitude greater affinity ($K_D \sim 10^{-8}$ M) than the CCP–Cyt c adduct ($K_D \sim 10^{-5}$ M).

The preparation of peptide-capped (see section 1.2) nanoparticles is rapid, simple, and amenable to high-throughput approaches and allows, in a single step, the production of stable and functional nanoparticles[41]. This provides robust and scalable methodologies for controlling the nanoparticle surface. However, even though these studies demonstrated the potential of the peptide-capped gold nanoparticles a number of scientific challenges remain to be addressed: (a) how to control the surface composition and topology on the molecular level, (b) how to control the dynamic exchange of the peptides and, the greater challenge, (c) the formulation-function problem, that is, which combinations of peptides gives rise to the most effective surface?

1.4 Self-assembly of dynamic structures

Self-assembly is the spontaneous organization of molecules into ordered aggregates without external control[50,51]. The driving force for formation are mutual interactions, such as electrostatic interactions, hydrophobic interactions, coordination bonds, hydrogen bonding etc. The noncovalent bond formation between the constituents makes that these systems typically form in a reversible manner, whichs creates a fundamental difference with covalent structures. During the last decades a big effort has been made in developing synthetic self-assembly systems[51,52] starting

from simple building blocks[50]. A wide variety of examples of supramolecular self-assembled systems are found in literature[53].

Also the self-assembly of alkane thiols on gold nanoparticles to form Au NPs is a reversible and spontaneous process[54]. Nonetheless, the composition of self-assembled monolayers (SAMs) on Au NPs is typically still of rather low complexity[55]. This mainly originates from the use of synthetic protocols for mixed SAM formation (e.g., place exchange), which do not give full control over the final composition, require purification of each single NP system, and suffer from issues related to the characterization of mixed SAMs both in terms of composition and morphology.

SAMs are formed through self-assembly, and, indeed, the dynamic nature of the system was used by Rotello to study the adaptation of a Au NP system to an α-helical peptide. They reported the use of trimethylammonium-functionalized Au NP (MMPCs **2**) for the binding and stabilization of a tetra-aspartate peptide in completely aqueous solution[56]. Peptide **1** (Figure 1.6a) was used to test the ability of MMPCs **2** to recognize and stabilize the α-helix of a peptide sequence (Figure 1.6b). The binding of the peptide to the nanoparticle was studied by fluorimetry. The addition of the MMPC **2** to a peptide solution resulted in a partial reduction of the fluorescence intensity (Figure 1.6c). Next, the formation of the α-helices was monitored by circular dichroism (CD). An increase in the α-helicity was observed (at 208 nm and 222 nm), indicating the formation of the α-helices induced by MMPCs **2** The resulting α-helicity from each addition was analyzed and plotted against the MMPCs **2** concentrations (Figure 1.4d). The addition of the MMPCs **2** resulted in a strong increase in the helicity (60 %) compared to that of the peptide alone (4 %). Also the α-helical content increased in time suggesting an adaptation of the thiols in MMPC **2** towards a surface with a higher affinity for the α-helix.

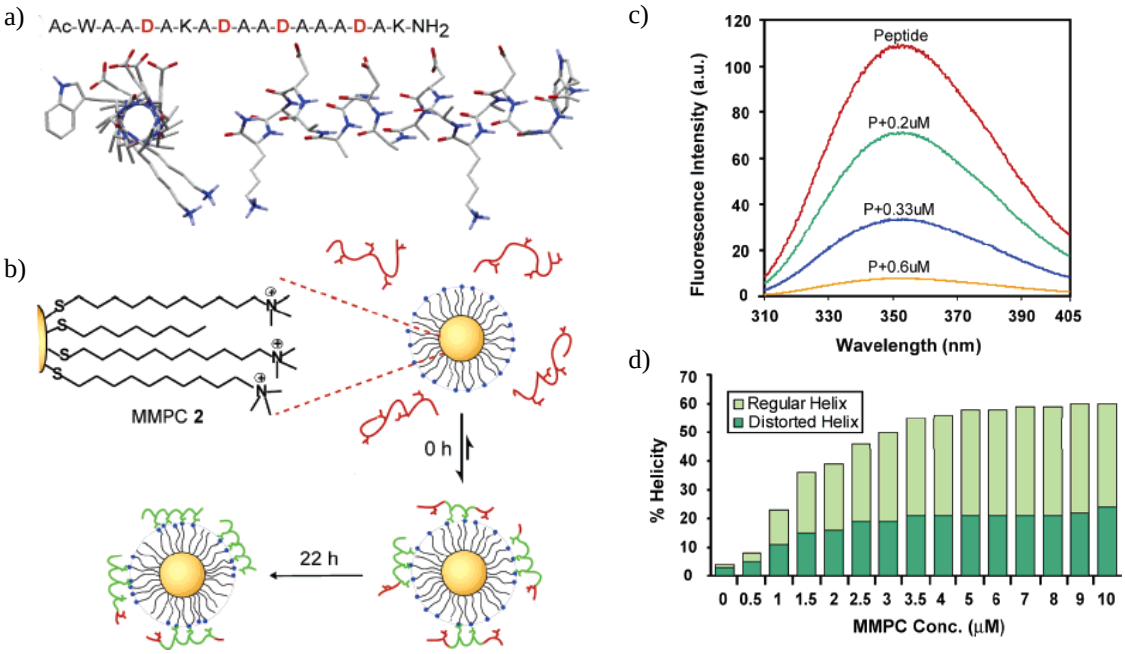

Figure 1.6. (a) Peptide **1** sequence. (b) General scheme of the work. (c) Fluorimetric assays. (d) Representation of the helicity against to MMPCs **2** concentration.

These studies by Rotello and co-workers illustrated that in principle the dynamic nature of the self-assembled monolayer can lead to adaptation. However, the study also shows practical limitations originating from the slow dynamics of the system. For that purpose, alternative strategies have been developed in which the Au NP is taken as a multivalent scaffold on which small molecules are self-assembled using noncovalent interactions. Thus, the dynamic nature is shifted from *in* the monolayer to *on* the monolayer.

This different approach of exploiting self-assembly processes in combination with Au NPs has been studied recently by the Prins'group. Au NPs containing 1,4,7-triazacyclononane (TACN)•Zn^{2+} head groups (Au NP **1**) are attractive scaffolds for the formation of multivalent supramolecular structures (Figure 1.7). These Au NP **1** present many features that make them appealing. Here, two of them will be discussed, which are the ability to catalyze the chemical transformation of bound molecules, and, importantly, the ability to concentrate small molecules on the monolayer surface[57].

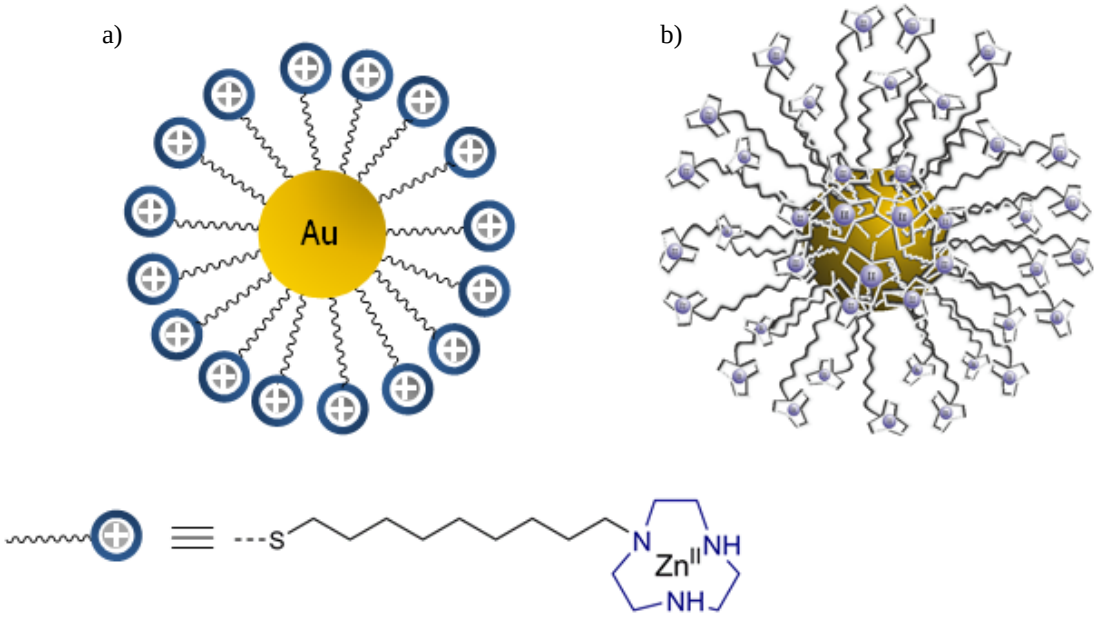

Figure 1.7. (a) Representation of Au NP **1** (b) 3D structure of Au NP **1**.

Au NP **1** has the capability to catalyze the transphosphorylation of HPNPP (2-hydroxypropyl-4-nitrophenyl phosphate)[58] which is a model compound used for mimicking RNA-hydrolysis[31]. Rate accelerations up to 4×10^4 were observed compared to the background reaction. Studies showed that this catalytic activity results from the formation of catalytic pockets by two neighboring TACN·Zn^{2+} complexes in the monolayer[58] since a sigmoidal curve is observed for the initial rate as a function of the amount of Zn^{2+} added. It is possible to modulate the catalytic activity of the Au NP **1** through competition between the HPNPP-substrate and anionic probes. The anionic probes occupy the binding sites preventing access of HPNPP to the active sites (Figure 1.8).

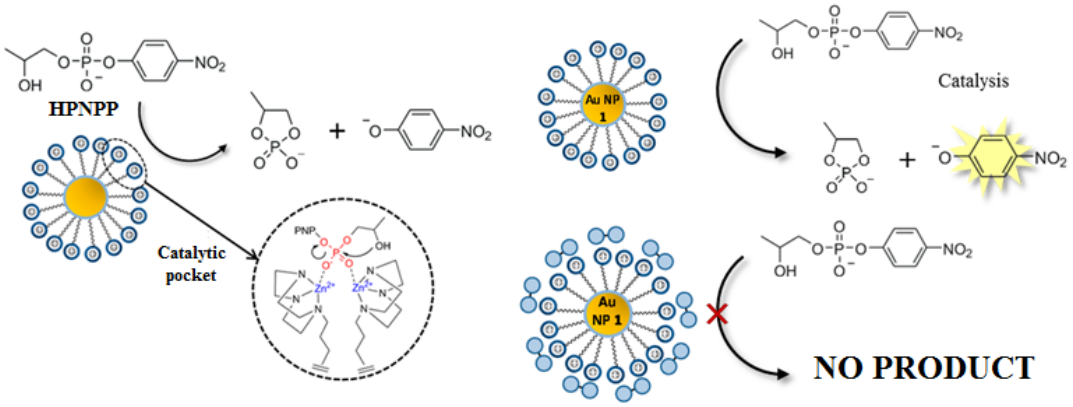

Figure 1.8. Catalytic pocket and schematic representation of the inhibition study.

On the other hand, the polycationic nature of the Au NP **1** surface causes a high affinity for small negatively charged molecules[59] such as oligonucleotides (ATP_F, ATP and ADP) and small peptides (Ac-DDD and NBD-GDDD). Those anions spontaneously assembly on the surface of Au NP **1** in water through a combination of electrostatic interactions and hydrophobic interactions. (Figure 1.9). It has been shown that this property is highly attractive for the development of responsive multivalent surfaces[60].

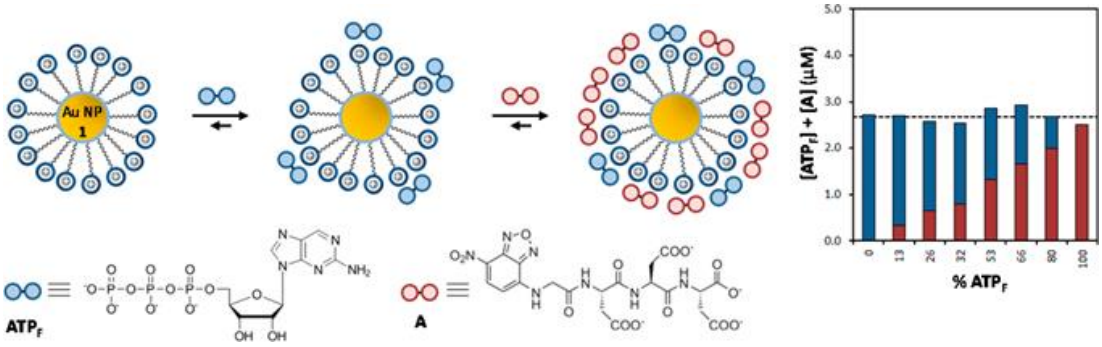

Figure 1.9. Co-assembly of ATP_F and peptide A on Au NP **1** leads to a heterogeneous surface composition.

Binding interactions between small molecules and Au NP **1** are typically studied in two ways: either by using a fluorescence titration or by means of a displacement assay.

The affinity of the cationic surface of Au NP **1** for a compound can be studied by measuring the fluorescence intensity as a function of the amount of compound added to a solution of Au NP **1**. (Figure 1.10). This titration relies on the ability of Au nanoparticles to highly efficiently quench the fluorescence of bound fluorophores[61]. The probes are quantitatively bound to the surface up to the surface saturation concentration (SSC). After having reached the SSC, the additional amount of fluorescent probe remains free in solution and, consequently, in that concentration regime the fluorescence intensity increases linearly as a function of the amount of probe added.

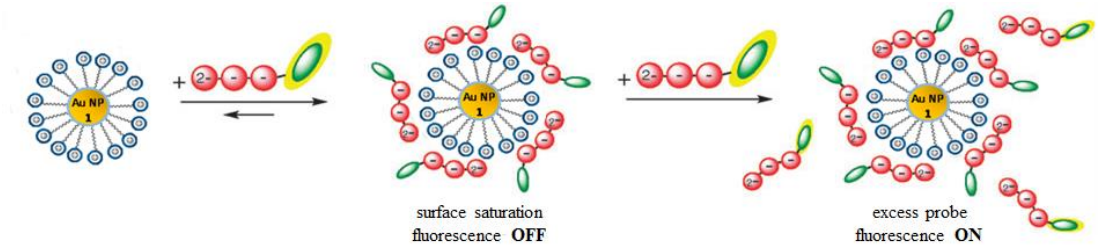

Figure 1.10. Schematic representation of binding assay.

Alternatively, the displacement assay relies on the dynamic nature of the system, which causes the displacement of a fluorescent probe from the surface of Au NP **1** surface upon the addition of increasing amounts of a (non-fluorescent) competitor (Figure 1.11). This allows determination of the relative affinities of different probes compared to the same competitor. The displacement can be simply monitored by measuring the fluorescence intensity originating from the displaced fluorescent probe as a function of the concentration of added inhibitor.

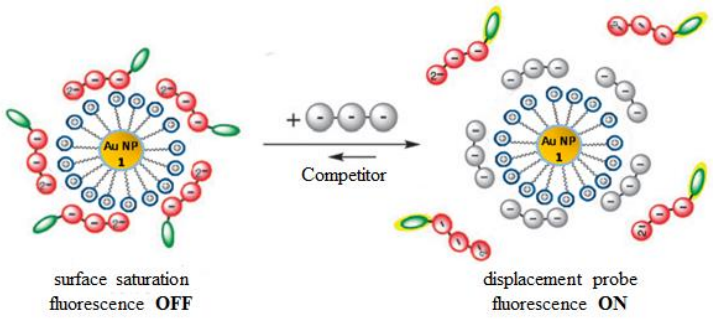

Figure 1.11. Schematic representation of the displacement experiment.

1.5 Scope of this Thesis

The examples discussed in the introduction have demonstrated the power of conjugating peptides and gold nanoparticles for the purpose of biomolecular recognition and more. However, based on the results obtained so far in the Prins' group we are challenged by the idea of creating a new kind of nanoprotein by self-assembling peptide fragments noncovalently on the monolayer.

With this approach some of the limitations present in the systems seen before will be overcome. Since the peptides will not be covalently bound to the Au NP **1**

surface, it will be easier to change the composition of the surface simply by changing the ratio of the peptides added. Moreover, since the formation of the final structure depends on self-assembly, additional functionalities can be simply introduced by changing the sequences of the peptide fragments (Figure 1.12a). Thus the creation of structural diversity will no longer require the cumbersome separate synthesis and purification of each functionalized nanoparticle system.

Also, due to the non-covalent nature of the interactions, the surface will be highly dynamic and self-adaptable. This implies that exposure to a protein target could in principle lead to a reorganizing, spontaneously selecting those peptides able to form a synthetic protein surface that is best adapted to interact with the protein target (Figure 1.12b).

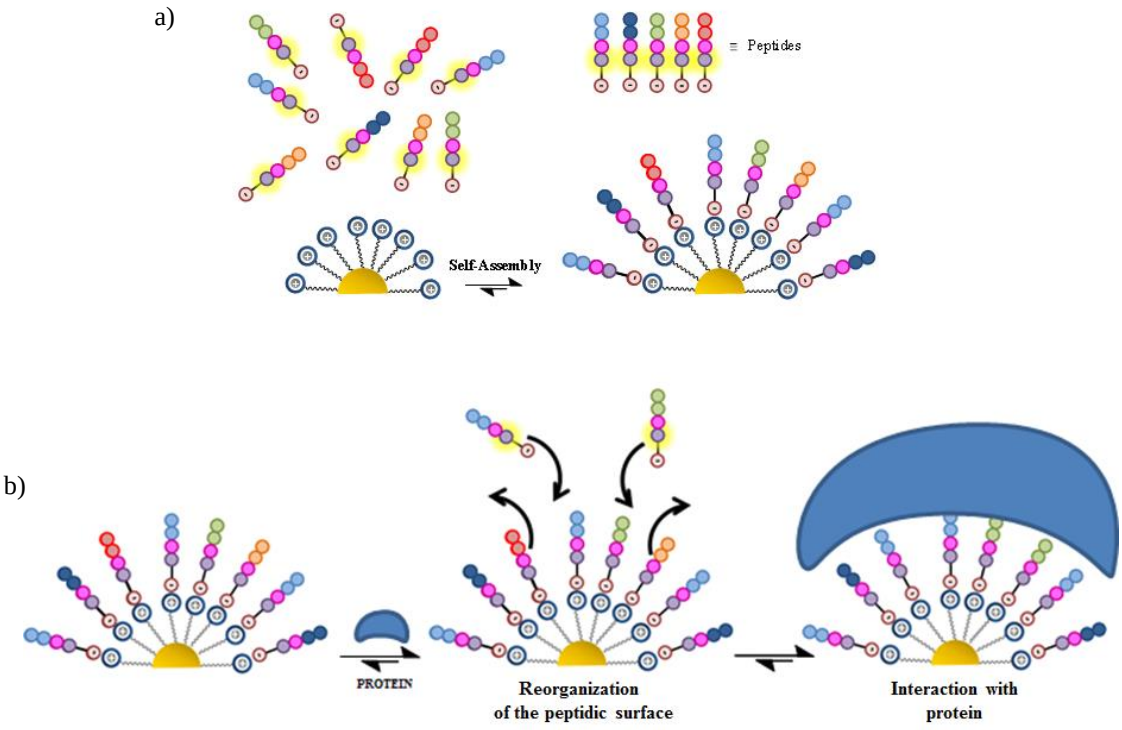

Figure 1.12. (a) Schematic representation of the self-assembled system and (b) reorganization of the peptidic surface and further interaction with protein.

CHAPTER 2: Self-assembly of small peptides on monolayer-protected gold nanoparticles

2.1 Summary

In this chapter the interaction of different small peptide and peptide-like molecules with the Au NP **1** surface is studied with the scope of identifying the minimal structure required for binding under saturation conditions. Then, the selected structure is used to synthesize a peptide library containing selected amino acids that cover the complete range of functionalities present. Next, the interaction of the small peptide library with Au NP **1** is evaluated. In first instance the peptides are used separately and, finally, the peptides are combined and self-assembled simultaneously on the surface of Au NP **1** to yield a dynamic multivalent peptide surface.

2.2 Small peptide fragments as recognition unit

In order to maximize the number of peptides bound to Au NP, our initial aim was to find minimal peptides that would bind Au NP **1** under saturation conditions at low micromolar concentrations at physiologically relevant conditions.

The main prerequisite for the peptides is the presence of a negative charge to interact electrostatically with the polycationic surface of Au NP **1**. In order to determine which groups would cause strong binding a series of small molecules were selected that combine a negative charge with additional functionalities that may favor binding to the monolayer: the presence of a pyridine in picolinic acid **2** and, isonicotinic acid **3**, the presence of a thiol for coordinating Zn^{2+} (*N*-Ac-Cys **4** using *N*-Ac-Met, **5** as a reference), or the presence of an apolar side chains (H-Val-OH **6**, *N*-Ac-Val, **7**) (Chart 2.1).

The relative affinity of each compound for the Au NP **1** surface was evaluated by means of a displacement experiment (see section 1.4). As mentioned before, these displacement experiments rely on the competition of two compounds

for binding to the surface of Au NP **1**. Displacement of a (quenched) fluorophore from the surface of Au NP **1** upon the addition of a competitor leads to a turn-on of its fluorescence, which can be measured. In this case the tripeptide Ac-WDDD-OH (*N*-Ac-Trp-Asp-Asp-Asp-OH) was used as a fluorescent high affinity probe.

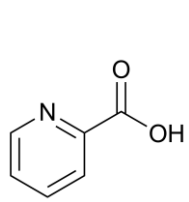

Picolinic acid
2

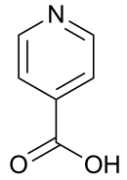

Isonicotinic acid
3

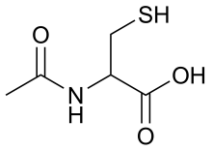

N-Ac-L-Cys-OH
4

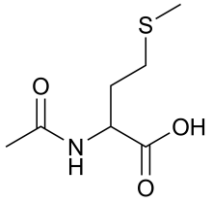

N-Ac-L-Met-OH
5

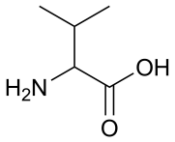

L-Val-OH
6

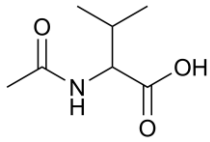

N-Ac-L-Val-OH
7

Chart 2.1.

Unfortunately, none of the candidates (**2**-**7**) were able to displace significant amounts of Ac-WDDD-OH (2.4 μM) from the surface of Au NP **1** ([TACN-Zn^{2+}] = 10 μM) even after additions exceeding 20 μM. This indicates that these recognition units have an affinity for Au NP **1** that is too low to effectively compete with the high affinity binder Ac-WDDD-OH.

For this reason, it was decided to study the interaction between the library and Au NP **1** in an alternative manner. An catalytic inhibition assay was used that is more sensitive to detect the interaction of small anions with Au NP **1.** As discussed in section 1.4, this assay exploits the inhibition of the catalytic activity of Au NP **1** in the transphosphorylation of HPNPP by small molecules able to compete with HPNPP for binding to Au NP **1**. The higher sensitivity of this assay results from the fact that in this case the compounds compete with HPNPP which has a much lower affinity for Au NP **1** compared to Ac-WDDD-OH. For these studies, two additional candidates were added to the library: Fmoc-Ser(PO_2H_3)-OH (**8**) and Fmoc-His-OH (**9**) (Chart 2.2).

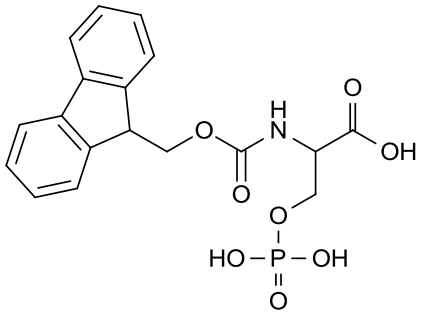

Fmoc-L-Ser(PO_3H_2)-OH
8

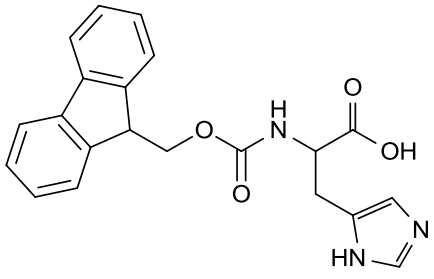

Fmoc-L-His-OH
9

Chart 2.2.

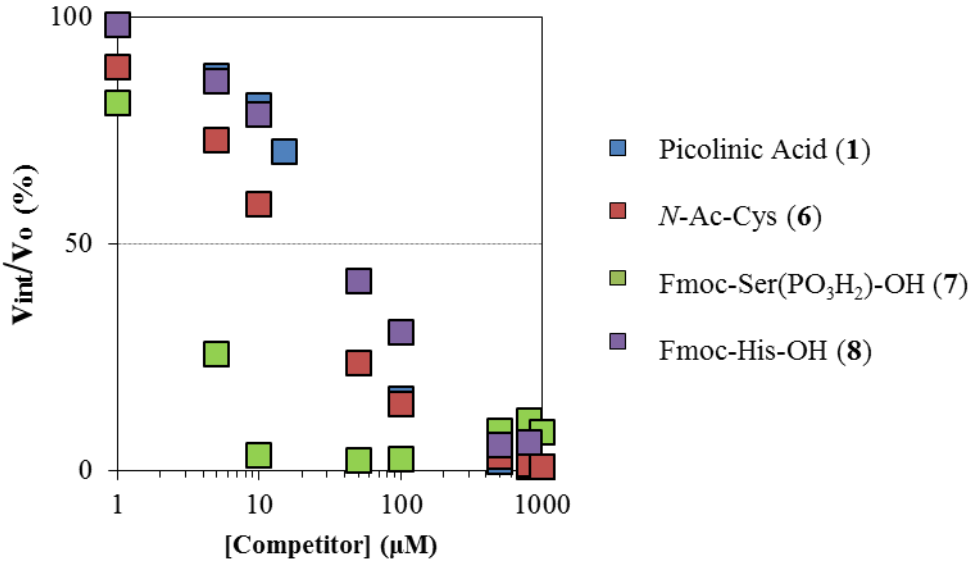

Figure 2.3. v_{init}/v_0 (x 100 %) as a function of the concentration of competitor. Experimental conditions: measured at λ=405 nm of *p*-nitrophenol. Conditions: [TACN-Zn^{2+}] = 20 µM, [HPNPP] = 2 mM in [HEPES] = 10 mM, pH = 7.5 at T = 40ºC.

Thus, increasing amounts of competitors ranging between 0-1 mM were added to a solution containing Au NP **1** (([TACN-Zn^{2+}] = 20 µM) in HEPES buffer at pH = 7 and T = 40ºC. The absorbance at 405 nm originating from the formation of *p*-nitrophenol was measured as a function of time. Initial rates were determined by dividing the slope (taking the 10 first minutes) by the molar extinction coefficient of *p*-nitrophenol at pH = 7.5 (ε = 13135 $M^{-1}cm^{-1}$). Tthe initial rate (v_{init}/v_0) as a function of the concentration of competitor is shown in Figure 2.3.

Analysis learned that only four of the eight molecules were able to inhibit significantly the transphosphorylation reaction (some of the other molecules showed

weak inhibition at concentrations higher than 1 mM). The concentration required to cause a 50% inhibition ($v_{int}/v_0 = 0.5$) was taken as a value to quantify the inhibitory effect. It was found that 26 µM of **2** was sufficient for 50% inhibition, whereas the regioisomer **3** (with the carboxylic acid group in *p*-position) did not show any significant inhibition up to 1 mM. This clearly indicates that a combination of electrostatic interactions with coordination bonding to the Zn^{2+} metal ions in the monolayer through the chelate effect can provide strong affinity binders. This was also observed in the case of **9** where a negative charge is combined with an imidazole-moiety. This compound had a similar inhibitory effect as compared to **2** (38.2 µM). This seems further confirmed by the strong inhibitory power of **4** (13.76 µM) and the weak binding of **5** (no inhibition) which indicates the involvement of the thiol bond in metal coordination. The most impressive data was obtained for **8**, which at a 3.3 µM concentration caused 50% of inhibition. These inhibition experiments yielded four structures with a potential high affinity for the monolayer surface: **2**, **4**, **8** and **9**. Hence, the next step was to evaluate the affinity for Au NP **1** using a direct fluorescence titration, *i.e.* in the absence of a competitor such as Ac-WDDD-OH or HPNPP.

Fluorescent analogues of the four candidates were synthesized by SPPS (Solid Phase Peptide Synthesis) conjugating the molecules to Trp as a fluorescent unit. A leucine residue was added to the peptide sequences in order to facilitate purification of the peptides by precipitation. The use of picolinic acid (**2**) was abolished since the addition of a new residue would lead to the loss of the negative charge. This was compensated for by adding a new candidate to the library: aspartic acid (Chart 2.3). Binding assays were also performed in the presence of other metal ions than Zn^{2+} (*i.e.* Cu^{2+}, Ni^{2+}, Co^{3+} and Fe^{3+}) to assess whether this would affect the binding properties. The concentration of metal ions stock solution (Zn^{2+}, Cu^{2+}, Ni^{2+}, Co^{3+} and Fe^{3+}) were determined by atomic absorption spectroscopy. The concentration of the peptides in the stock solution were determined by UV spectroscopy at pH 7.0 ($\varepsilon_{280\,(Trp)} = 5579\ M^{-1}cm^{-1}$).

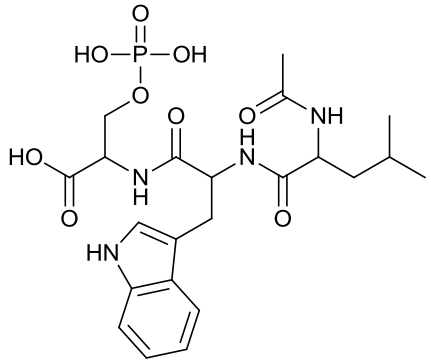

Ac-(LLL)-Leu-Trp-Ser(PO_3H_2)-H
LWS(p)
10

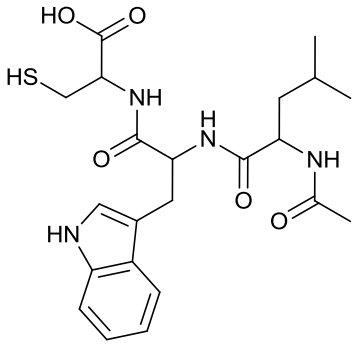

Ac-(LLL)-Leu-Trp-Cys-H
LWC
11

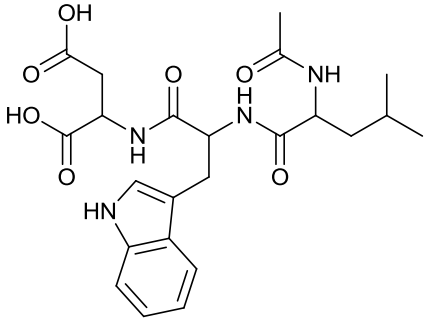

Ac-(LLL)-Leu-Trp-Asp-H
LWD
12

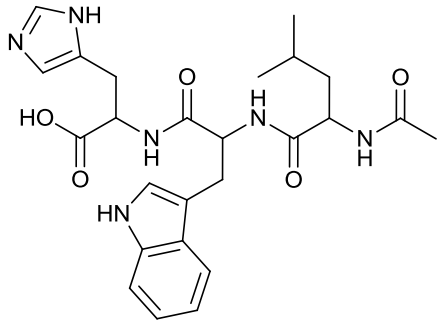

Ac-(LLL)-Leu-Trp-His-H
LWH
13

Chart 2.3.

In these titrations, the fluorescent intensity was plotted as a function of the concentration of the probes **10**-**13** (Figure 2.5). The resulting graphs are characteristic of Au NP **1**-peptide complex formation under saturation conditions. Since in the absence of binding the hypothetical increase in fluorescence is given by $y = ax + b$, the surface saturation concentration (SSC) could be calculated by extrapolation of the linear part of the curve (Table 2.1). Furthermore, the shallowness of the curve provides qualitative information on the affinity for the surface. The more shallow the curve, the lower is the affinity.

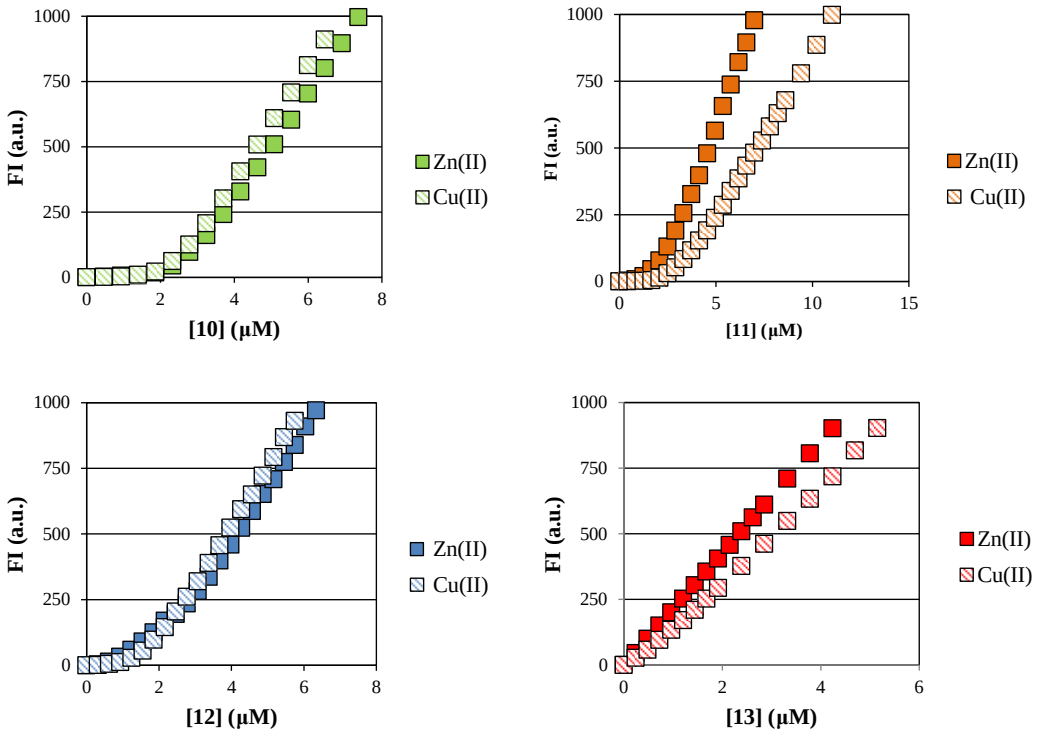

Figure 2.5. Binding assays: fluorescent intensity (a.u.) as a function of **10**, **11**, **12** and **13** concentration (µM) in presence of Zn^{2+} (left) and in presence of Cu^{2+} (right) measured at λ_{ex}=280 nm, λ_{em}=360 nm. Conditions: [TACN-Zn^{2+}] = 10 µM, [HEPES] = 10 mM, pH = 7, T = 25 °C.

The results showed that when Zn^{2+} and Cu^{2+} are present in the monolayer of Au NP **1** all molecules bind, except for **13**. However, no binding was observed when Ni^{2+}, Co^{3+} and Fe^{3+} were used, except for **9** that even in the presence of those metals showed some degree of binding (section 2.5.5 - Figure 2.15).

Table 2.1. SSC values of **10**, **11**, and **12** obtained from their binding assays.

	SSC (µM)	
	Zn^{2+}	**Cu^{2+}**
LWS(p) (**10**)	2.66	2.33
LWC (**11**)	2.14	3.09
LWD (**12**)	1.15	1.61

Looking at the SSC (Table 2.2) in the presence of Zn^{2+}, a significant difference between **10** and the other two peptides was observed. The SSC of **10** (2.66 µM) was the highest one indicating that more molecules of **10** can be simultaneously accommodated on the surface of Au NP **1**. Interestingly, in the presence of Cu^{2+} it

was found that **11** presented the highest SSC (3.09 μM), making it potentially the best candidate. However, since other studies have shown that thiol-containing peptides can promote place-exchange reactions with the thiols of the monolayer[62] it was decided not to continue with **11** as the lead compound. Therefore, comparing **10** to **12** it was observed that the SSC of **10** was significantly higher than that of **12**. In addition, the shallowness of the curve measured for **12**, indicated a lower affinity for the Au NP **1** surface.

These results point to an important role of the phosphate group in regulating binding, which was in line with previous results obtained for the interaction between ATP and Au NP **1**[63]. In addition, the fact that the SSC of **10** is higher compared to that of ATP (2.5 μM), allows a high number of peptides to be bound simultaneously to the monolayer surface thus yielding a nanosystem with a higher valency. Consequently, compound **10** was chosen as a lead for follow-up studies.

2.3 Peptide library

In the next phase compound **10** was used as the starting point for the construction of a small peptide library able to decorate Au NP **1**. Additional amino acid residues were chosen to study the effect of additional charges (positive and negative) and polarities (hydrophobic/hydrophilic) on the affinity of the peptides for Au NP **1** with the final scope of creating a dynamic peptide surface on Au NP **1** as functionally diverse as possible (Chart 2.4). All residues were added twice in order to mimic previously studied systems in which Au NPs were functionalized with dipeptide-terminated thiols and in order to reinforce the effect of the added functionality.

Asp was added to provide the system with an additional negative character whereas Arg and Lys introduced a positive charge. Leu and Phe were chosen as hydrophobic residues and, finally, Ser and Asn as neutral polar residues. The eventual combination of these peptides would enable the formation of multivalent peptide surfaces with the chemical diversity required for the interaction with the protein surface. All peptides were synthesized by SPPS and characterized by RP-UPLC and MALDI-TOF.

After the synthesis and purification, the affinity of the peptides for the Au NP **1** surface was evaluated by fluorescence titrations. As before, the binding assays were monitored by measuring the fluorescent intensity (Trp fluorescence, λ_{ex}=280 nm, λ_{em}=360 nm) after the addition of increasing amounts of peptide. Then, the fluorescent intensities were plotted as a function of the concentration of the peptides (Figure 2.6).

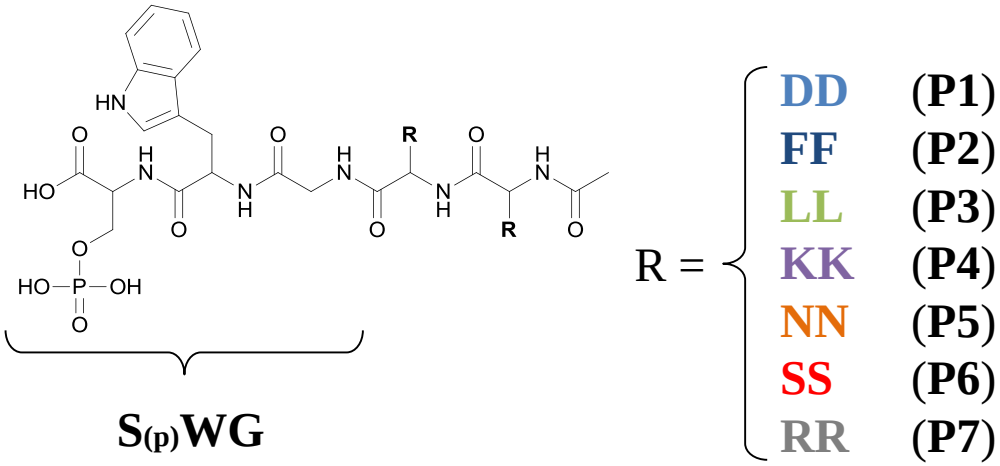

Chart 2.4.

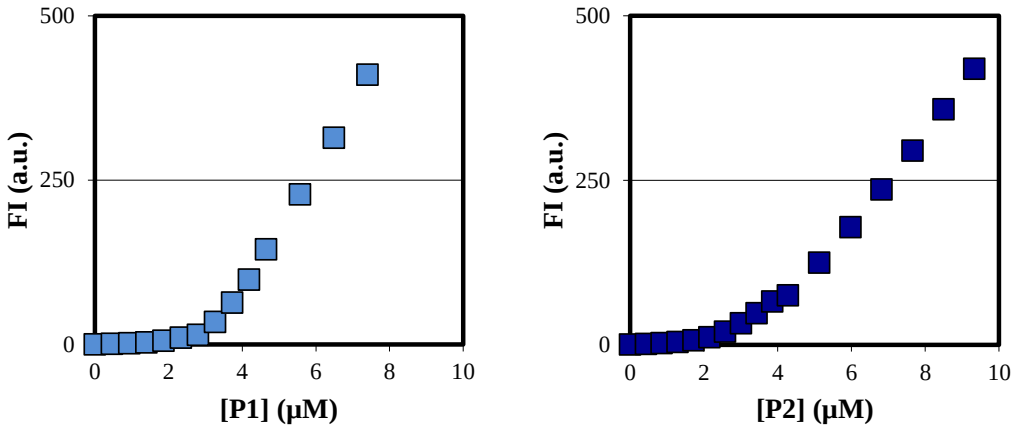

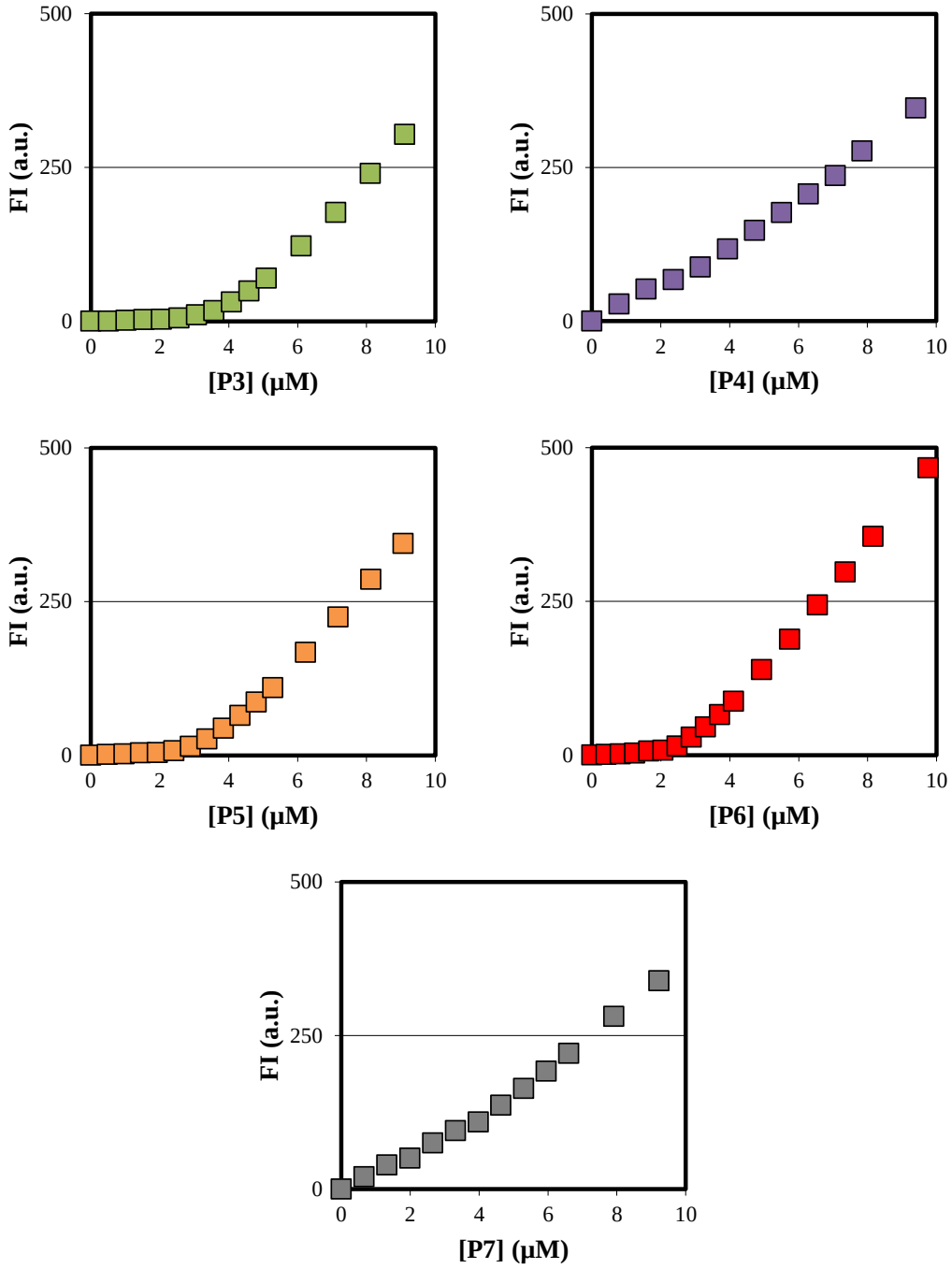

Figure 2.6. Binding assays: fluorescent intensity (a.u.) as a function of **P1** (light blue), **P2** (blue), **P3** (green), **P4** (lilac), **P5** (orange), **P6** (red) and **P7** (grey) concentration (μM) measured at λ_{ex}=280 nm, λ_{em}=360 nm. Conditions: [TACN-Zn^{2+}] = 10 μM, [HEPES] = 10 mM, pH = 7, T = 25 °C.

The titrations confirmed a strong binding for **P1**, **P2**, **P3**, **P5** and **P6**, whereas for **P4** and **P7** no binding was observed. That could be due to the repulsion between the positively charged residues of **P4** or **P7**, (Lys and Arg respectively), and the positively charged surface of Au NP **1**. An alternative explanation is the formation of intramolecular electrostatic interactions between the positively and negatively

charged residues in **P4** and **P7**. Consequently, **P4** and **P7** were dismissed from further studies. The SSCs were determined as mentioned before[64]. The obtained SSC showed similar values for all of the peptides except for **P3** (Table 2.2). This difference could be attributed to the intermolecular hydrophobic interactions between Leu-residues causing a more compact packing of the peptides on the surface.

Table 2.2. SSC and $[ADP]_{50\%}$ (μM) values of the peptide library.

	SSC (μM)	**$[ADP]_{50\%}$ (μM)**
P1	3.1	17.3
P2	3.6	5.3
P3	4.9	4.8
P5	3.6	3.9
P6	3.1	3.0

In order to determine the relative affinity of each peptide for the surface of Au NP **1**, displacement experiments were performed using ADP as a non-fluorescent competing probe. Displacement experiments were carried out by measuring the fluorescent intensity of Trp (fluorescence, λ_{ex}=280 nm, λ_{em}=360 nm) upon addition of increasing amounts of ADP to Au NP **1** covered with peptides **P1**-**P3** and **P5**, **P6**. (Figure 2.7).

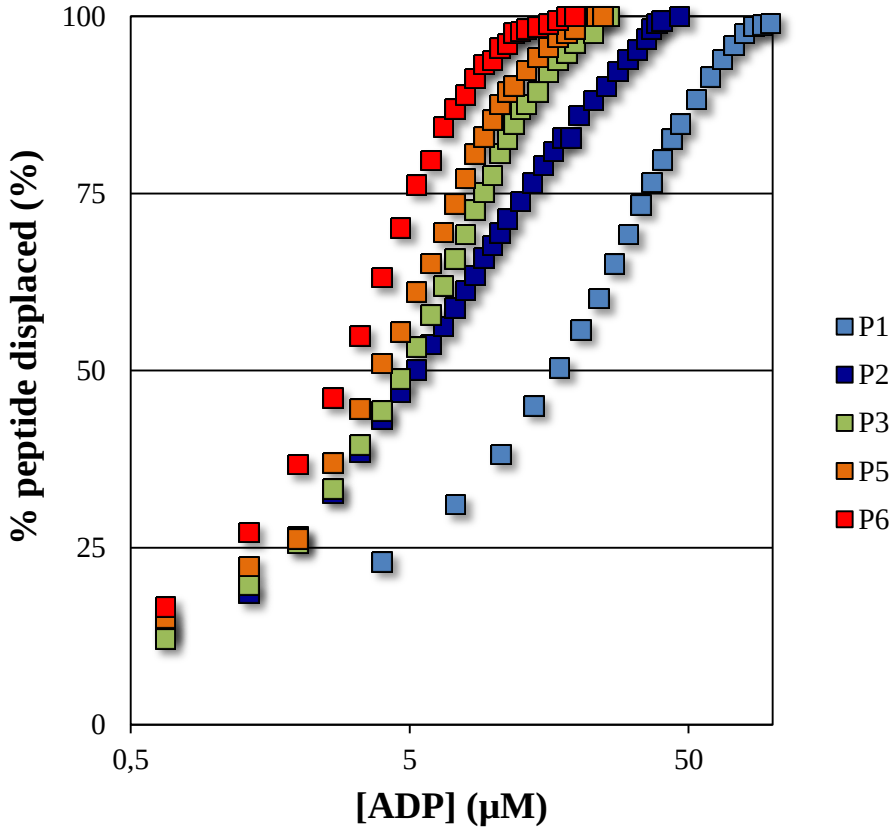

Figure 2.7. Displacement experiment: fluorescent intensity (a.u.) as a function of [ADP]. **P1** (light blue), **P2** (blue), **P3** (green), **P5** (orange) and **P6** (red) concentration (µM) measured at λ_{ex}=280 nm, λ_{em}=360 nm. Conditions: [TACN-Zn^{2+}] = 10 µM, [HEPES] = 10 mM, pH = 7, T = 25 °C.

The ADP-concentration required to displace a 50% of peptide can be taken as a value that quantifies the relative affinity of the peptides for the Au NP **1** surface (Table 2.2). The higher the concentration of ADP needed to displace the peptide from the surface, the higher the affinity of the peptide for the surface Au NP **1**. **P1** has five negative charges (at pH = 7), which explains the higher affinity for Au NP **1** compared to the other peptides ($[ADP]_{50\%}$ = 17.3 µM) . The relatively high affinity of **P2** could be a result of the presence of the hydrophobic Phe-residues. Other studies have indeed shown that hydrophobic interactions with the alkyl chains of the monolayer can significantly enhance the affinity of small molecules for the surface[65]. This seems to be confirmed by the relative low affinity of peptide **P6** which has two polar Ser-residues ($[ADP]_{50\%}$ = 3.0 µM).

.

2.4 A multivalent protein-like surface

Next, we were interested to find out whether the combined use of peptides **P1** to **P6** would result in the formation of a dynamic multivalent peptide surface on Au NP **1**. Hence, to study the behavior of a mixture of peptides in the presence of Au NP **1** a binding assay was performed using the same conditions as before. The binding was monitored by measuring the fluorescent intensity of Trp (λ_{ex}=280 nm, λ_{em}=360 nm) upon the addition of increasing amounts of an equimolar peptide mixture containing **P1**, **P2, P3, P5** and **P6** (Figure 2.8). The resulting curve showed that the different peptides could indeed be accommodated simultaneously on the surface Au NP **1** without affecting the binding properties. The SSC for the peptide mixture was determined at 2.4 µM.

Finally, a displacement experiment was performed by adding increasing amounts of ADP to Au NP **1** saturated with the peptide mixture (1.9 µM, corresponding to around 80% of the SSC). The results showed a release of peptides upon addition an increasing amounts of competitor confirming the binding, which is in line with the behavior observed for the single peptides. It is worth noticing that the different affinities of each peptide for Au NP **1** makes the displacement curve less smooth compared to the individual curves.

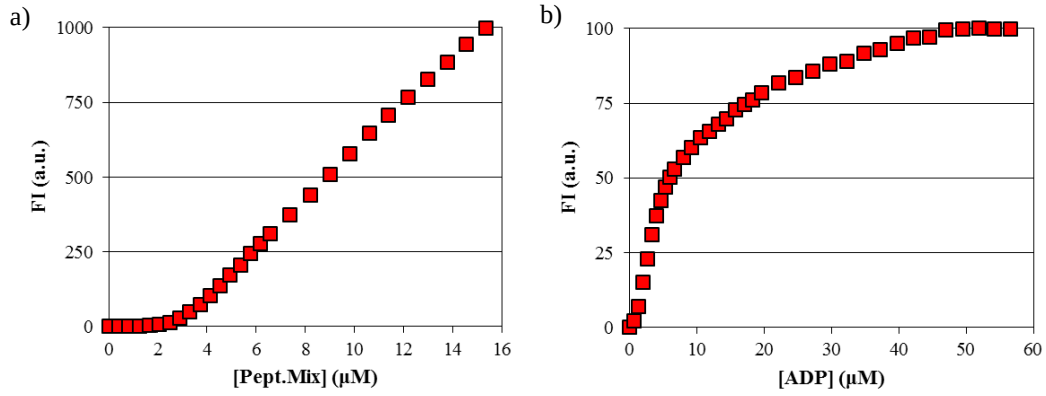

Figure 2.8. (a) Binding assay: fluorescent intensity (a.u.) as a function of Peptide Mix concentration (µM) measured at λ_{ex}=280 nm, λ_{em}=360 nm. Conditions: [TACN-Zn^{2+}] = 10 µM, [HEPES] = 10 mM, pH = 7, T = 25 °C. (b) Displacement experiment: fluorescent intensity (a.u.) as a function of [ADP] (µM). Conditions: [TACN-Zn^{2+}] = 10 µM, [Pept.Mix] = 1,9 µM [HEPES] = 10 mM, pH = 7, T = 25 °C.

The simultaneous assembly of multiple peptides on the surface of Au NP **1** results in a large pool of different dynamic peptide surfaces. This number, *C*, can be calculated using a simple model that assumes degenerate binding sites:

$$C = \frac{(N+1)\times(N+2)\times\ldots(N+k-1)}{2\times3\times\ldots(k-1)} \qquad \textbf{Equation 2.1.}$$

where N = number of binding sites on Au NP **1** and k = size of the peptide library.

If it is considered that the ratio head group/peptide is 4.2 (10 μM/2.4 μM (SSC average of the peptides)) and that there are around 70 thiols[66] per gold nanoparticle, it is found that the number of binding sites, *N*, is roughly 17. Then, for k = 5, it emerges that 5985 different surface combinations are present in solution.

These studies demonstrates the possibility to build an heterofunctionalized system containing just five different peptides. The library size can be controlled by changing the peptide ratios and, in addition, easily enhanced by adding additional peptides with different sequences.

2.5 Conclusions

The studies have identified four potential candidates for binding to Au NP **1** of which the tripeptide LWS(p) (S(p) = phosphoserine) had the highest affinity. From a series of studies in which the metal-ion in the monolayer has been varied, it emerged that Zn^{2+} gave the best results. Using LWS(p) as a lead structure a small peptide library has been synthesized successively in which additional amino acid residues have been attached to the binding unit. Amino acids containing negatively or positively charged, polar and apolar side chains have been chosen in order to create a chemical diverse library. Subsequent binding studies have shown that all peptides had a very high affinity for Au NP **1**, apart from the peptides containing positively charged amino acids. Afterwards, the peptide library has been used to self-assembly a dynamic nanoprotein by adding all peptides simultaneously to Au NP **1**. Binding studies have revealed that binding occurred under saturation conditions at

low micromolar concentrations in aqueous buffer at pH = 7. The addition of a competitor for binding resulted in a complete displacement of the peptides demonstrating the dynamic nature of the surface. In this way it has been demonstrated that it is possible to build up a complex multivalent system in a straightforward manner.

2.6 Experimental section

2.6.1 Instrumentation

NMR Analysis

^{1}H-NMR spectra were recorded using a Bruker AV300 spectrometer operating 300 MHz for ^{1}H, respectively. Chemical shifts (δ) are reported in ppm using D_2O residual solvent value as internal reference[67]. Diffusion-ordered ^{1}H NMR spectra were recorded using the "longitudinal-eddy-current-delay" (LED) pulse sequence[68].

TEM Analysis

TEM images were recorded on a Jeol 300 PX electron microscope. One drop of sample was placed on the sample grid and the solvent was allowed to evaporate. TEM images were elaborated using the freeware software ImageJ (http://rsb.info.nih.gov/ij/).

DLS Analysis

Dynamic light scattering measurements were recorded on a Zetasizer Nano-S (Malvern, Malvern, Worcestershire, UK) equipped with a thermostatted cell holder and an Ar laser operating at 633 nm.

TGA Analysis

Thermogravimetric analysis (TGA) was run on 1-2 mg nanoparticle samples using a Q5000 IR model TA instrument from 30 to 1000 °C under a continuous air flow.

pH measurements

The pH of buffer solutions was determined at room temperature using a pH-meter Metrohm-632 equipped with a Ag/AgCl/KCl reference electrode.

UV-Vis and Fluorescence spectroscopy

UV-Vis measurements were recorded on a Varian Cary50 spectrophotometer, while fluorescence measurements were recorded on a Varian Cary Eclipse Fluorescence spectrophotometer. Both the spectrophotometers were equipped with thermostatted cell holders.

Preparative HPLC, Analytical HPLC and UHPLC-MS

HPLC purifications were performed on a preparative HPLC Shimadzu LC-8A equipped with a Shimadzu SPD-20A UV detector. HPLC analysis were performed on a analytical Shimadzu LC-10AT equipped with a Shimadzu SPD-10A UV detector. For the UPLC analysis an Agilent Technologies 1290 Infinity equipped with a DAD detector and a Quadrupole LC/MS.

Mass measurments

ESI-MS measurements were performed on an Agilent Technologies 1100 Series LC/MSD Trap-SL spectrometer equipped with an ESI source, hexapole filter and ionic trap.

AB SCIEX MALDI TOF/TOF was used for characterizing the peptide library. α-Cyano-4-hydroxycinnamic acid (CHCA) was used as matrix.

2.6.2 Materials

All the compounds were purchased from Sigma Aldrich. L-aminoacids were purchased from Sigma Aaldrich or Iris Biotech. $Zn(NO_3)_2$ and $Cu(NO_3)_2$ were analytical grade products. In all cases, stock solutions were prepared using deionized water filtered with a MilliQ-water-purifier (Millipore) and stored at 4 °C.

2.6.3 Synthesis and characterization of Au NP 1[59]

S-(9-bromonyl) ethanethioate (**A**)

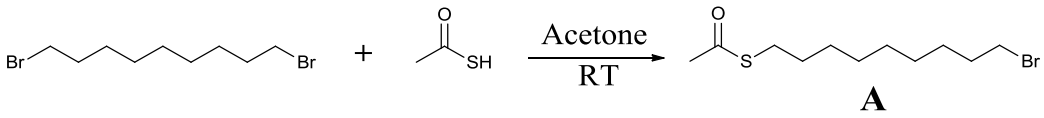

A

1,8-Dibromononane A (5,60 g, 19,6 mmol) was dissolved in acetone (50 mL). Potassium thioacetate was added (2,23 g, 19,6 mmol) and the resulting mixture was kept at room temperature under nitrogen overnight. The resulting suspension was then filtred and after solvent evaporation, the crude product was purified by flash chromatography (silica gel, eluent: EP/CH_2Cl_2: 60/40). 2,79 g (37%) of **A** were obtained as a colorless oil.

^{1}H NMR: (δ ppm, CDCl3, 300K, 200 MHz): 3.38 (t, J = 6.8 Hz, 2H), 2.84 (t, J = 7.2 Hz, 2H), 2.30 (s, 3H), 1.95 – 1.69 (m, 2H), 1.56 (m, 2H), 1.53 – 1.07 (m, 10H).

^{13}C NMR: (δ ppm, CDCl3, 300K, 75 MHz): 195.8, 33.8, 32.7, 30.5, 29.4, 29.1, 29.0, 28.9, 28.7, 28.6, 28.0.

Di-tert-butyl 7-(9-(acetylthio)nonyl)-1,4,7-triazanonane-1,4-dicarboxylate

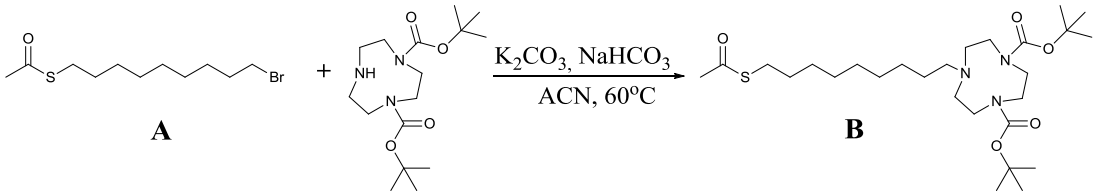

A **B**

Compound **A** (0,344g, 1,224 mmol) and Di-tert-butyl 1,4,7-triazanonane-1,4-dicarboxylate (0,335g, 1,02 mmol) were added to a suspension of K_2CO_3 (0,418g, 3,03 mmol) and $NaHCO_3$ (0,255g, 3,03 mmol) in MeCN (10 mL). The suspension was stirred at 60°C for 3 hours the suspension was filtred under a gooch filter. After evaporation under reduced pressure the crude product was purified by flash

chromatography (silica gel, eluent: CH2Cl2/MeOH: 97/3). 0.345 g (46%) of **B** was obtained as a slightly yellow oil.

^{1}H NMR: (δ ppm, CDCl3, 300K, 250 MHz): 3.43 (m, 4H), 3.22 (mbr, 4H), 2.81 (t, J = 7.2 Hz , 2H), 2.59 (m, 4H), 2.44 (m, 2H), 2.29 (s, 3H), 1.57 (m, 2H), 1.44 (s, 18H), 1.24 (sbr, 12H).

^{13}C-NMR: (300 MHz, d-ACN) δ: 196.35, 156.11, 155,97, 155,81, 79.72, 79.68, 7.41, 54.50, 54.09, 50.98, 50.82, 50.63, 50.41, 50.14, 31.06, 31.00, 29.97, 29.87, 29.53, 29.19, 29.01, 28.63, 28.48, 28.33, 27.91, 27.81

MS (ESI,+, MeOH): *m/z* $[M+H]^+$, 530.4, *m/z* $[M+Na]^+$, 552.4, ($[M+H]^+$, calc. 529.4; $[M+Na]^+$, calc. 552.3)

9-(1,4,7-triazanonan-1-yl)nonane-1-thiol

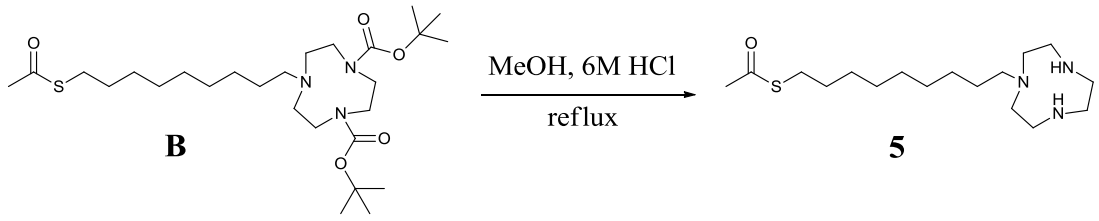

Compound **B** (121 mg, 0,23mmol) was solubilized in MeOH (2 mL) and HCl 6M (2 mL) was added. The resulting solution was stirred for 4 hours at 60°C and after evaporation of the solvant under reduced pressure 17 mg of the thiol **5** (99%) was obtained as a white solid.

^{1}H NMR: (δ ppm, CDCl3, 300K, 250 MHz): 3.43 (s, 4H), 3.25 (m, 4H), 3.10 (m, 4H), 2.75 (m, 2H), 2.29 (t, J = 7 Hz, 2H), 1.43 (m, 4H), 1.34 (sbr, 12H).

Nanoparticles syntehsis

$HAuCl_4 \cdot 3H_2O$ (105.2 mg, 0.27 mmol), weighed in a dry-box, was dissolved in H_2O (mQ; 7 mL). Separately, a solution of TOABr (1,75 g, 3 mmol) in degassed toluene (250 mL) was prepared (sonication for 1 h). The aqueous solution of Au(III)

was extracted with the TOABr-solution (3×15 mL) causing the transfer of $[AuCl_4]^-$ ions into the organic phase (red-orange color). The organic phase was brought together with the remaining amount of the TOABr solution in a 250-mL round bottom flask and di-n-octylamine (4,4 mL, 14 mmol) was added (with a plastic syringe). The solution was vigorously stirred for 30 min under N_2, resulting in a progressive decoloration (red, yellow, green; few minutes). Subsequently, $NaBH_4$ (50,5 mg, 1,2 mmol) dissolved in H_2O (mQ; 2 mL) was added under vigorous stirring, resulting in the formation of the Au nanoparticles (brown coloring). The solution was stirred for an additional 3 h under N_2, after which the aqueous phase was removed with a separating funnel. Then, thiol **5** (89,17 mg, 0,27 mmol) solubilized in a minimum quantity of DMF (1 mL) was added quickly: the solution became colorless and after several minutes a brown precipitate was formed. The obtained suspension were stored under an inert atmosphere overnight. Then, H_2O (mQ; 5 mL) was added and the solutions were stirred for further 30 minutes under N_2. Finally, the aqueous phase was separated and washed with diethyl ether (2×15 mL), toluene (2x15 mL), ethylacetate (2x15 mL), and again diethyl ether (2x15 mL). The resulting dark brown aqueous phase was concentrated and passed through a Sephadex G-25 (mQ water). Finally, the collected brown fraction was concentrated and passed through a Sephadex LH-20 using MeOH.

Au NP **1** was characterized by ^{1}H-NMR, TEM, DLS and TGA analysis. In general, by carrying out ^{1}H-NMR experiments using a "longitudinal-eddy-current-delay" (LED) pulse sequence it is possible to differentiate molecules based on their diffusion coefficients. This provide an unequivocal proof that thiols are bound to the Au NP surface (broad signals) as well as a way to assess the purity of the samples. The obtained NMR spectra with (b) and without (a) the diffusion filter showed that only minimal amounts of unbound additives were present in the final sample (Figure 2.9).

TEM, DLS and TGA analyses provide information about the size and morphology of functionalized gold nanoparticles. TEM analysis proved that the synthesized nanoparticles were nicely mono-dispersed, with a gold core diameter = 2.5 ± 0.5 nm (Figure 2.10c). The hydrodynamic radius observed by DLS was 6.1 ±

1.2 nm (Figure 2.10b), which is in agreement with the thiol length (ca. 1.7 nm). Finally, the weight loss measured by TGA was 51.8% (Figure 2.10d).

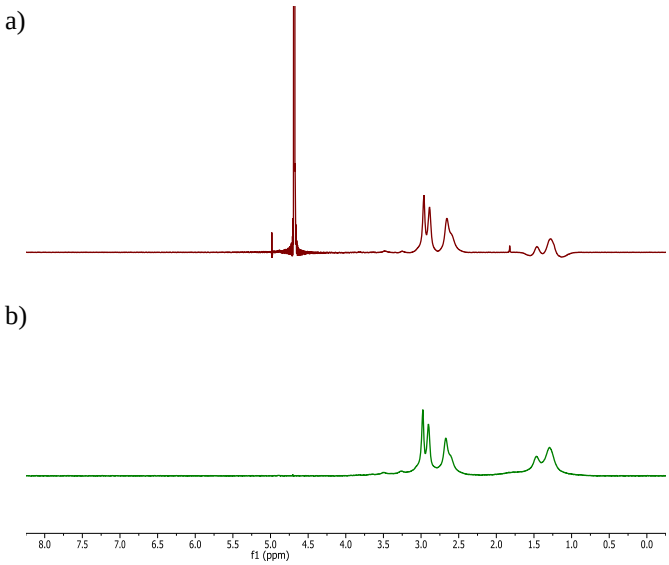

Figure 2.9. ^{1}H-NMR spectra of a solution of Au NP **1** in D_2O. (a) ^{1}H-NMR without the diffusion filter, (b) ^{1}H-NMR with the diffusion filter.

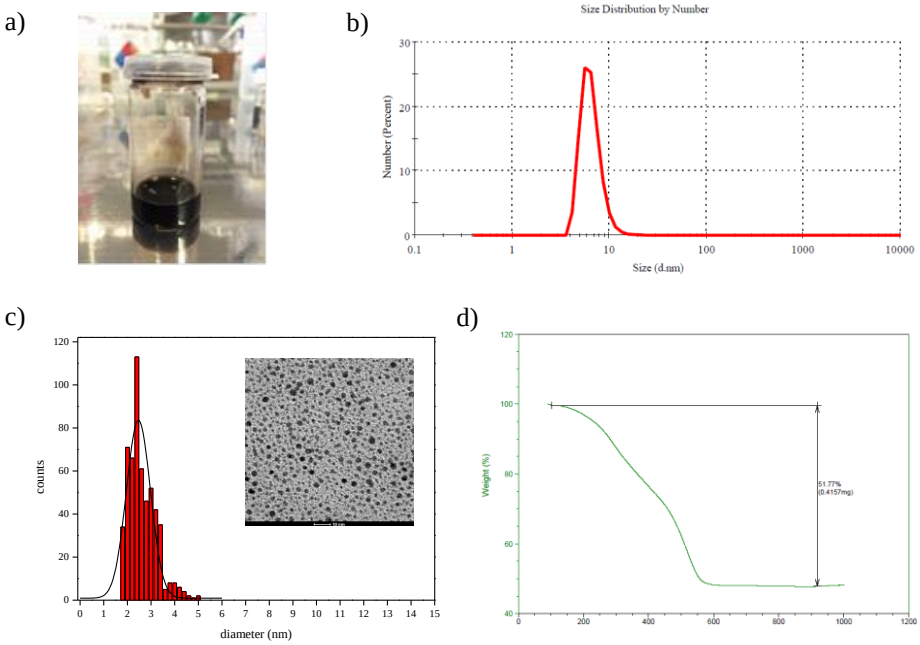

Figure 2.10. (a) picture of a batch of Au NP **1**. (b) DLS analysis. (c) TEM image (scale bar = 10 nm) together with the corresponding ImageJ elaboration. (d) TGA analysis.

The absence of the surface plasmon resonance band at 520 nm in the UV/Vis spectrum (Figure 2.11) gives additional proof for the presence of sub 3 nm sized Au NPs.

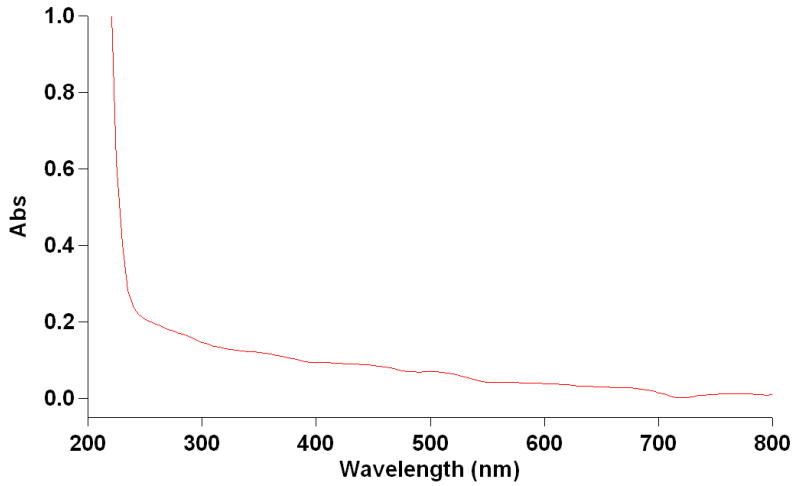

Figure 2.11. UV-Vis absorption spectrum of Au NP **1**, [TACN]=10µM, [HEPES]=10mM pH 7.

2.6.4 Determination of the stock solution concentrations

Zn^{2+} titration:

The concentration of TACN-headgroups was determined by kinetic titration using $Zn(NO_3)_2$ as reported previously[69].

Au NP titration:

In order to have a quick estimation of the head group concentration, a titration of the mother solution of Au NP **1** was performed in the presence of 2 µM of 2-aminopurine riboside-5'-O-triphosphate (ATP_F). An increasing amount of the stock solution was added to a solution of [ATP_F] = 2 µM, [$Zn(NO_3)_2$] = 10 µM in HEPES (10 mM, pH = 8). Upon the addition of a volume of stock solution leading to a 10 µM concentration of headgroups in the cuvette, the fluorescence is totally quenched (Figure 2.12).

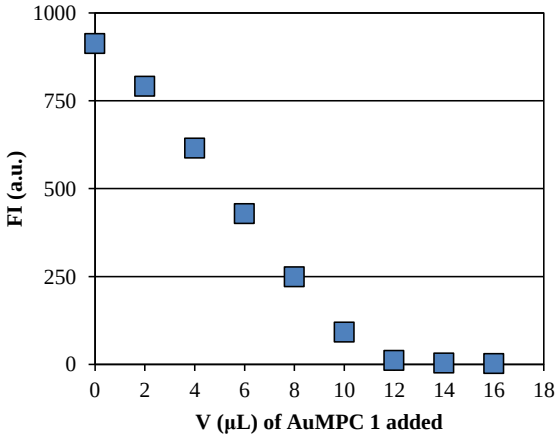

Figure 2.12. Au NP 1 titration in the presence of ATP_F

In this example, after the addition of 12 µL of the Au NP solution the fluorescence was quenched. As the saturation concentration of ATP_F at this pH is around 2 µM for 10 µM of TACN that means that C = $(3x10^{-3}x10x10^{-6})/(12x10^{-6})$ = 2.5 mM. Usually this approach leads to the obtainment of a value slightly lower than the one obtained by the zinc titration (20% lower)[59].

Surface saturation concentrations:

The fluorescence titrations were performed by adding consecutive amounts of a stocksolution of fluorescent probe in mQ water to a 3-mL aqueous solution (pH 7.0, HEPES = 10 mM) containing the [Au NP **1]** = 10 µM in terms of headgroups at 25°C. Then the fluorescence intensity is plotted in function of the concentration of probe (Figure 2.13).

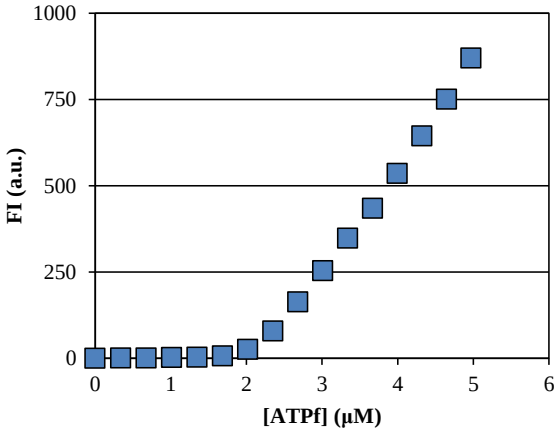

Figure 2.13. ATP_F titration.

In order to determine quickly the optimal parameters to use (mostly the slits parameters) the fluorescence emission spectra of a solution of fluorescent probe (C= 2-3 µM) was recorded by measuring the FI gradually opening the slits.

In order to avoid any kinetic problems, the first fluorescence titration with a new probe were always performed by following the evolution of the FI after each addition of probe. (around 5 minutes between each adds).

The slope of the linear part of the SSC curve allows an estimation of FI in function of the concentration of the free probe in solution in presence of the Au NP. This value can be used in order to verify the maximum of FI that should be expected for a full displacement of the probe from the surface in a displacement experiment with a competior.

2.6.5 Displacement experiments

The displacement experiments were performed by adding consecutive amounts of a stocksolution of ADP in mQ water to a 3-mL aqueous solution (pH 7.0, HEPES = 10 mM) containing the Au NPs coated with the fluorescent probe at 80-90% of the saturation concentration at 25°C.

At the end of the displacement it was verified that the maximum value was close to the value obtained by the extrapolation of the linear part of the titration curve (see above). Then this value was used to normalize the FI and to plot the percentage of probe displaced in function of the concentration of competitor added. To ensure that a stable signal was obtained the displacement studies were performed by measuring the fluorescence intensity in time after each addition until a constant value was obtained.

2.6.6 Synthesis and purification of the peptides

The synthesis of the fluorescent analogues (LWC, LWS(p), LWH, LWD) was carried out by Fmoc-strategy SPPS (Solid Phase Peptide Synthesis) using Wang resin (f=1.1 mmol/g) for (LWC, LWS(p), LWH) and Fmoc-Asp(tBu)-OH Wang resin (f=0.8 mmol/g) for (LWD). The swelling was done using DCM and DMF (30 min each). The active sites of the resin were capped using Ac_2O/pyr 1:1 (2 x 15 min). As usual, 20% piperidine in DMF (2 x 10 min) was used to the Fmoc deprotection.

The coupling step was performed using 3 eq Fmoc-aa-OH, 3 eq HOBt and 3 eq DIPCDI. Finally, for the cleavage of the peptide from the resin was used an acidic mixture (TFA/H_2O/TIS, 95:2.5:2.5) which after filtering was removed by evaporation. Cold ether (x 4) was added for the precipitation and washing of the peptide.

Peptide	**Resine (mg)**	**mg peptide theoretical (mg)**	**mg peptide obtained (mg)**	**Yield (%)**
LWC (**10**)	397.6	202.1	104.8	52
LWS(p) (**9**)	495.5	286.8	99.6	35
LWH (**12**)	441.9	241.8	103.2	43
LWD (**11**)	226.6	86.0	51.6	60

The purification of the peptides was performed by RP-HPLC using A: H_2O + TFA 0.1% and B: ACN + TFA 0.1% as eluents and a C18 Jupiter 4 u Proteo 90A, 250 x 21,1 mm reverse phase column. After the purification the peptides were lyophilized.

Peptide	**Gradient**	**RT (min)**	**Purity (%)**	**MALDI-TOF (m/z)**	**MALDI-TOF calc. (m/z)**
LWC (**10**)	45%-60% B in 30 min	15.1	≥ 99	$[M+H]^+$ = 463.5	$[M+H]^+$ = 462.2
LWS(p) (**9**)	20%-35% B in 30 min	6.4	≥ 97	$[M+H]^+$ = 527	$[M+H]^+$ = 526.2
LWH (**12**)	30%-60% B in 30 min	4.9	≥ 99	$[M+H]^+$ = 497.5	$[M+H]^+$ = 496.2
LWD (**11**)	45%-60% B in 30 min	9.2	≥ 98	$[M+H]^+$ = 475.5	$[M+H]^+$ = 474.2

The synthesis of the fluorescent analogues (**P1**, **P2**, **P3**, **P4**, **P5**, **P6**, **P7**) was carried out by Fmoc-strategy SPPS (Solid Phase Peptide Synthesis) using 2-Chlorotrytil resin (CTC resin) (f=1.6 mmol/g). The swelling was done using DCM and DMF (30 min each). The active sites of the resin were capped using DCM/MeOH/DIEA 17:2:1 (3 x 10 min). As usual, 20% piperidine in DMF (2 x 10 min) was used to the Fmoc deprotection. The coupling step was performed using 5 eq Fmoc-aa-OH, 5 eq HOBt and 5 eq DIPCDI. Finally, for the cleavage of the

peptide from the resin was used an acidic mixture (TFA/H_2O/TIS, 95:2.5:2.5) which after filtering was removed by evaporation. Cold ether (x 4) was added for the precipitation and washing of the peptide.

Peptide	**Resine (mg)**	**mg peptide theoretical (mg)**	**mg peptide obtained (mg)**	**Yield (%)**
P1	216.1	241.8	20.9	8.6
P2	160.5	196.0	4.8	2.4
P3	149.8	166.7	2	1.3
P4	157.6	182.9	36.4	19.9
P5	148.7	165.9	33.3	20.1
P6	150.1	154.5	2.8	1.8
P7	163.5	204.4	53.9	26.4

The purification of the peptide library was performed by RP-HPLC using A: H_2O + TFA 0.1% and B: ACN + TFA 0.1% as eluents and a C18 Jupiter 4 u Proteo 90A, 250 x 21,1 mm reverse phase column. After the purification the peptides were lyophilized. They were characterized by UHPLC and MALDI-TOF.

Peptide	**Gradient**	**RT (min)**	**Purity (%)**	**MALDI-TOF (m/z)**	**MALDI-TOF calc. (m/z)**
P1	20%-35% B in 30 min	4.1	≥ 99	$[M+H]^+$ = 699.3	$[M+H]^+$ = 700.2
P2	40%-55% B in 30 min	8.2	≥ 98	$[M+H]^+$ = 763.4	$[M+H]^+$ = 764.3
P3	20%-80% B in 30 min	16.3	≥ 99	$[M+H]^+$ = 695.4	$[M+H]^+$ = 696.3
P4	20%-35% B in 30 min	3.8	≥ 97	$[M+H]^+$ = 725.4	$[M+H]^+$ = 726.3
P5	20%-35% B in 30 min	3.8	≥ 97	$[M+H]^+$ = 697.3	$[M+H]^+$ = 698.2
P6	20%-60% B in 30 min	4.2	≥ 99	$[M+H]^+$ = 643.2	$[M+H]^+$ = 644.2
P7	20%-35% B in 30 min	10.1	≥ 99	$[M+H]^+$ = 781.4	$[M+H]^+$ = 782.3

2.6.7 Miscellaneous

WDDD binding:

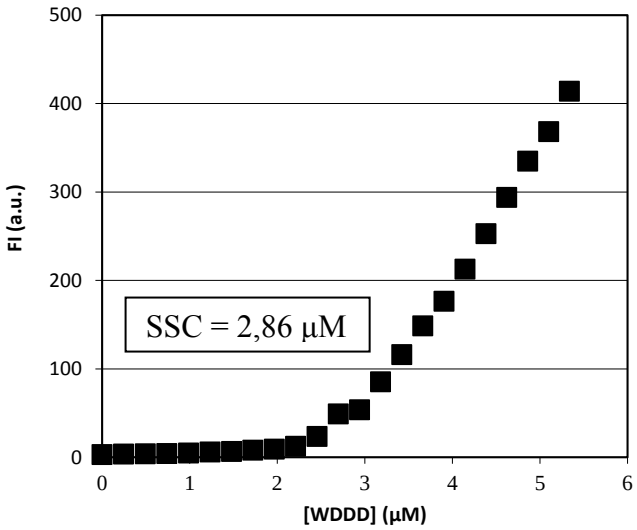

Figure 2.14. Binding assay of WDDD. Conditions: [TACN-Zn^{2+}] = 10 µM, [HEPES] = 10 mM, pH = 7, T = 25 °C.

Binding assay of **10** with different metals in the monolayer:

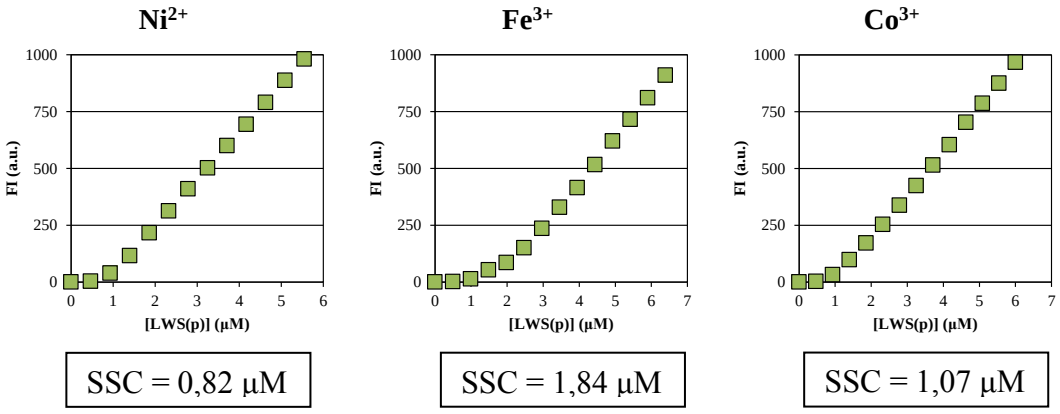

Figure 2.15. Binding assay of **10**. Conditions: [TACN-M^{n+}] = 10 µM, [HEPES] = 10 mM, pH = 7, T = 25 °C.

CHAPTER 3: Self-selection of peptides on Au NPs

3.1 Introduction

The discovery of biologically active substance requires finding molecules that interact selectively with certain biological targets[70]. Combinatorial chemistry (CC) in the past, and, most recently, dynamic combinatorial chemistry (DCC) approaches have been used to simplify the discovery of such substances. In DCC[71], a dynamic combinatorial library (DCL) of oligomers is generated from a set of building blocks through reversible interactions, which can either be covalent or noncovalent[72]. Consequently, the composition of a DCL is determined by the relative thermodynamic stabilities of its components.

A key feature of a DCL is that it can respond to external influences. That is, changes (pH, light, addition of a target molecule, etc.) will change the energy landscape and the DCL will adapt in order to maximize the concentration of the species that is more stable under the new conditions. This has also been referred to as 'amplification of the fittest' in analogy to Darwinian evolution. As illustrative example, a recent system by Giuseppone and Lehn will be discussed, in which the response of a dynamic system based on imines to a physical stimulus (temperature) and a chemical effector (H^+) was studied[73]. A set of imines **A**-**D** was generated from a stoichiometric mixture of 1-naphtylamine (**1)**, 2-aminoanthracene (**2**), 9-anthracene carboxaldehyde (**3**), and 1-azulenecarboxaldehyde (**4**) (Figure 3.1a) that were chosen because the absorption spectra of the imines permitted a straightforward monitoring of changes in the library. A 3D diagram was used to illustrate the complex behavior of the system. Here, multiple expression domains were identified as a function of the two parameters: acidity and temperature (Figure 3.1b). Three domains, one at 308 K and two at 358 K, of high conversion presented noticeably different expressions. **C** and **A** preponderated at low $[H^+]$/high *T*. Instead, on the central ridge, **B** and then **A** were in majority as *T* increases. Lastly, **A** and then **D** predominated over the whole *T* range at moderate and high $[H^+]$ respectively. With these results they showed the versatility of the system upon physical and chemical stimulus. However, the high

complexity of the system did not permit the quantitative explanation of the structures and the mechanism.

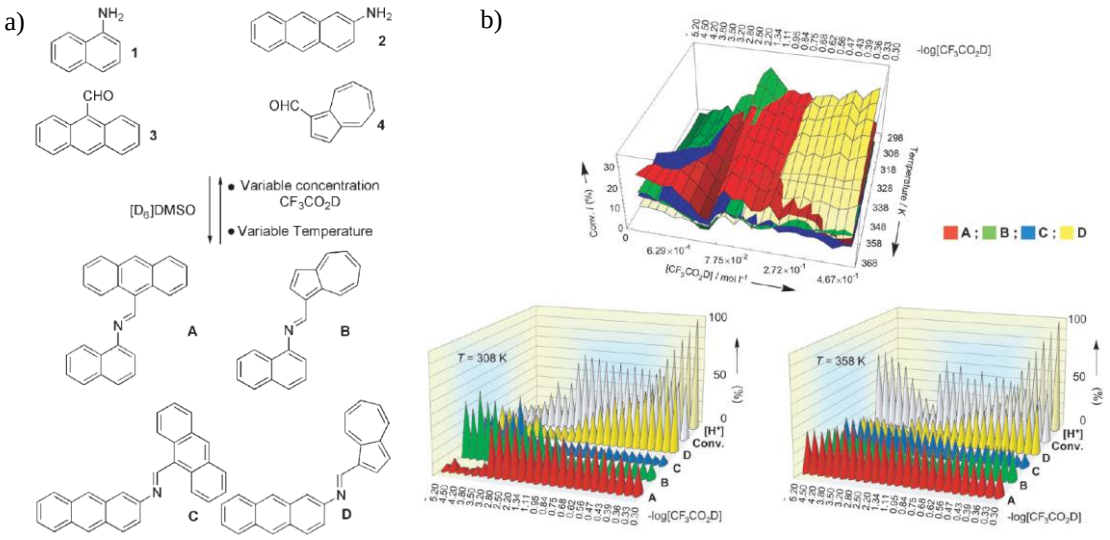

Figure 3.1. (a) Dynamic library of the four components **1**–**4** and the four constituents **A**–**D**. (b) Top: Hypersurface for the expression of the four constituents **A**–**D** as a function of temperature and acid concentration. Bottom: Distributions of imines **A**–**D** at two temperatures as a function of acidity [H^+].

DCC has been extensively used to develop systems for many applications such as synthetic receptors[74,75], catalysts[76,77], ligands for biomolecules[78] and sensory systems[79]. However, apart from some exceptions, a typical limitation of these systems is the small library size and the rather low structural complexity of the library members. A main challenge is still the development of complex functional systems able to interact with biological targets in aqueous media. Thus, structurally biocompatible systems are demanded. As we have seen in Chapter 1 monolayer protected gold nanoparticles can accomplish these requirements. Indeed, very recently the first applications of DCC in combination with Au NPs have appeared.

Kay's group has demonstrated how to procure reversible control over the nanoparticle functionalization by dynamic covalent exchange in the monolayer[80]. They synthesized a series of gold nanoparticles bearing a homogeneous monolayer of *N*-aroylhydrazones (Figure 3.3a). It is known that hydrazones undergo covalent exchange reactions in the presence of acid or nucleophilic catalysts[81,82,83] making them attractive to develop dynamic covalent systems. Due to the low resolution of the ^{1}H-NMR spectra of Au NPs, Kay and coworkers incorporated fluorine labels (red

and blue) to exploit the significant shift dispersion and excellent sensitivity of ^{19}F-NMR spectroscopy for studying the composition of the hydrazone monolayer (Figure 3.3b). Using ^{19}F-NMR spectroscopy it was possible to follow hydrazone exchange between AuNP-**1** and **5** hydrazine by adding increasing amounts of **5** hydrazine in real time and the effects of surface confinement on reactivity as well as the reversibility of the dynamic covalent exchange process by adding again the **6** hydrazone to AuNP-**2**.

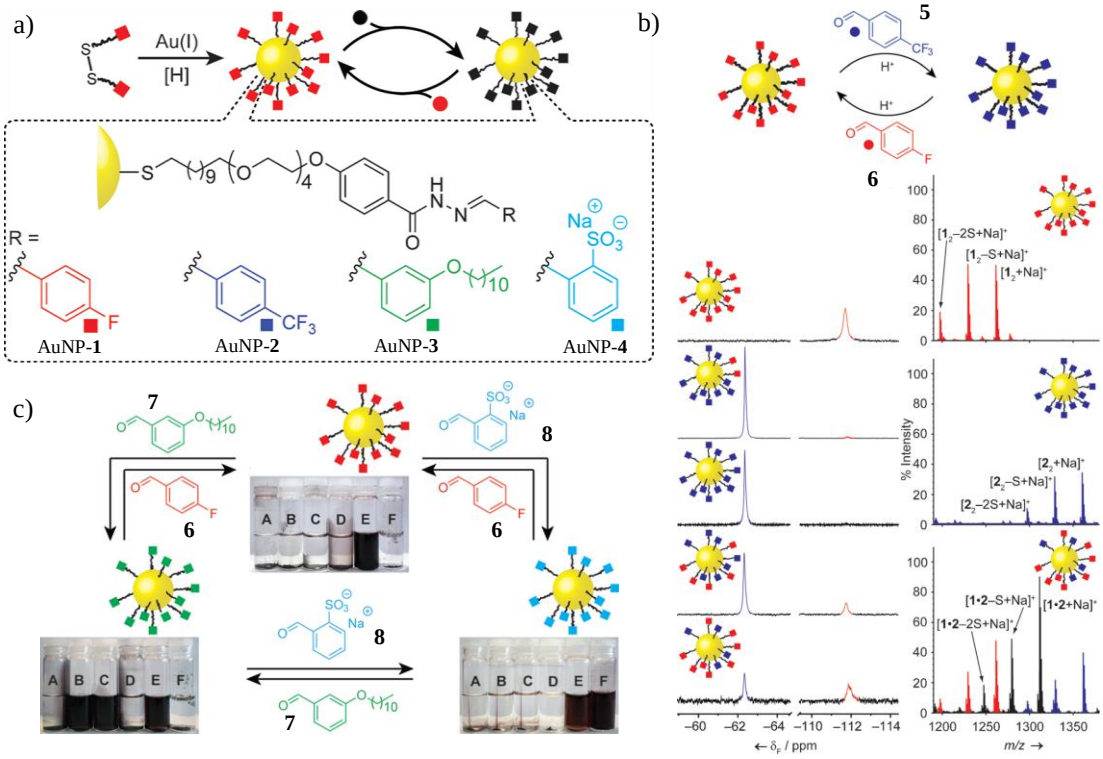

Figure 3.3. (a) Preparation and reversible surface modification of a dynamic covalent NP building block. (b) Hydrazone exchange by ^{19}F-NMR and Partial LDI-MS spectra. (c) Reversible switching of Au NP solvophilicity properties by hydrazone exchange.

Then, they went further by demonstrating the potential of the dynamic covalent exchange. They introduced different aldehyde exchange units with different solubility characteristics (Figure 3.3c). Different solvents were used to test the dynamic exchange against the solubility of the different units (**A** = hexane, **B** =chloroform, **C** = tetrahydrofuran (THF), **D** = methanol, **E** = DMF and **F** = water). The experiment showed that after exchange between AuNP-**1** and **8** (soluble only in DMF) to AuNP-**4** the solubility in water increases maintaining that in DMF. A further exchange from AuNP-**4** to AuNP-**3** led to a more apolar environment (soluble

in chloroform and THF). These results showed an easily manner to change the solubility of the Au NP just by covalent exchange between aldehydes-headgroups with different solvophilic characteristics.

A second example of DCC on nanoparticles was reported by Otto *et al*[84]. They designed gold nanoparticles that were water soluble (**L1** ligand) and contain aldehyde groups (**L2** ligand) (Figure 3.4b) for the reversible formation of imines by DNA templating (Figure 3.4a). In an aqueous environment, the equilibrium for imine formation was strongly disfavored and imines are not formed if aldehydes and amines were present in (sub)millimolar concentrations. This was an advantageous property because this way imine formation in the absence of template (DNA) was avoided.

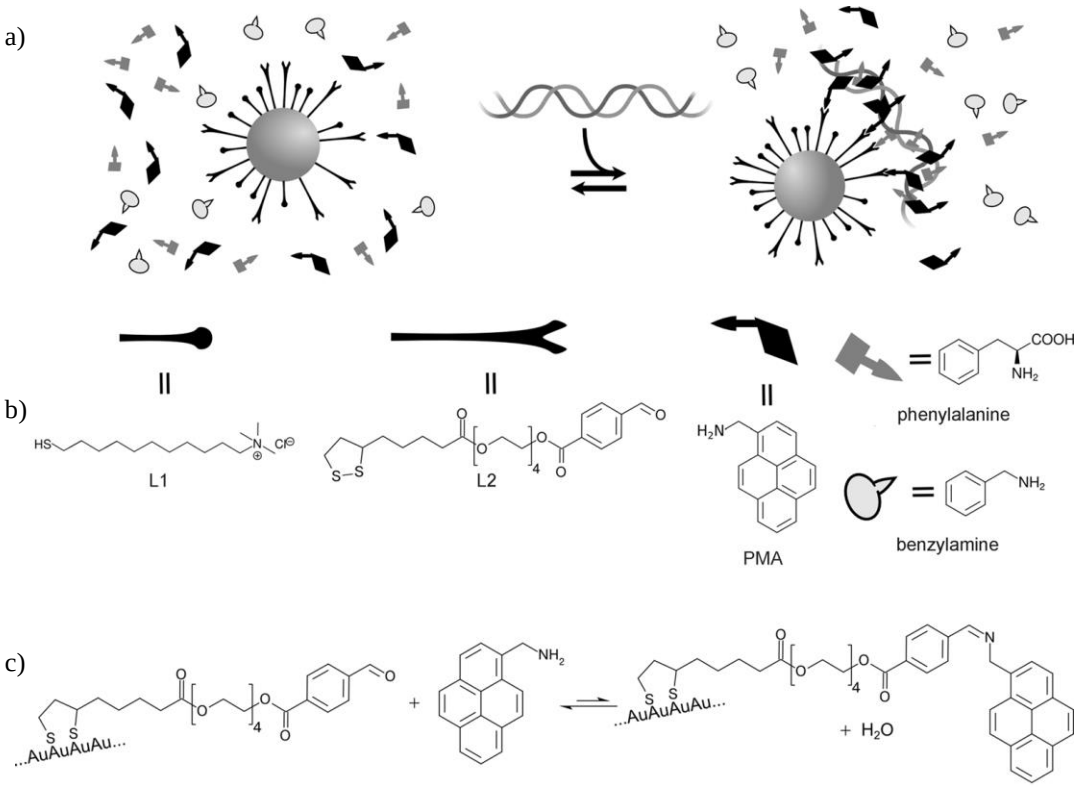

Figure 3.4. (a) A DNA template directs the surface functionalization of the nanoparticles, which leads to the formation of a complementary receptor. (b) Ligands used to stabilize the nanoparticles and recognition units. (c) Reaction between **L2** and PMA under thermodynamic control.

Simple libraries composed of pyrenemethylamine (PMA), Au NPs and 16-meric double-and stranded DNA $(CG)_8$ were prepared. PMA is known to be a good DNA intercalator and, in addition, has an amine group for imine-formation (Figure

3.4c). To analyze the library they performed a procedure based on centrifugal filtrations equipped with a membrane that is only permeable to small molecules and not to nanoparticles or DNA(Figure 3.5a). Analysis of the filtrate by HPLC was used to quantifiy the unbound amines which then yielded information on the amines captured on the nanoparticles.

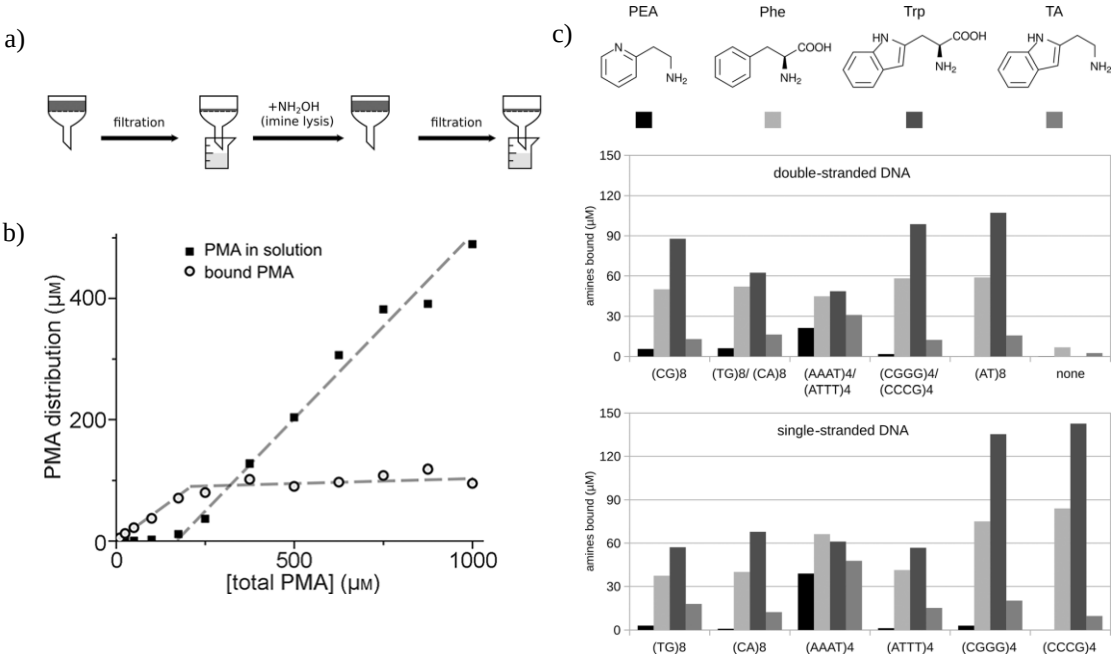

Figure 3.5. (a) Analysis of the dynamic combinatorial libraries. (b) Analysis of DCLs with different total PMA concentrations. (c) Influence of the DNA sequence on the functionalization of nanoparticles with different amines.

They investigated the degree of surface functionalization for a series of libraries with different PMA or DNA concentrations. At low PMA concentrations, all the amines were attached to the nanoparticles. Upon increasing the concentration, the excess of amine could no longer be attached to the nanoparticles and so, the concentration of NP-bound PMA reached a plateau (Figure 3.5b). A lack of Au NP functionalization in the absence of the template was consistent with imine bonds being too labile to be formed without external stabilization provided by the multivalent template. Furthermore, they investigated whether DNA binders could be selectively incorporated on the nanoparticles surface from a mixture of amines (Figure 3.4b). An experiment in the presence of all three amines led to the selective uptake of PMA, while also some l-phenylalanine was bound but not benzylamine.

Encouraged by these results it was investigated to what extent the DNA sequence affects surface functionalization. Au NP libraries with several non-intercalating amines and templated them with double- and single-stranded hexadecameric DNAs with different sequences (Figure 3.5c). The single-stranded C/G-rich templates promoted amine incorporation most efficiently. Most DNA sequences showed a pronounced preference for Trp, followed by Phe, while PEA and TA were in most cases incorporated less efficiently. This way, Otto and coworkers presented a method to locally functionalize gold nanoparticles using dynamic combinatorial chemistry and DNA template. Moreover, the system presented selectivity among a pool of compounds in the presence of DNA.

Also in early 2015, Prins *et al.* reported a dynamic system composed of Au NPs and a mixture of four nucleotides[85]. This work was based on a previous paper[86] in which Au NP **1** (see Chapter 1) was used for the development of a sensing system able to detect Hg^{2+}. As discussed in section 1.4 the surface of Au NP **1** can accommodate negatively charged probes at low micromolar concentrations. Also, it was shown that the number of negative charges present in the probes strongly affects the affinity for Au NP **1**. Pioneering work of Ono and Togashi demonstrated that Hg^{2+} highly selectively binds to the DNA nucleobase thymine (T), forming a $T{\cdot}Hg^{2+}{\cdot}T$ sandwich complex[87]. Thus, in the NP system Hg^{2+} induced the dimerization of TDP (monophosphate nucleotide) leading to the formation of a ternary $TDP{\cdot}Hg^{2+}{\cdot}TDP$ complex which has a much higher affinity for Au NP **1** than TDP alone. Consequently, the ternary complex displaced (quenched) fluorescent probe **A** from the surface of Au NP **1** resulting in a turn-ON of the fluorescence.

In this way, the Prins' group studied the selectivity of $TDP{\cdot}Hg^{2+}{\cdot}TDP$ complex in the presence of other monophosphate nucleotides (dAMP, dCMP, dGMP) (Figure 3.6a). As demonstrated in the previous paper[86] Au NP **1** and molecules that are non-covalently bound to the monolayer do not permeate PES-membranes with a 10 kDa MW cut-off upon centrifugation (12000 rpm), whereas unbound molecules do. Thus, a fixed concentration of Au NP **1**, probe **A**, nucleotides were mixed together. Then, analysis of the dialysate by LC/MS (in SIM detection mode) were carried out in the presence and in the absence of Hg^{2+} in order to analyze the concentration of the four nucleotides (Figure 3.6b). The addition of Hg^{2+} caused

a significant decrease of only the TMP concentration (25%), indicating that the presence of Hg^{2+} resulted in the near exclusive capture of TMP (4.3 μM) on the surface of Au NP **1** (Figure 3.6c). The addition of a new metal to the mixture (Ag^{+}) was evaluated. Ag^{+} forms ternary complex with cytosine ($C{\cdot}Ag^{2+}{\cdot}C$)[88]. The selectively experiments revealed, unexpectedly, the formation of a ternary complex with dGMP (Figure 3.6d).

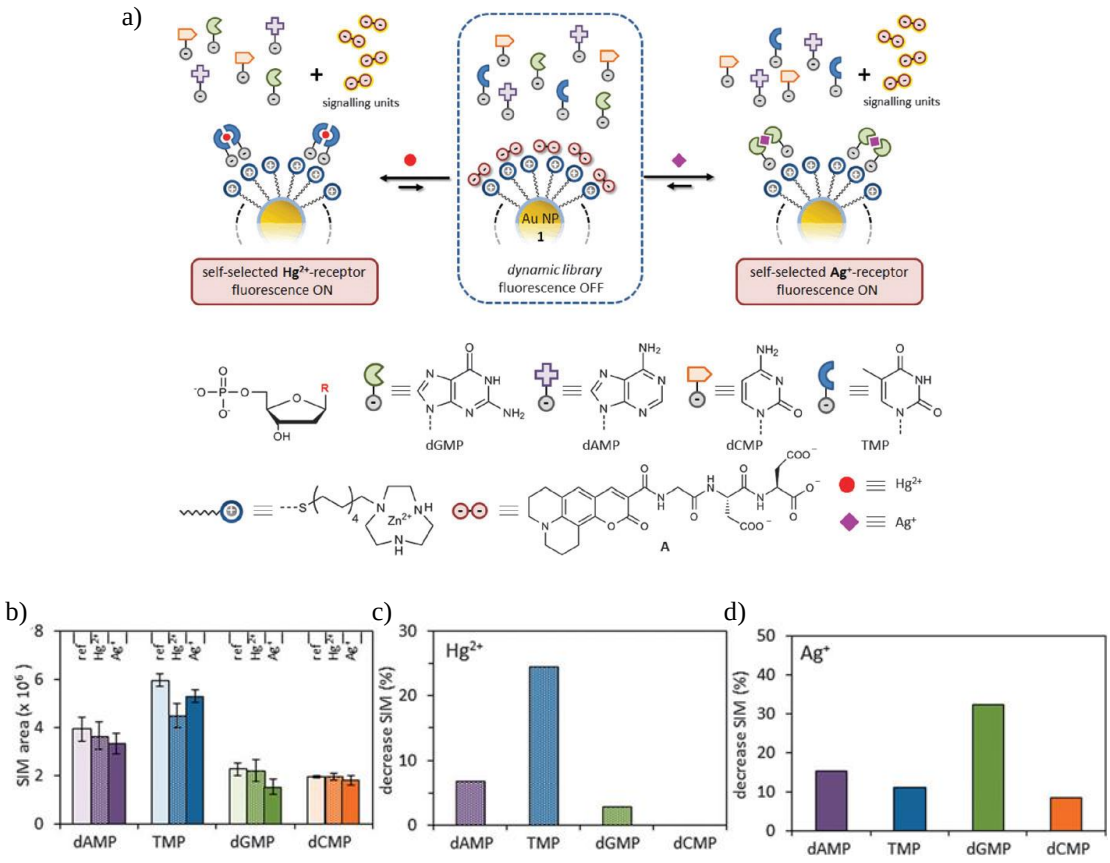

Figure 3.6. (a) Schematic representation of the self-selection. (b) SIM areas of the deoxynucleotides in the dialysate before and after the addition of Hg^{2+}/Ag^{2+}. Relative decrease (%) of the SIM area of each deoxynucleotide before and after addition of (c) Hg^{2+} (d) Ag^{2+}.

Fluorescence studies to confirm the results of self-selection experiments were done by titrating Ag^{+} to a solution containing Au NP **1**, probe **A** and either one of the nucleotides dGMP, dAMP, dCMP, and TMP (Figure 3.7). It gave a strong increase in signal intensity only when dGMP was present, a result in line with the self-selection experiments.

With this work it was demonstrated how to apply dynamic combinatorial chemistry on Au NPs by using non-covalent interactions, in this case, for the identification of the best recognition unit for Hg^{2+} and Ag^{+}. The ability to apply

dynamic combinatorial chemistry on a nanoparticle offers an enormous potential for the development of multivalent receptor systems of high complexity.

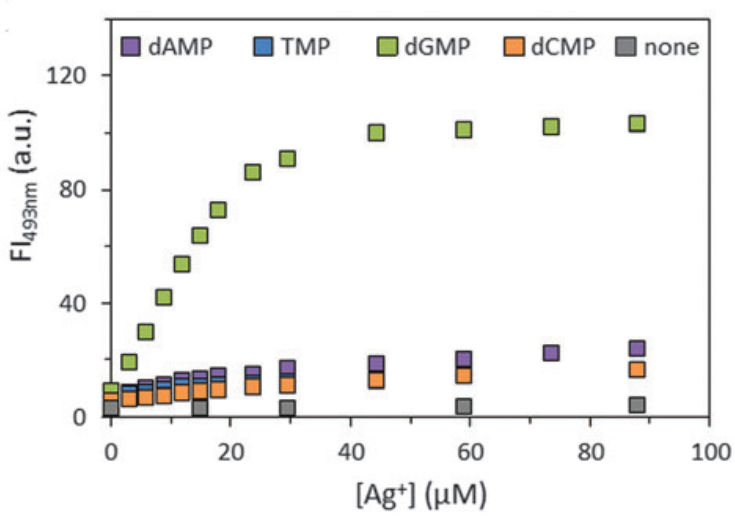

Figure 3.7. Fluorescence intensity (a.u.) at 493 nm (caused by the displacement of probe **A**) as a function of the concentration of Ag^+ added.

Based on these results, we were challenged by applying this concept on a more complex system, exploiting the self-assembled peptide-nanoparticle structures developed in the previous chapter.

3.2 Methodology for studying the surface composition

The fluorescence titration experiments described in Chapter 2 provided evidence for the formation of a dynamic peptide surface on Au NP **1.** However, fluorescence spectroscopy is not able to provide information on the type of peptides that are bound to Au NP **1**. Thus, the first challenge was to determine a methodology that would allow an identification of the type of peptides bound to Au NP **1**.

In order to do so, a new methodology based on the use of membranes with a defined molecular weight (MW) cut-off was developed. Such ultracentrifugal filters are commonly used for concentrating proteins, relying on the fact that large molecules cannot pass through the membrane whereas small ones can. We hypothesized that, in the same way, peptides that are free in solution would be able

to pass through the membrane whereas peptides bound to the monolayer surface of Au NP **1** would be unable to do so. The analysis of the filtrate (containing the unbound peptides) by LC/MS would then provide indications about the surface composition of the peptide-Au NP **1** complex. This methodology required the optimization of some parameters such as type of membrane and MW cut-off, measurement technique, centrifugation procedure and overall conditions.

Hence, the type of membrane and its MW cut-off was optimized first. The peptides had to be able to pass through the membrane without adsorbing on it. Different membranes were tried such as VIVASPIN polyethersulfone (PES), AMICON regenerated cellulose and NANOSEP modified polyethersulfone. Besides, different MW cut-off were also studied (3 kDa, 5 kDa, 10 kDa). The studies consisted of filtering a known peptide mixture composition and, then, analyzing the filtrate by LC/MS. The results were compared to that of non-filtered samples at the same conditions and concentrations. This procedure provided quantitative information on the amount of peptide adsorbed to the membrane. It was found that VIVASPIN PES (10 kDA) showed to be optimal to perform these experiments, since almost 100% of the amount of peptides passed through the membrane (Figure 3.8). NANOSEP filters did not allow peptides to pass through the membrane at all, whereas AMICON filters showed a significant adsorption of **P1** and **P2**.

Also the parameters related to the LC/MS analysis had to be optimized. It was observed that the peaks of the peptides and the buffer (HEPES) (after filtering) were overlapping (Figure 3.8 (VIVASPIN filters) and Figure 3.9) in the chromatogram (λ=280 nm). For that reason it was decided to use selected-ion monitoring mode (SIM mode) to analyze the peptides[89]. Using the SIM mode it was possible to use one channel for each peptide (Figure 3.9c).

Another parameter to take into account was the centrifugation step. Changing the total volume of the solution affects the concentration of the dissolved species which could affect also the equilibrium between bound and free peptides. Thus, the filtrate volume should be as low as possible in order not to change too much the initial conditions, but at the same time, high enough to have as sizeable volume for

injection into the UPLC. It was found that a 15 second centrifugation at 12.000 r.p.m. led to a filtrate volume of around 100 uL.

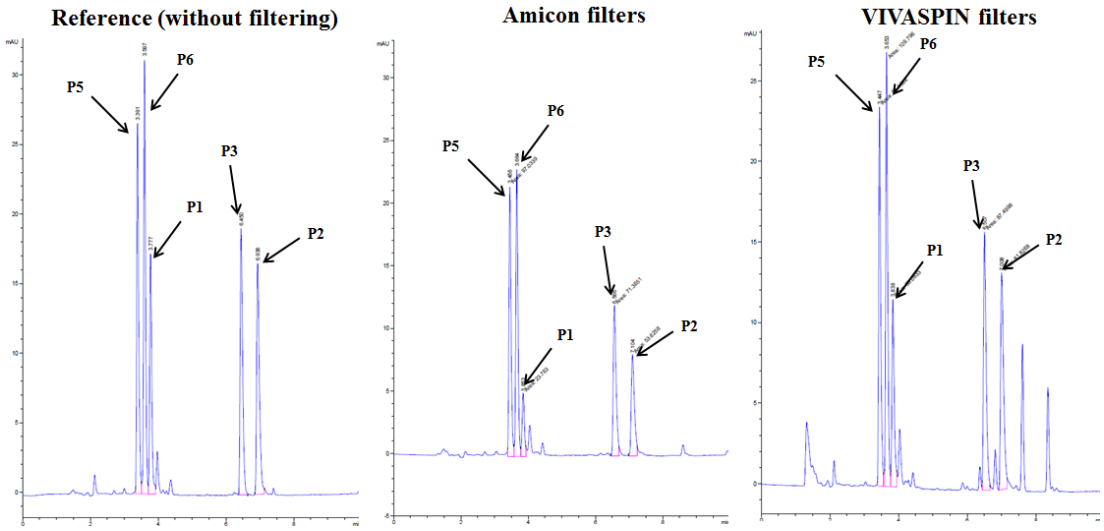

Figure 3.8. Chromatograms of peptide mixture (50 µM) using different filters.

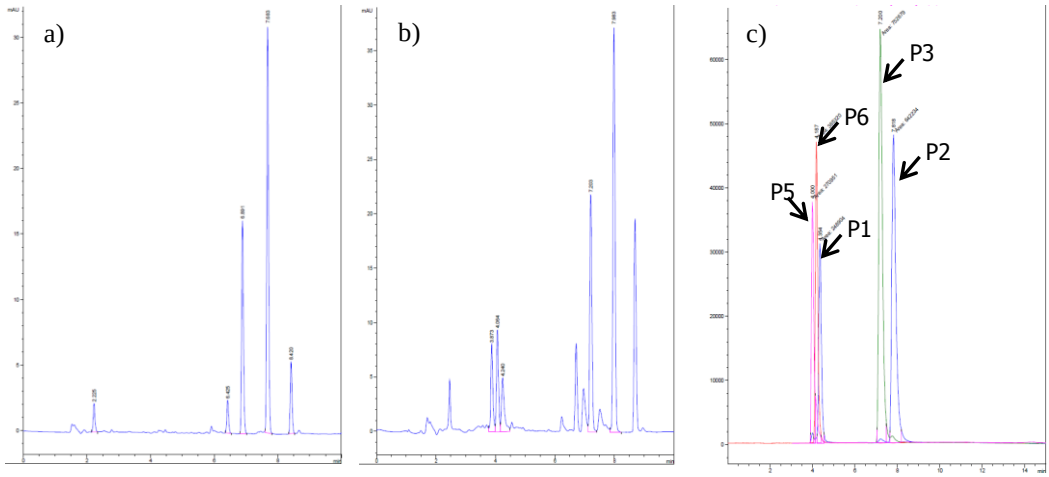

Figure 3.9. Chromatograms after filtering of: (a) 5 mM HEPES pH=7, (b) 10 µM Peptide Mixture, 5 mM HEPES pH=7. Conditions: 10-80 %B in 30 min, 0.208 mL/min; A: H_2O+0.1% HCOOH B: ACN+0.1% HCOOH mesured at 280 nm. (c) SIM mode chromatogram.

This implied a reduction in the original volume ≤ 20% , which was considered acceptable. Finally, the concentrations of Au NP **1**, the peptide mixture and HEPES buffer were altered to meet the sensitivity of the ESI-MS. The quantitative detection of the peptides required higher concentrations compared to those used in the fluorescence measurements. Therefore, the TACN-Zn^{2+}

concentration was raised to 50 µM. The necessity to use 50 µM of TACN required a renewed determination of the SSCs at that concentration (Figure 3.10).

In order to ensure that the higher Au NP **1** concentration did not affect the interaction with the peptides, the fluorescence binding assay was repeated at the new TACN-Zn^{2+}-concentration of 50 µM and [HEPES] = 5 mM (pH = 7, T = 25 °C, λ_{ex}=280 nm, λ_{em}=360 nm) by adding increasing amounts of the peptide mixture and measurement of the fluorescence intensity (Figure 3.10a). In addition, a displacement experiment was also performed by measuring the fluorescent intensity (λ_{ex}=280 nm, λ_{em}=360 nm) after addition of increasing amounts of ATP as a non-fluorescent competitor. The fluorescent intensity was plotted as a function of the concentration of the probes (Figure 3.10b).

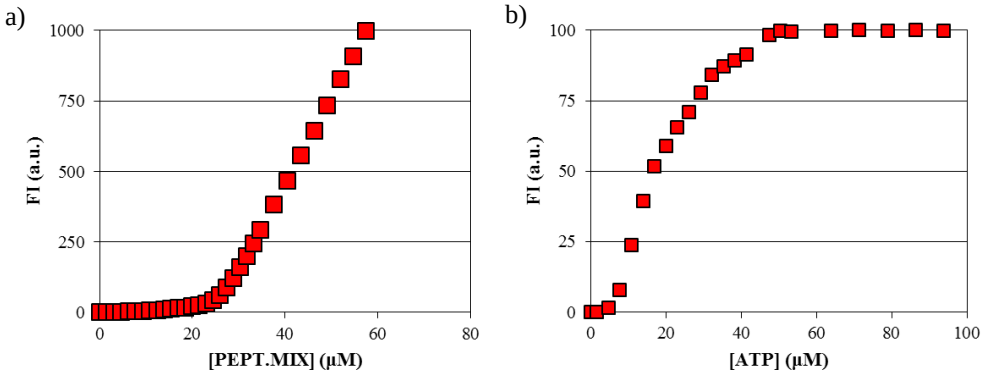

Figure 3.10. (a) Binding assay: fluorescent intensity (a.u.) as a function of Peptide Mixture concentration (µM). (b) Displacement experiment: percentage of peptides displaced (%) as a function of [ATP]. Measured at λ_{ex}=280 nm, λ_{em}=360 nm. Conditions: [TACN-Zn^{2+}] = 50 µM, [Peptide mixture]= 20 µM (80% SSC) and [HEPES] = 5 mM at pH = 7 and T = 25 °C.

The displacement experiment confirmed the binding of the peptides at the new conditions, but, interestingly, the results showed an increase in the SSC to 25.6 µM. This saturation concentration suggested a TACN-Zn^{2+}/peptide mixture ratio of 2:1 which is higher than previously observed when using [TACN-Zn^{2+}] = 10 µM (≈3:1). This indicates a shift of the equilibrium towards the multivalent Au NP **1** peptide complex upon the increase of the concentration of Au NP **1**.

3.3 Self-selection experiments

The scope of these experiments was to demonstrate two important concepts: dynamics and self-selection. With this approach we wanted to study changes in the composition of the peptidic surface and, more importantly, whether some of the peptides would be selected over the others in case an excess of peptides was present.

The experiments consisted of a titration of increasing amounts of a peptide mixture composed of peptides **P1**, **P2**, **P3**, **P5** and **P6** (total peptide concentration is 25, 50, 75, 100 or 125 μM) to a constant concentration of Au NP **1** (50 μM) followed by centrifugation at 1200 r.p.m. during 15 sec. using VIVASPIN 500 10kDa PES-membrane. Subsequently, the filtrates were analyzed by UHPLC/MS in SIM mode (Scheme 3.1).

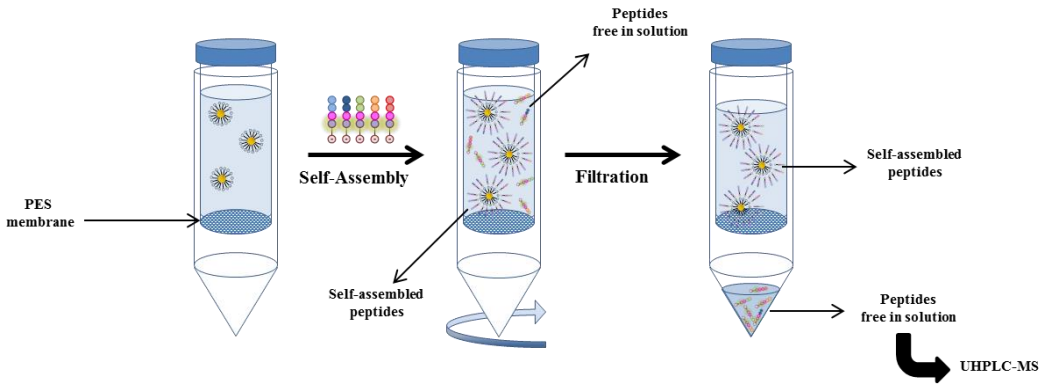

Scheme 3.1. Representation of cut-off membrane filters experiments.

All experiments were performed five times and the average values were reported together with the error margin. Each peptide concentration was quantified by comparing the intensity to the reference peaks obtained from centrifuged examples of identical compositions, but in the absence of Au NP **1**. In Figure 3.11 the percentages of the peak areas are given relative to value of the area of each single peptide filtered in the absence of Au NP **1**. The absence of unbound peptides in sample **I** (25 μM) confirmed that at this concentration all peptides are bound to Au NP **1** (Figure 3.11a). This represents the situation of maximum system complexity (see section 2.4). Upon adding the peptide mixture at concentrations higher than the SSC (50 to 125 uM), *i.e.* samples **II-V**, changes in the surface composition are observed, favoring the self-assembly of peptides P1 and P2. These results clearly

indicated a self-selection of peptides **P1** and **P2** out of the peptide mixture. In this process, the complexity of the self-assembled system is reduced reaching a situation in which only two peptides (**P1** and **P2**) were present on the surface.

It is noted that a perfect quantification of the surface composition was hindered by the adsorption of nanoparticles and peptides on the membrane. This led to a relative large error in particular at lower concentrations of peptides. This prevented a precise determination of the surface composition under this conditions. Nonetheless, it was possible to accurately determine the composition at the highest peptide concentration (125 μM): 70 % of **P1** and 30 % of **P2**.

As expected, these results are consistent with the displacement experiments (Figure 2.7) and indicated that self-selection as driven by the relative affinity of the peptides for Au NP **1** (**P1** > **P2** ≥ **P3** > **P5** > **P6**). **P3**, **P5**, **P6** were detected as soon as the concentration of the peptide mixture was increased confirming their lower affinity for Au NP **1**. These results show that self-selection on the surface of Au NP **1** occurs driven by the non-covalent interactions between the peptides and the Au NP **1** surface.

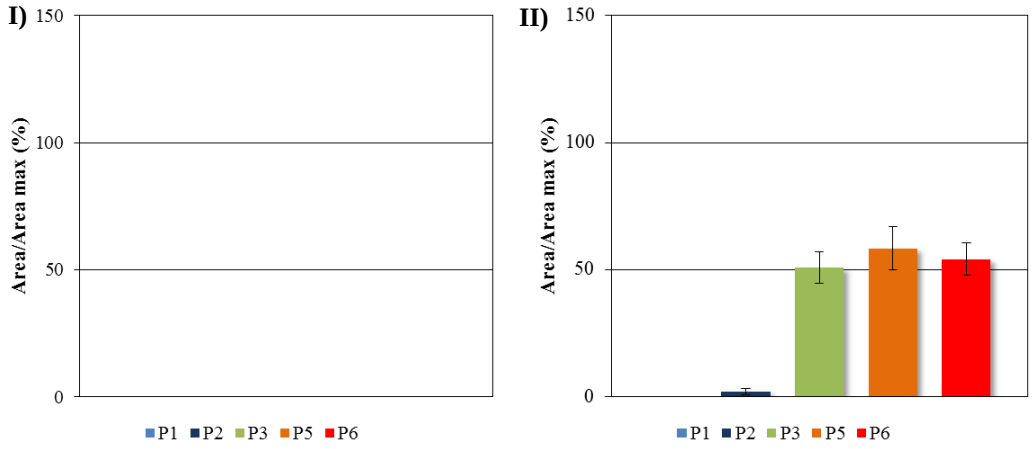

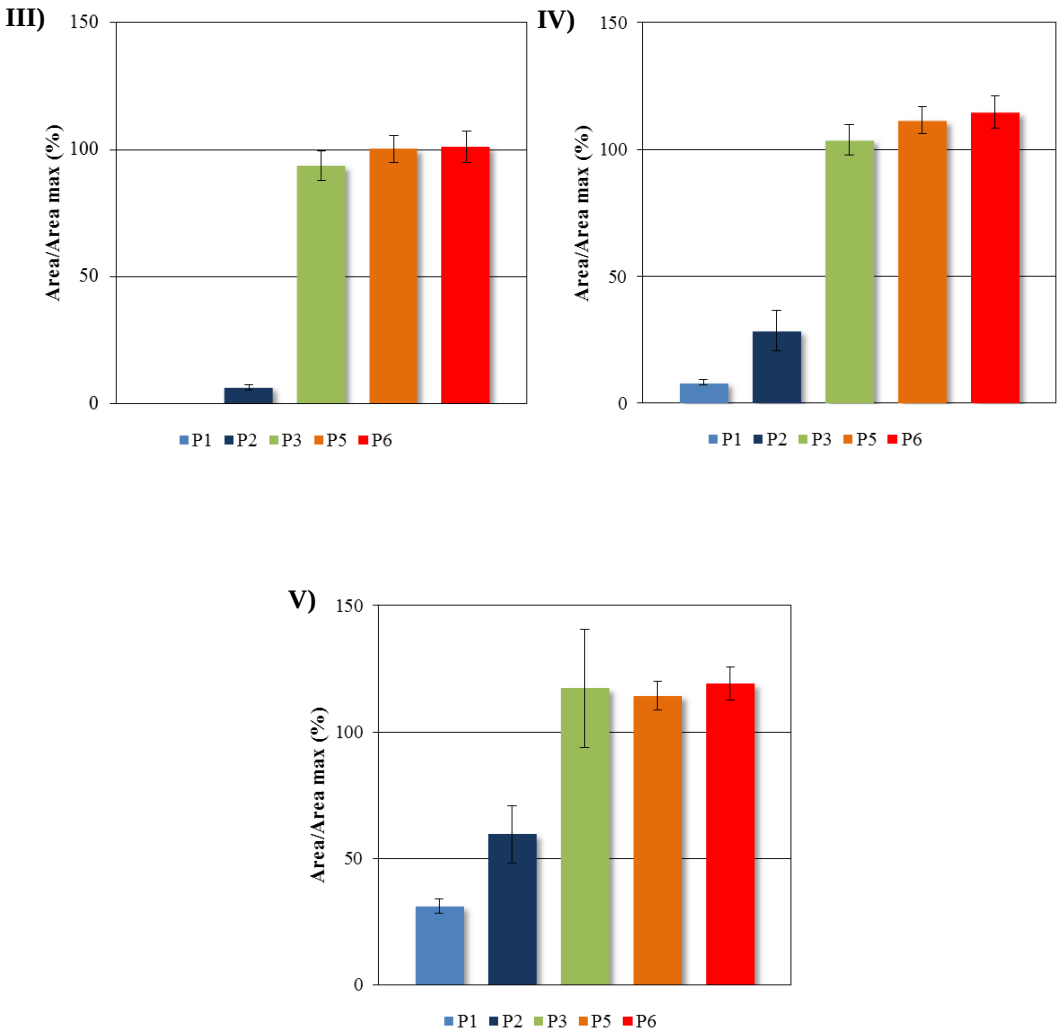

Figure 3.11. Cut-off membrane filter experiments: Conditions: [TACN-Zn(II)]=50 μM, [HEPES]=5 mM, pH=7, (I) 25 μM [Pept.Mix.], (II) 50 μM [Pept.Mix.], (III) 75 μM [Pept.Mix.], (IV) 100 μM [Pept.Mix.], (V) 125 μM [Pept.Mix.]. Determined by mass spectrometry (SIM Mode). (P1, P2, P3, P5, P6).

As a control experiment, the identical experiments were also performed in the presence of an excess of ATP (200 μM) in order to suppress binding of the peptides to Au NP **1**. Fluorescent experiments had demonstrate that 200 μM of ATP were enough to completely displace the peptides from the surface (Figure 3.10b).In Figure 3.12 it is shown that all peptides are free in solution in the presence of ATP, which is consistent with the displacement studies. Again, the large errors originate from the difficult quantification of peptides at low concentrations.

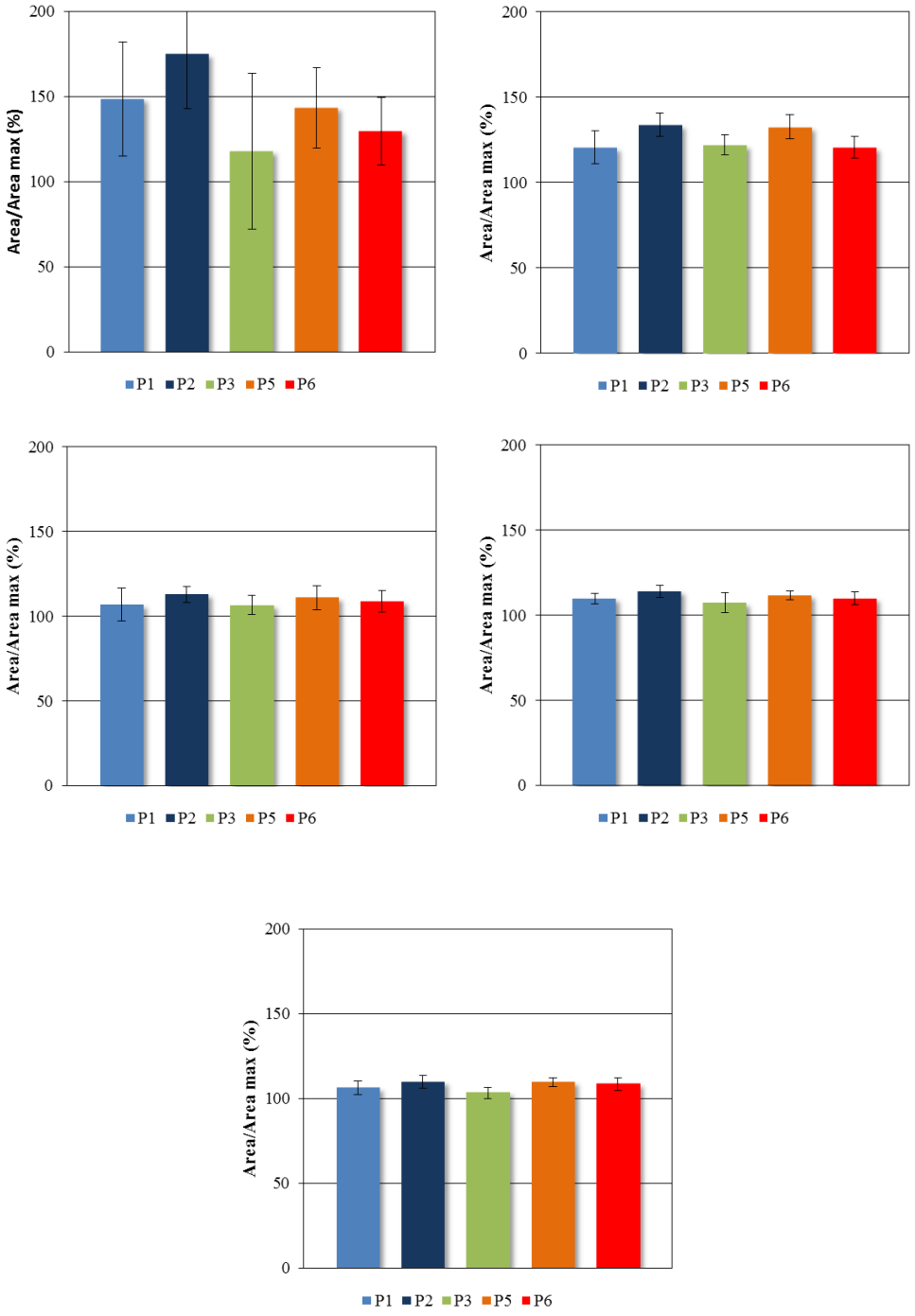

Figure 3.12. Cut-off membrane filter experiments: Conditions: [TACN-Zn(II)]=50 µM, [ATP]=200 µM, [HEPES]=5 mM, pH=7, (I) 25 µM [Pept.Mix.], (II) 50 µM [Pept.Mix.], (III) 75 µM [Pept.Mix.], (IV) 100 µM [Pept.Mix.], (V) 125 µM [Pept.Mix.]. Determined by mass spectrometry (SIM Mode). (P1, P2, P3, P5, P6).

3.4 Conclusions

The dynamic nature of the system has been exploited in a series of self-selection experiments, aimed at determining how the surface composition on Au NP **1** would change when an excess of peptides would be present. A new protocol relying on the use of ultracentrifugation filters containing a MW cut-off membrane has been developed for the purpose of analyzing the surface composition. The results have shown a spontaneous self-selection of the peptides with a higher affinity for Au NP **1** upon increasing the overall concentration of the peptide library.

3.5 Experimental section

3.5.1 Instrumetation

UHPLC-MS

For the analysis of the filtrate in the ultracentrifugation experiments an Agilent Technologies 1290 Infinity LC equipped with a quadrupole MS was used.

Ultracentrifugation

For the centrifugation of the samples an Eppendorf MiniSpin centrifuge was used.

3.5.2 Materials

VIVASPIN 500 ultracentrifugation filters (Sigma Aldrich, Z614025) equipped with a PES (polyethersulfone) membrane with a 10 kDa of cut-off were used. They have a 500 μL capacity.

3.5.3 Ultracentrifugation experiments

The ultracentrifugation experiments were performed by preparing five different samples containing different peptide mixture (equimolar **P1**, **P2**, **P3**, **P5** and **P6)** concentrations (25 µM, 50 µM, 75 µM, 100 µM and 125 µM) and Au NP **1** [TACN-Zn(II)] = 50 µM in [HEPES] = 5 mM at pH = 7 and 25 ^{o}C reaching a final volume of 500 µL. Next, the solution were equilibrated for 15 min before centrifugation was started with a duration of 15 sec and 12.000 r.p.m.. The total volume was reduced by around 20 %.

A 20 µl (using glass insertor, Sigma Aldrich code: 24707) sample was injected in the UPLC equipped with a Zorbax Eclipse Plus C18 column with a length of 150 mm and an internal diameter of 2.1 mm and 1.8-mm fused silica particles at a flow rate of 0.2 mL/min. A solvent gradient from 10% (v/v) ACN+0.1% HCOOH in H_2O+0.1% HCOOH to 80% (v/v) ACN+0.1% HCOOH in H_2O+0.1% HCOOH (10 min) was used. This concentration was kept constant for 12 min after which a gradient to 10% (v/v) ACN+0.1% HCOOH in H_2O+0.1% HCOOH was imposed (15 min). The column temperature was set at 40 ^{o}C. The peptides were monitored using SIM mode (selected-ion monitoring mode) (Figure 3.13) with a separate channel dedicated to each of the peptides(Figure 3.14). The following figure represents the instrumental parameters that were used to obtain the profiles showed before (Figure 3.13)

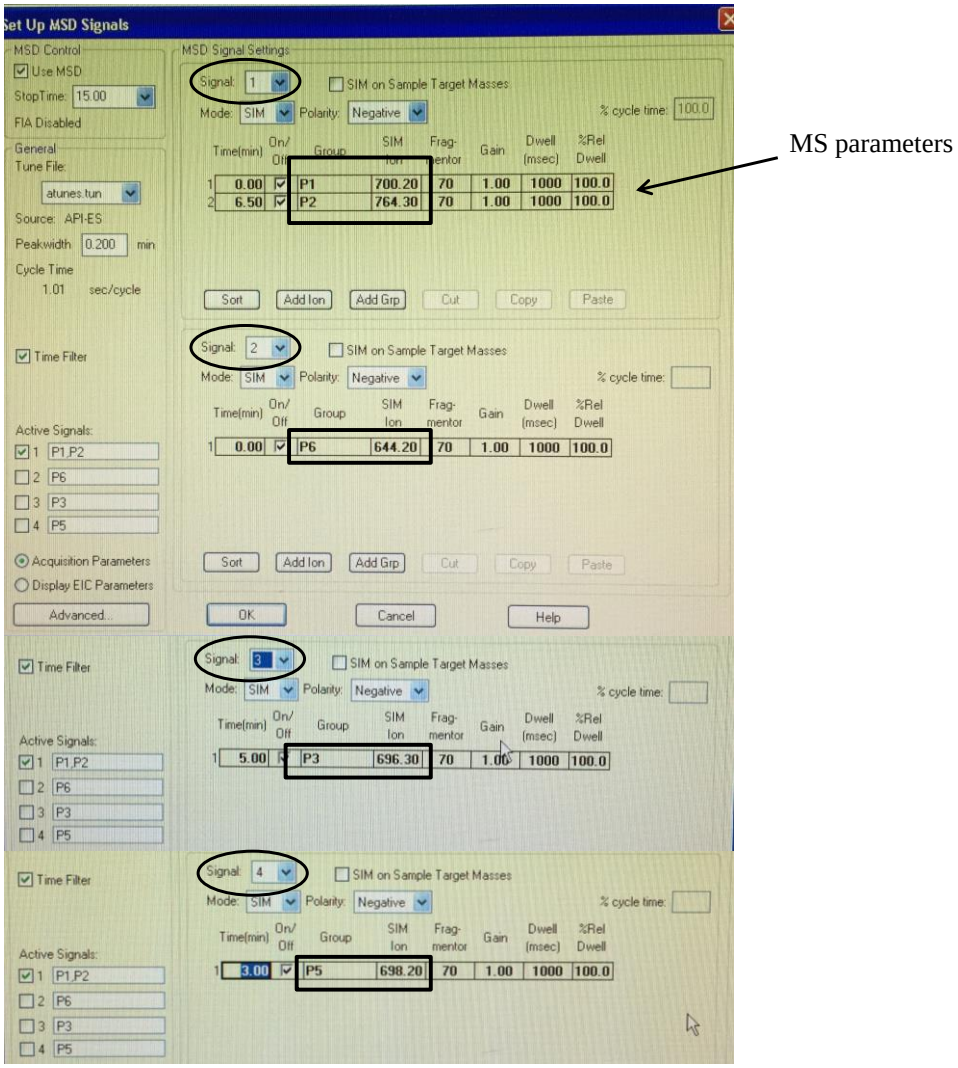

Figure 3.13. Mass parameters for the SIM mode.

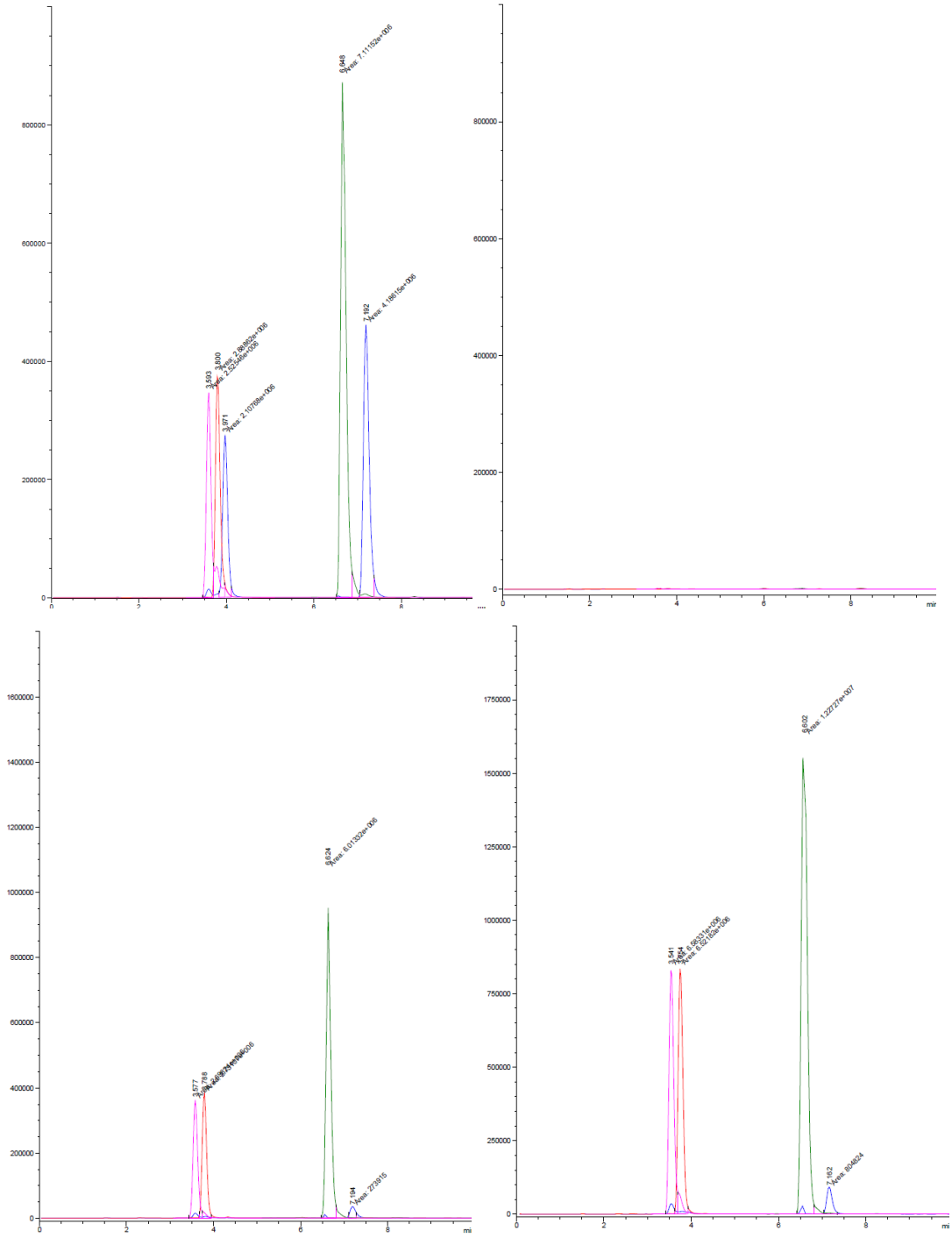

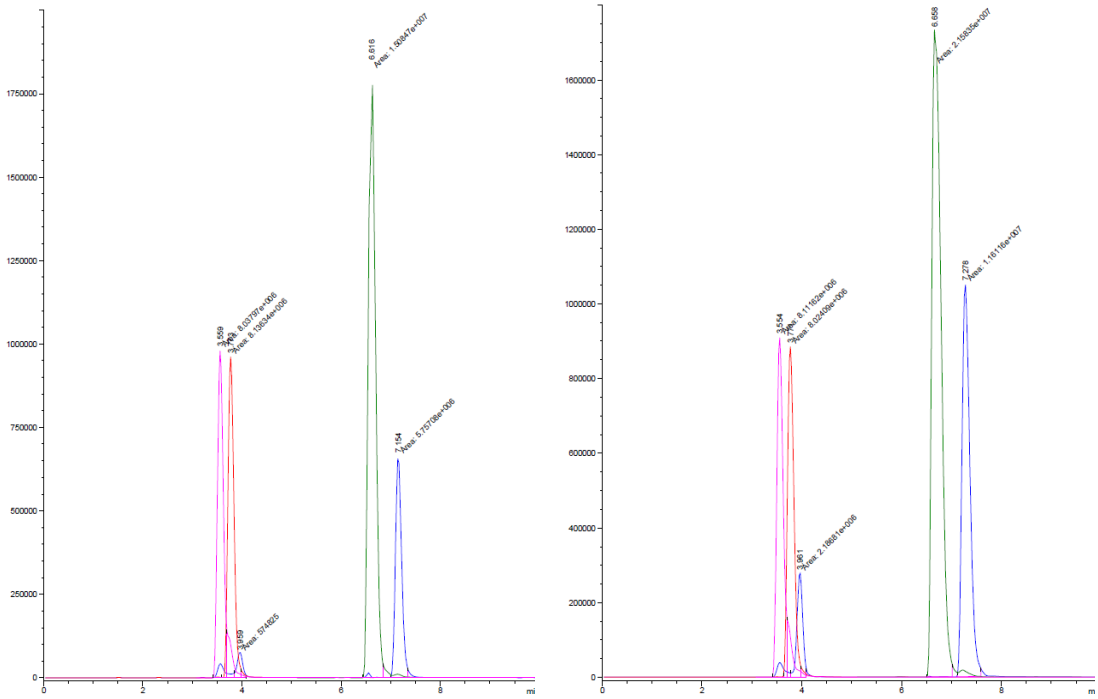

Figure 3.14. Examples of the chromatograms obtained at different concentrations: (a) Control (without AuMPC **1**) at 25 µM, (b) 25 µM, (c) 50 µM, (d) 75 µM, (e) 100 µM, (f) 125 µM.

The same experiments were performed but in presence of [ATP]=200 µM (Figure 3.15).

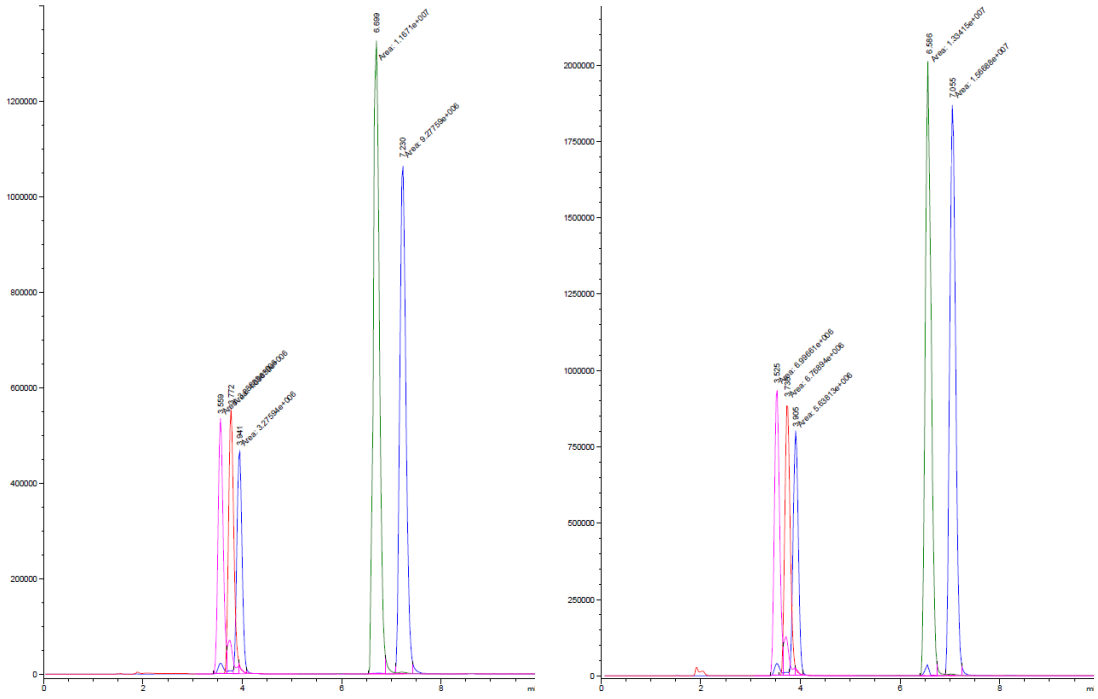

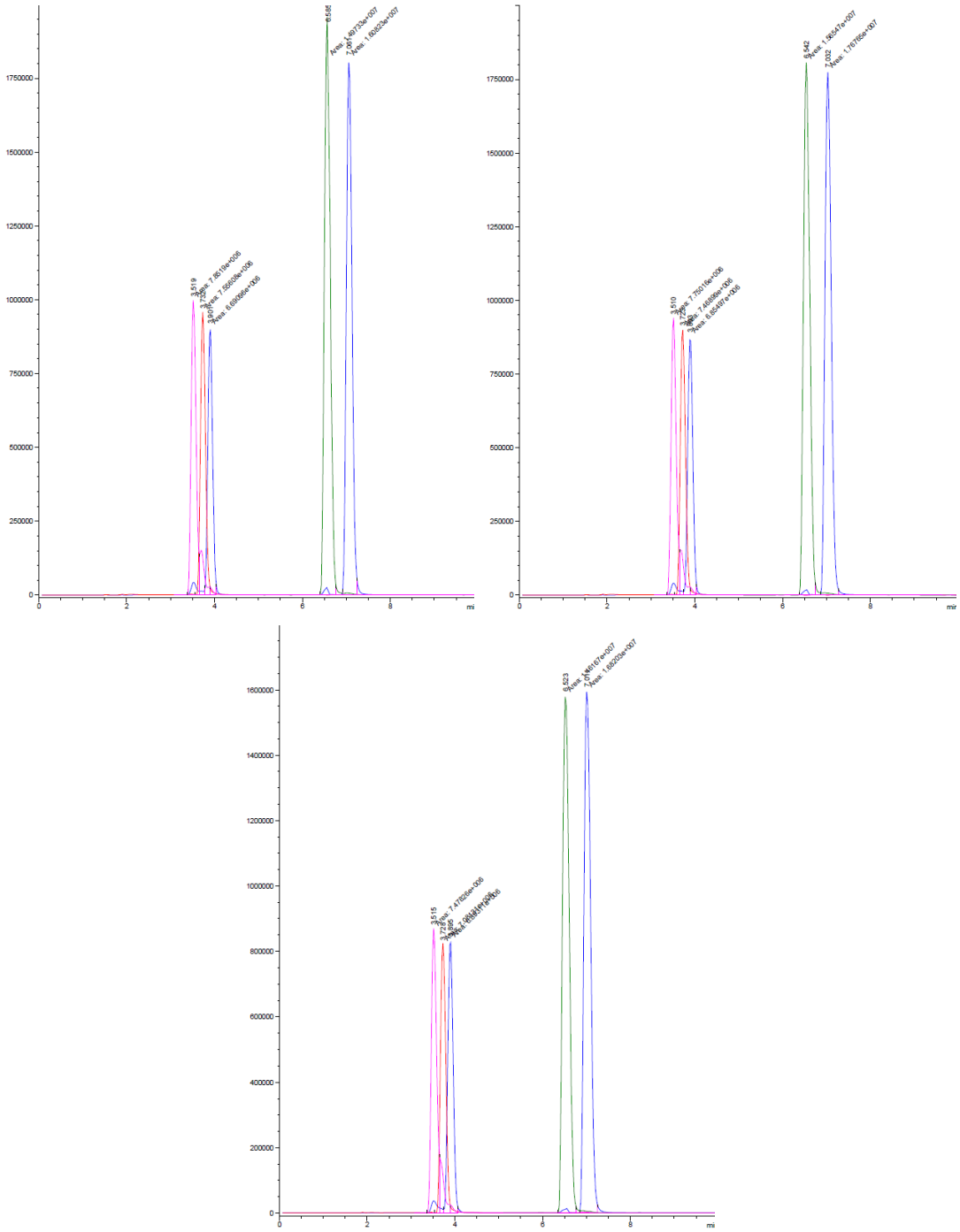

Figure 3.15. Examples of the chromatograms obtained at different concentrations of the peptides mixture: (a) 25 µM, (b) 50 µM, (c) 75 µM, (d) 100 µM, (e) 125 µM.

CHAPTER 4: Multivalent dynamic peptide surfaces for protein recognition

4.1 Introduction

As discussed in Chapter 1, proteins perform a vast array of functions within living organisms. Every protein contains a unique distribution of functional groups (charged, hydrogen bonding, and hydrophobic) on its exterior surface[90]. These regions are involved in important interactions to other proteins (PPIs) as part of multi-subunit complex systems involved in metabolic or signal transduction pathways, for example[91]. For that reason, the development of synthetic agents able to recognize protein surfaces is of a great interest.

The serine proteases represent interesting targets for protein surface recognition due to their central role in biological and medicinal chemistry[92]. Thus, α-chymotrypsin (ChT) ((pI = 8,25)[93]), a serine protease of 25 kDa, provides an excellent system for studying the protein surface recognition. It is an extensively characterized protein with well-defined geometry, and enzymatic activity[44]. UV response after cleavage substrate usually are used to evaluate the ChT activity which makes easier the detection of enzyme activity. The crystal structure of chymotrypsin (Figure 4.1a) reveals that, Ser195 assisted by His57 and Asp102 residues (Figure 4.1b), form a catalytic triad, a feature repeated for many hydrolytic enzymes. This triad operates within a well-defined binding site that is lined with nonpolar amino acids capable of van der Waals interactions with polypeptide substrates containing aromatic side chains. Importantly, the active site of ChT is surrounded by hydrophobic residues and also by a ring of cationic residues. Such a surface "hot spot" is advantageous for interaction with a large object such as Au NPs[94].

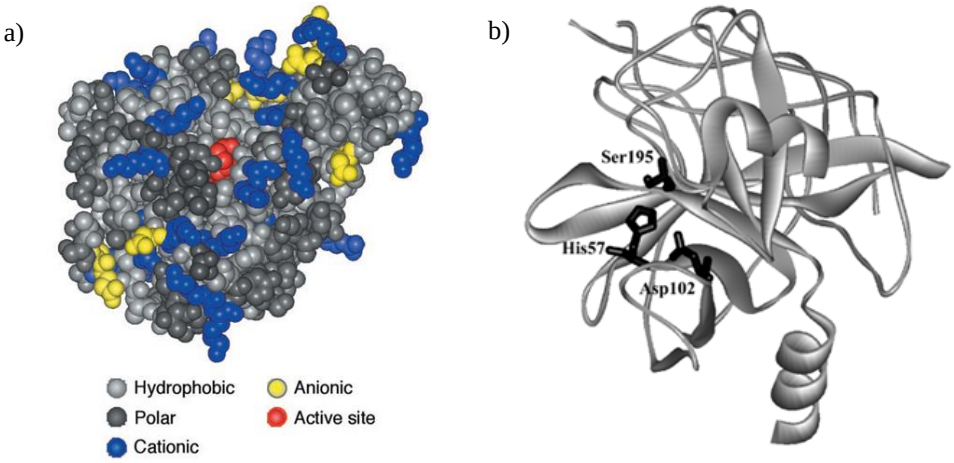

Figure 4.1. (a) Space-filling model of ChT. (b) The crystal structure of α-chymotrypsin showing the catalytic triad of amino acid side chains. (Adapted from Blevins, R. A., and Tulinsky, A. (1985))[95]

The key features of the mechanism (Scheme 4.1) are the participation of the serine hydroxyl as a nucleophile whose attack on the carbonyl of the substrate is facilitated through proton abstraction by the imidazole nitrogen of His57 and its redonation to the amine-leaving group. Deacylation of the enzyme follows general base catalysis of water attack again by His57 and the return of the enzyme to its resting state. Catalysis of the chemical process through the participation of the side chains of an enzyme in proton, hydride, and electron transfer is a hallmark of enzyme catalysis and can occur efficiently in the confines of the active site owing to the optimal alignment and juxtapositioning of the substrate for chemical reaction.

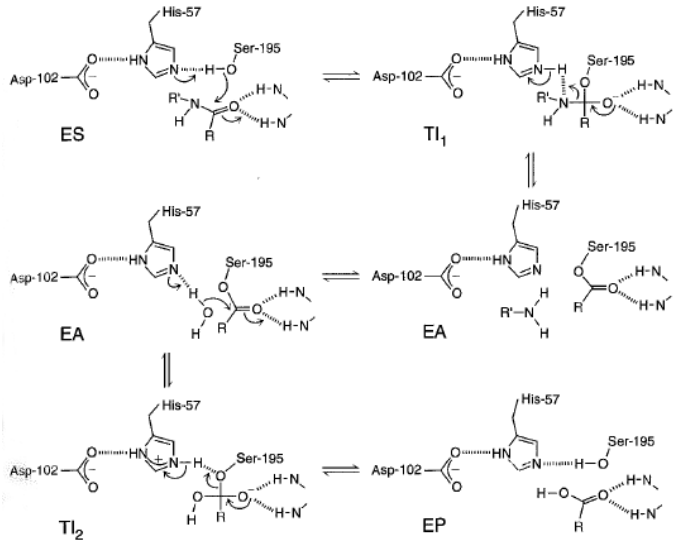

Scheme 4.1. The mechanism of amide hydrolysis by α-chymotrypsin[96].

As seen in Chapter 1, Rotello demonstrated that by incorporating simple L-amino acids in the monolayer Au NPs exhibited different inhibition activity of ChT. Complementary electrostatic interaction between nanoparticles and ChT was proven to be the predominant driving force contributing to the complex formation, but the hydrophobic interaction between the hydrophobic patches of receptors and proteins enhanced the complex stability[44].

This promising example was an excellent starting point for our purpose. Hence, the question to be addressed was whether the dynamic protein surface obtained by assembly simultaneously negatively charged, polar and hydrophobic peptides on the surface of Au NP **1** would be able to recognize the ChT-surface. Furthermore, would the dynamic nature of the surface allow an adaptation to the protein target in order to spontaneously form the surface with the highest complementarity.

4.2 Stability studies in the presence of ChT

Before studying the interaction of the dynamic nanoproteins with ChT, some initial control experiments were performed. As mentioned above, ChT is a protease that cleaves peptides, especially those with hydrophobic residues. Thus, in order to study the stability of the peptides **P1**-**P3**, **P5**, **P6** in the presence of ChT stability tests were performed (Figure 4.4). The concentration of each peptide in solution was monitored by selected-ion monitoring mode (SIM mode) during as a function of time in the presence of ChT (Figure 4.3). Constant concentrations of peptides ($[P_x]$ = 25 μM) and enzyme ([ChT] = 1.5 μM) were used in [HEPES] = 5 mM at pH = 7.

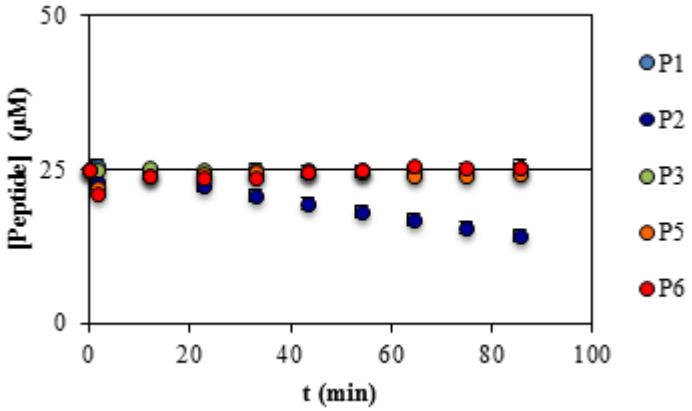

Figure 4.4. Concentration of each peptide during time. Conditions: [Px] = 25 μM, [HEPES]=5 mM, pH=7. Determined by mass spectrometry (SIM Mode).

The results showed that all the peptides were stable in the presence of ChT over time, except for **P2**, which was gradually consumed (with a 44 % decrease in concentration after 80 minutes). Presumably, the lower stability of **P2** originates from the presence of two Phe residues in **P2**, which is in line with the specificity of ChT to cleave close to hydrophobic residues. Thus, to avoid further complications **P2** was dismissed from the following studies.

Another parameter that could be affected by the addition of a protein to the nanosystem is the binding of the peptides to the Au NP **1** surface. Hence, it was necessary to determine whether the presence of ChT would affect the interaction of peptides **P1**, **P3**, **P5**, **P6** to Au NP **1**. Thus, a series of fluorescence titrations were performed in the presence/absence of ChT (conditions: [TACN-Zn^{2+}] = 50 μM, [ChT] = 1.5 μM in [HEPES] = 5 mM, pH = 7, T = 25 °C, λ_{ex}=280 nm, λ_{em}=360 nm). The fluorescent intensity at 360 nm was plotted as a function of the concentration of the peptides (Figure 4.5).

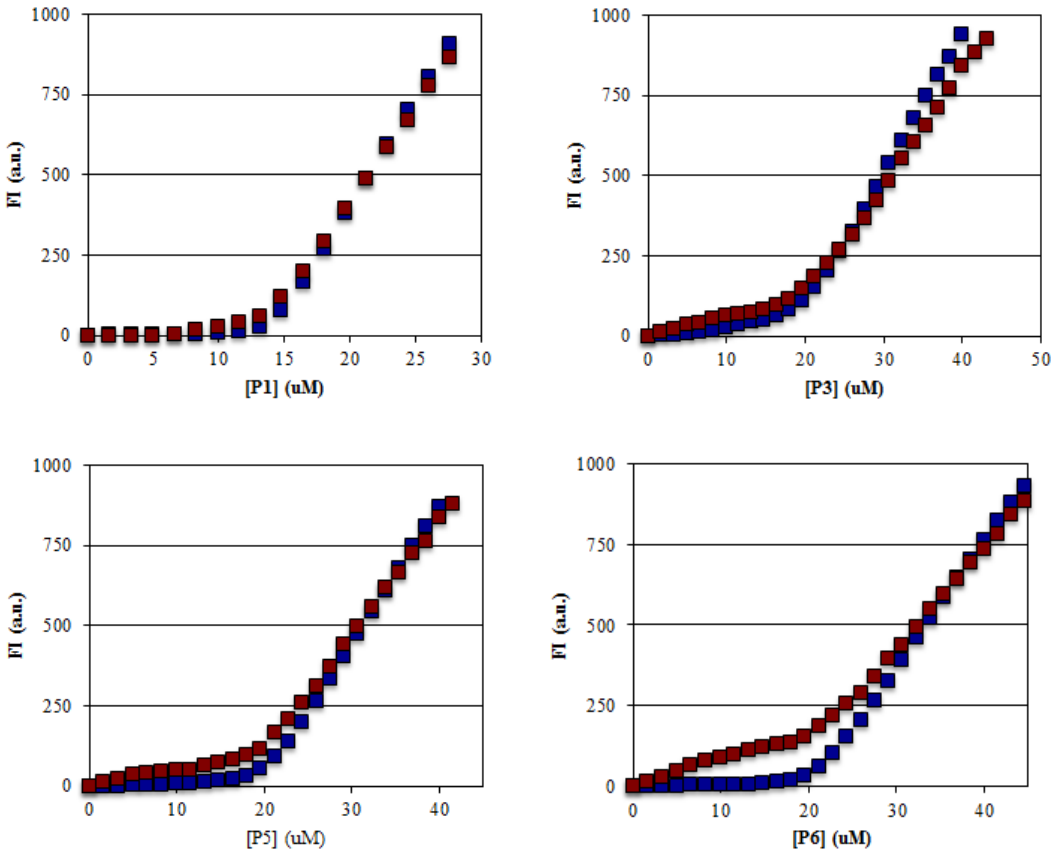

Figure 4.5. Curve binding assay: fluorescent intensity (a.u.) as a function of peptide concentration (μM) measured at λ_{ex}=280 nm, λ_{em}=360 nm. Peptide + AuMPC **1** (blue); Peptide + AuMPC **1** + ChT (red). Note: The intrinsic ChT fluorescence was taken as zero value.

The results showed that the presence of ChT does not significantly affect the interaction between the peptides and Au NP **1**. In some cases (**P5** and **P6**) only slight differences in the first part of the curve were observed (at low peptide concentration), which might be due to a weak competition between the peptides and the ChT. The saturation concentrations of the peptides at this conditions were 13.2 μM, 18.5 μM, 19.7 μM and 20.6 μM for **P1**, **P3**, **P5** and **P6**, respectively.

After having confirmed that the self-assembled nanoproteins are stable in the presence of ChT we proceeded by studying the interactions between the nanoproteins and ChT. There were two main questions: Does the presence of Au NP **1** decorated with the peptides affect ChT activity and does the presence of ChT affect the distribution of peptides on the surface of Au NP **1** under self-selection conditions *i.e.* with excess of peptide present?

4.3 Influence of Au NPs on the activity of ChT

To study the effect of the complex Au NP **1**-peptide on the ChT activity, the ChT-catalyzed hydrolysis of SPNA was examined (Chart 4.1). A screening of the cleavage rate of SPNA by ChT was performed in the presence of peptides and in the presence/absence of Au NP **1**.

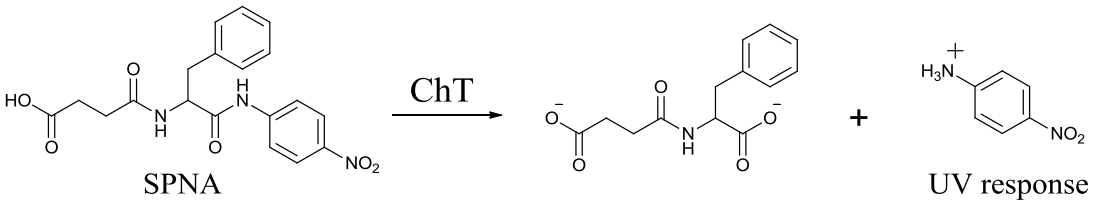

Chart 4.1.

For Au NP **1**-peptide complexes the saturation concentrations of each peptide on Au NP **1** were used (Figure 4.5). The conditions were the same as those used by Rotello in studying the peptide-functionalized Au NPs (see above)[44,97,98,99]. Therefore, the ChT concentration (1.5 μM) was chosen based on the concentration of Au NP **1** (50 μM). Taken into account that the concentration of TACN-Zn^{2+} headgroups is 50 μM and there are around 70 thiols per gold cluster the ratio between Au NP/ChT resulted in around 1:2, which is similar to the ratio used by Rotello *et al.*

The increasing amount of *p*-nitroaniline (*p*NA) formed because of the cleavage of SPNA was monitored by UHPLC at 380 nm for approximately one hour. The initial rate was determined dividing the concentration of *p*NA by time (*i.e.* the regime where the absorbance intensity linearly increases). The initial rates of each single peptide or Au NP **1**-peptide complex were compared to that of just ChT (E+S) (Figure 4.6).

The results showed an increase in the ChT activity when Au NP **1** was present (E+S+Np, **violet**). However, a similar increase in activity was observed also when Au NP **1** was added in the absence of Zn^{2+} (E+S+NP-Zn). It has been reported that cationic additives such as tetrabutylammonium bromide (TBABr), cetyltributylammonium bromide (CTBABr) and p-octyloxybenzyltributyl-ammonium bromide (pOOTBABr) can activate ChT, but a satisfactory explanation

for this observation has not yet been provided[100,64]. Rotello also observed an increase in ChT-activity when using **NP_L-Arg** in the example discussed before. They hypothesized that positively charged additives could interact with negatively charged regions of the ChT which would produce a more hydrophobic microenvironment and a consequent increase in the nucleophilicity of the catalytic serine residue[64]. In any case, the mechanism is still unclear.

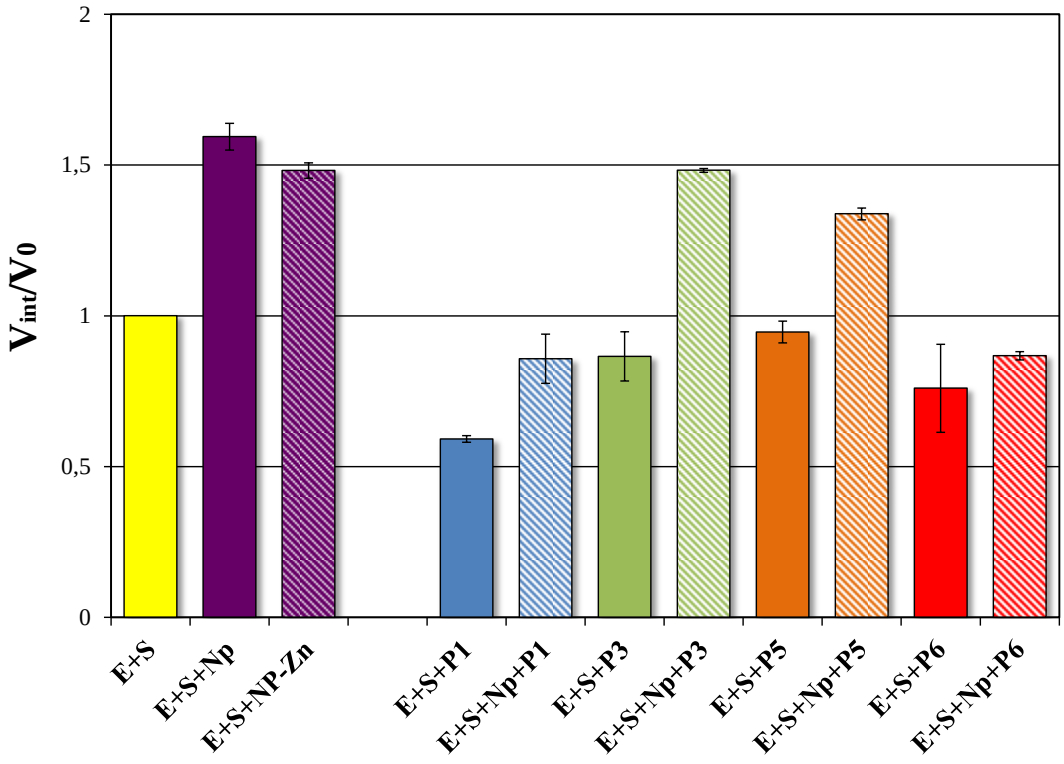

Figure 4.6. Results of the screening of the ChT assay. The activities of ChT in the presence of Au NP **1** (violets)**,** Au NP **1**-peptides (plain) and peptides alone (striped) were normalized to that of free ChT (yellow). Conditions: the formation of *p*-nitroaniline was mesured using 5-95 %B in 5 min, 0.200 mL/min; A: H_2O+0.1% HCOOH B: ACN+0.1% HCOOH at 380 nm. Note: E = enzyme (ChT), S = substrate (SPNA) and Np = Au NP **1**. Conditions: [TACN-Zn^{2+}] = 50 µM, [ChT] = 1.5 µM, [SPNA] = 1 mM in [HEPES] = 5 mM at pH = 7, T = 25 ^{o}C.

The possible interaction between Au NP **1** and ChT was studied by fluorimetry. Thus, ChT was titrated in a solution containing HEPES buffer (30 mM) in the absence/presence of Au NP **1** (50 µM). As expected, the results showed no binding of ChT to Au NP **1**. Hence, the reason by why Au NP **1** increases the ChT activity is still unknown.

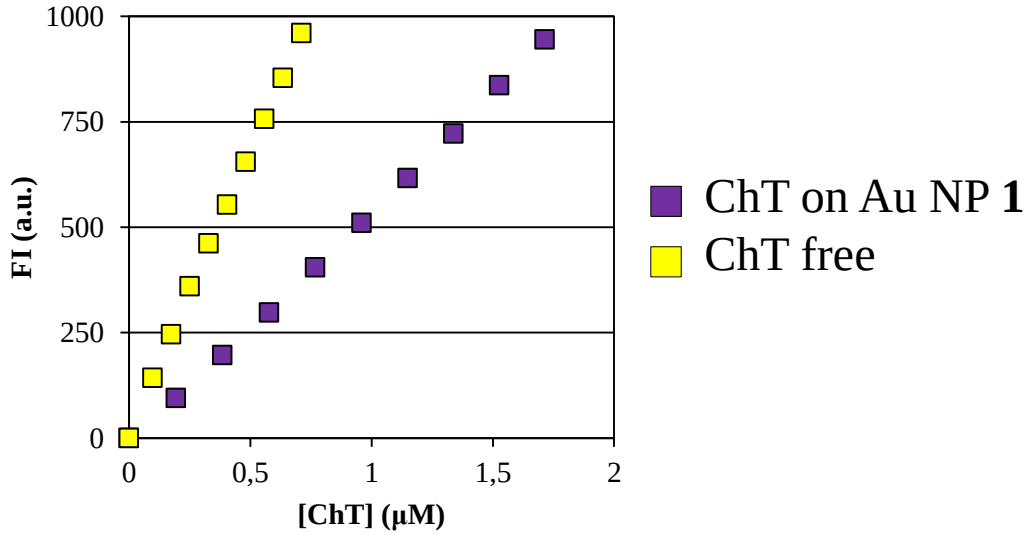

Figure 4.7. Titration of ChT in the presence/absence of Au NP **1.** Conditions**:** [TACN-Zn^{2+}] = 50 µM, [ChT] = 1.5 µM, [HEPES]=30 mM at pH=7 and T = 25 ^{o}C.

Regarding the kinetic studies, a different behavior was observed in the presence of the peptides. In the absence of Au NP **1**, **P1** caused a roughly 50% decrease in ChT activity, which could be explained by interaction between the highly negatively charged **P1** and the cationic ring surrounding the hot spot of ChT. A weaker effect was observed for the other peptides.

This changed when peptides were added in the presence of Au NP **1**. It was possible to divide the peptides in two different groups (in terms of similarity in induced effect): **P1**, **P6** (**blue**&**red**) and **P3**, **P5** (**green**&**orange**). In the case of **P1** and **P6** no change in activity was observed compared to free ChT (**yellow**), whereas for **P3** and **P5** a similar effect to that of Au NP **1** (**violet**) was observed. In other words, the first group (**P1**/**P6**) seemed to counteract the activation of the ChT by the Au NP **1** (see above). On the other hand, **P3** and **P5** gave a similar degree of activation compared to Au NP **1** alone. This could have indicated that **P3** and **P5** were not totally bound to the nanoparticle surface and the observed higher activity was a result of Au NP **1**. However, the previously discussed fluorescence titration studies had indicated that this was not the case and that under these conditions all peptides are bound to Au NP **1**. For that reason, it was hypothesized that the addition of SPNA could change the experimental conditions. In particular, it was found that the addition of the SPNA-substrate (1 mM) at the buffer concentration of 5 mM caused a slight change in the pH (- 0.8 pH units). It is reminded that these conditions

(substrate and buffer) were based on a previous literature report by Rotello *et al.* which had not taken into consideration this effect on the pH. Hence, three solutions were prepared containing Au NP **1** [TACN-Zn^{2+}] = 50 µM, [ChT] = 1.5 µM and [SPNA] = 1 mM at three different HEPES concentrations: 5 mM, 10 mM and 30 mM at pH = 7. It was observed that when using 5 and 10 mM the pH decreased until 6.2 and 6.8 respectively upon the addition of SPNA. The pH remained stable when 30 mM of HEPES was used. Considering that the pH has an effect on the binding between the peptides and Au NPs and also on ChT activity, it was decided to repeat the assay using **P1** and **P3** (considering that these represented the two different groups) using 30 mM of HEPES to clarify whether this would affect the result (Figure 4.8).

Under these new conditions the difference between Au NP **1**-**P1** and Au NP **1**-**P3** had largely disappeared. In both cases now a slight activation of ChT was observed comparable to that of Au NP **1** by itself in the absence of peptides.

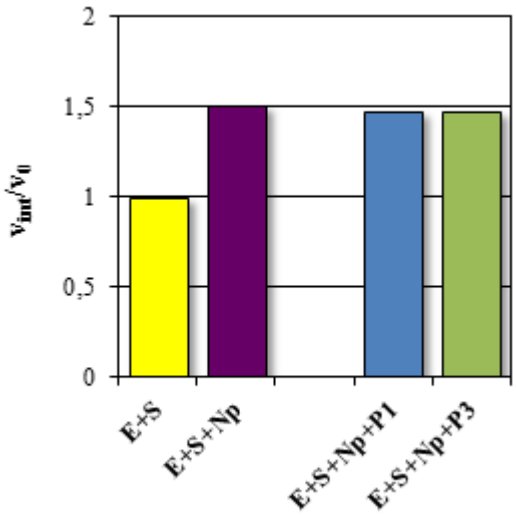

Figure 4.8. Results ChT assays. All the activities were normalized to that of free ChT (yellow). Conditions: the formation of *p*-nitroaniline was mesured using 5-95 %B in 5 min, 0.200 mL/min; A: H_2O+0.1% HCOOH B: ACN+0.1% HCOOH at 380 nm. Note: E = enzyme (ChT), S = substrate (SPNA) and Np = Au NP **1**. Conditions: [TACN-Zn^{2+}] = 50 µM, [ChT] = 1.5 µM, [SPNA] = 1 mM in [HEPES] = 30 mM at pH = 7, T = 25 ^{o}C.

Considering the absence of an observed difference for these different peptides and also considering the generally small magnitude of the effect, it was concluded that the nanoprotein only marginal affects ChT activity. However, the reason for

which the ChT activity increases in the presence of **P1**or **P3** and Au NP **1** has not been fully clarified yet.

4.4 Self-selection of peptide surfaces by a target protein

The previous assay was an indirect assay based on the expectation that an interaction between the nanoproteins and ChT would affect the catalytic activity. No convincing evidence that this indeed occurred was obtained. The reason may be that there is no interaction between the nanoprotein and ChT, but, alternatively, it could also be explained by the fact that the interaction between ChT and nanosystem does not affect the catalytic activity of the enzyme. That is why it was decided to study the interaction in a different manner aiming at a direct detection of binding. In addition, these new experiments would also permit also an assessment of the ability of the dynamic nanosystem to adapt to the protein.

For that purpose a series of experiments were designed using the previously developed ultracentrifugation methodology (Chapter 3). The scope of these experiments was to study possible changes in the distribution of two different peptides on the Au NP **1** surface upon the addition of a protein (ChT). It was decided to start with binary mixtures of peptides in order to reduce the complexity of the system. Thus, a series of two peptides at different ratios were used in these experiments: **P1**&**P3**, **P1**&**P5**, **P1**&**P6**, **P3**&**P5**, **P3**&**P6** and **P5**&**P6**.

The concentration of the peptides (25 μM, which is higher than the SSC of all of the peptides) was chosen such that there was always a part of the peptides free in solution. This is an essential condition for self-selection.

After centrifugation, the dialysates were analyzed by LC/MS in SIM mode to determine the ratio of peptides bound to Au NP **1**. The percentage of the area was represented for each single peptide relative to value of the area of each single peptide filtered in the absence of Au NP **1** and ChT ($\mathbf{P_X}$ + $\mathbf{P_Y}$) (Figure 4.9).

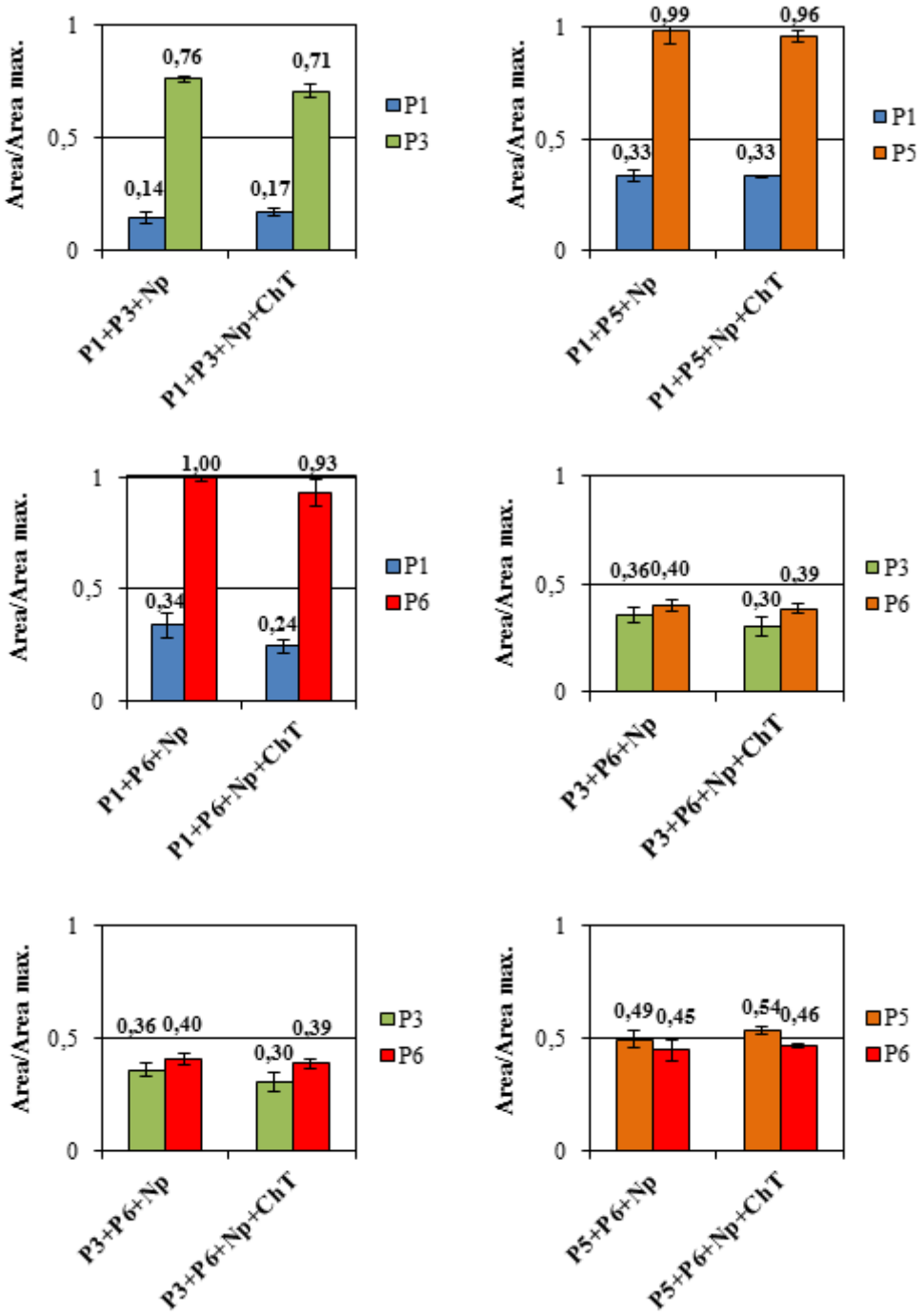

Figure 4.9. Self-selection experiments: Conditions: [TACN-Zn^{2+}]=50 μM, [ChT] = 1,5 μM, [HEPES]=30 mM, at pH=7. Determined by mass spectrometry (SIM Mode).

Regrettably, for none of the combinations studied, significant differences were observed in the peptide surface composition in Au NP **1** in the presence or absence of ChT. This might be caused by the ratio of Au NP **1**:ChT (1:2 ratio) and for that reason the experiments were repeated with a higher concentration of ChT (15 μM) (1:20 ratio). In this case only the combinations **P1**&**P3**, **P3**&**P5** and **P3**&**P6**

were tested (Figure 4.10). It was decided to keep **P3** so to have always an hydrophobic contribution.

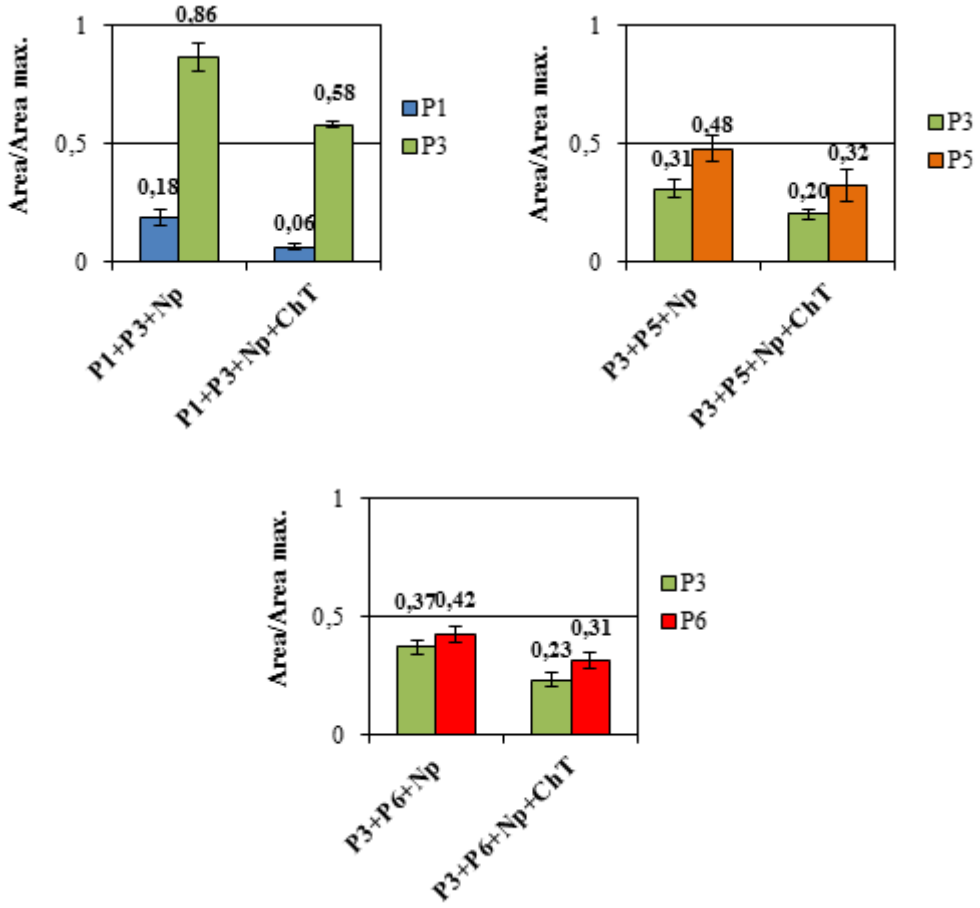

Figure 4.10. Self-selection experiments: Conditions: [TACN-Zn^{2+}]=50 µM, [ChT] = 15 µM, [HEPES]=30 mM, pH=7. Determined by mass spectrometry (SIM Mode).

Comparing the peptide concentrations in the presence and the absence of ChT, a general decrease of the peptide concentrations was observed when ChT was present. This fact could be explain if considering that a higher concentration of ChT can block the membrane of the centrifugal filter and does not allow the peptides to pass through it. This general effect of ChT was quantified for each peptide by determining the ratio of each peptide concentration in the absence and presence of ChT. This resulted in a constant value of around 1.5 for all of them, except for P1. For this peptide a 3-fold change was measured (0.18/0.06) (Figure 4.9, **P1**&**P3**). This could suggest that the concentration of **P1** in solution is more reduced by the presence of ChT compared to the other peptides.

This increase in retention of **P1** could be due to an interaction between **P1** and ChT, which would decrease the concentration of free **P1** (*i.e.* non-complexed) in solution. In fact, considering that **P1** is negatively charged, it could interact with the positively charged region of the ChT. These observations were in line with the previous activity studies that indicated an inhibition of ChT by **P1**.

This potential interaction was studied in another way[86], based on the expected different affinities of **P1** and the **P1**-ChT complex for the Au NP **1** surface between **P1** and the complex **P1**-ChT. Formation of a **P1**-ChT complex would result in a clustering of negative charges on ChT. It can be expected that such a complex would have a higher affinity for Au NP **1** compared to just **P1**, because of multivalency. If this is indeed the case, one would expect that the **P1**-ChT complex would be more efficient in displacing a (quenched) fluorescent probe from the surface of Au NP **1** in a competition experiment.

The complex formation (**P1**-ChT) was monitored following the fluorescence intensity of 2'-deoxy-3'-O-(*N'*-methylanthraniloyl)adenosine-5'-O-diphosphate (MANT-dADP) upon its release from the surface of Au NP **1** caused by the addition of **P1** either in the absence or presence of ChT (1.5 uM). The saturation concentration of MANT-dADP was previously evaluated by performing a binding assay at the same conditions (Figure 4.14). The fluorescence intensity was plotted as a function of the **P1** concentration (Figure 4.11).

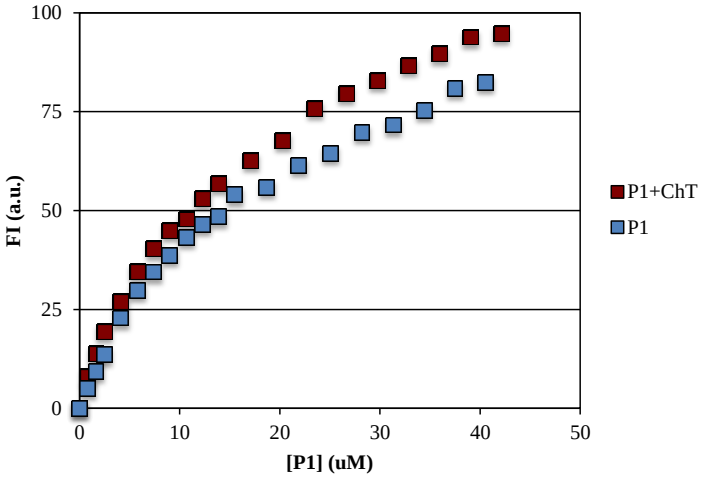

Figure 4.11. Displacement experiment: fluorescent intensity (a.u.) as a function of [P1] (μM) in the presence and in the absence of ChT measured at λ_{ex}=355 nm, λ_{em}=446 nm.

These displacement experiments clearly show that **P1** is more effective in displacing MANT-dADP from Au NP **1** when ChT is present. This suggests indeed the formation of a ternary complex in which **P1** is sandwiched between Au NP **1** and ChT. However, additional experiments such as isotherm titration calorimetry (ITC), dynamic light scattering (DLS) are needed to confirm the binding and the formation of the ternary complex between Au NP **1-P1**-ChT.

4.5 Conclusions

The ability of the nanoprotein to interact with natural protein surfaces has been investigated. A particular attention has been paid to exploitation of the dynamic nature of the assembly. The serine protease chymotrypsin (ChT) has been chosen as a target, because previous literature reports had already mentioned that peptide-functionalized Au NPs have been able to bind ChT. Binding assays have confirmed that the presence of ChT did not affect the interaction between the peptide library and Au NP **1**. Apart from peptide **P2**, none of the peptides was hydrolyzed by ChT. Enzyme activity studies in the presence of Au NP **1**-peptide systems did not provide conclusive data. The obtained data have showed a slight activation of ChT (1.5 times) in the presence of Au NP, irrespective of whether peptides were present or not. Such an activation of ChT by cationic agents has also been reported in other studies, but a clear explanation is not yet available. Since the measurement of enzyme activity is an indirect method of measuring the interaction between the nanoproteins and ChT, the attention have been shifted towards a direct method relying on the ultracentrifugation experiments developed earlier. The aim has been to investigate whether the surface composition would be affected by the addition of ChT. Initial data from the ultracentrifugation experiments and additional fluorescence studies seemed to suggest the formation of a ternary multivalent complex with peptide **P1** sandwiched between Au NP **1** and ChT. However, further experiments under different conditions and including other techniques (such as ITC and DLS) are required to confirm these results.

4.6 Experimental section

4.6.1 Instrumentation

See section 2.5.1 and 3.1.1.

4.6.2 Materials

α-Chymotrypsin from bovine pancreas, Type I-S (C7762) and *N*-succinyl-L-phenylalanine-*p*-nitroanilide (SPNA) (S2628) were purchased from SIGMA ALDRICH. For the rest of the materials see section 3.1.2. α-Chymotrypsin was solubilized in 1 mM HCl (2 mg/ml, 80 μM), yielding a clear solution and store at -20 °C. SPNA is solubilized in EtOH (20 mM, 7,7 mg/mL).

4.6.3 Stability studies

In a 2 mL eppendorf vial a solution that contains [Px] = 25 μM and [HEPES] = 5 mM was prepared to reach a final volume of 1800 μL. Three UPLC vials were filled with this solution (500 μL). Before injecting the enzyme was added ([ChT] = 1.5 μM) was added (H_2O is added to one of the vials instead of the enzyme and used as a reference). Zorbax Eclipse Plus C18 column with a length of 150 mm and an internal diameter of 2.1 mm and 1.8-mm fused silica particles at a flow rate of 0.2 mL/min. A solvent gradient from 5% (v/v) ACN+0.1% HCOOH in H_2O+0.1% HCOOH to 95% (v/v) ACN+0.1% HCOOH in H_2O+0.1% HCOOH (8 min) was used. This concentration was kept constant for 9 min after which a gradient to 5% (v/v) ACN+0.1% HCOOH in H_2O+0.1% HCOOH was imposed (10 min). The column temperature was set at 40 ^{o}C. The peptides were monitored using SIM mode (selected-ion monitoring mode) each 10 min for 85 min.

4.6.4 Binding studies in the presence of ChT

The binding assays were done as described before (Chapter 2). Due to the strong intrinsic fluorescence intensity of the ChT different slits were used in the binding assays for the experiments in the the presence/absence of ChT (λ_{ex} = 5 nm

and λ_{em} = 10 nm, and λ_{ex} = 5 nm and λ_{em} = 20 nm, respectively). In order to compare both binding assays the correlation of the fluorescence intensity and both slits settings was determined by titrating the peptides at both slits obtaining the ratio of the slopes for the two different slit settings (Figure 4.11). Then, the fluorescence intensity was corrected by multiplying the fluorescence intensity (of the λ_{ex} = 5 nm and λ_{em} = 10 nm) with this ratio (3.95). The results are reported as using λ_{ex} = 5 nm and λ_{em} = 20 nm slits.

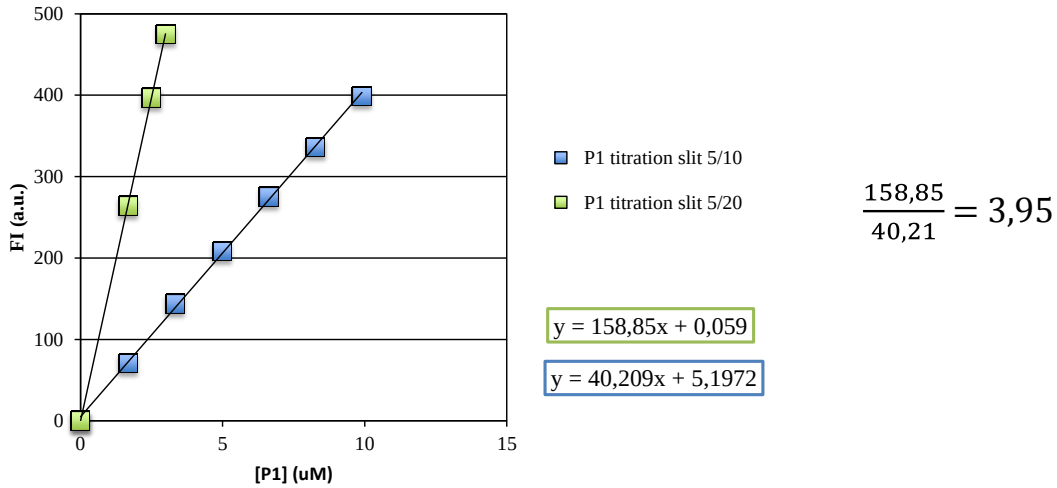

Figure 4.12. Example of how to determine the ratio between slits.

4.6.5 ChT assay: UHPL kinetics

In a UHPLC vial a solution was prepared containing [ChT] = 1.5 μM the Au NP **1** [TACN-Zn^{2+}] = 50 μM [Px] = SSC μM in [HEPES] = 5 mM/30 mM at pH = 7, and/or are added. Immediately before injecting [SPNA] = 1 mM was added to start the reaction. The reaction was monitored by UHPLC following the *p*-nitroaniline formed from the hydrolysis of the SPNA at 380 nm. The solution was sampled approximately 10.5 min for 60 min (Figure 4.12). Zorbax Eclipse Plus C18 column with a length of 150 mm and an internal diameter of 2.1 mm and 1.8-mm fused silica particles at a flow rate of 0.2 mL/min. A solvent gradient from 5% (v/v) ACN+0.1% HCOOH in H_2O+0.1% HCOOH to 95% (v/v) ACN+0.1% HCOOH in H_2O+0.1% HCOOH (8 min) was used. This concentration was kept constant for 9 min after

which a gradient to 5% (v/v) ACN+0.1% HCOOH in H_2O+0.1% HCOOH was imposed (10 min). The column temperature was set at 40 ^oC.

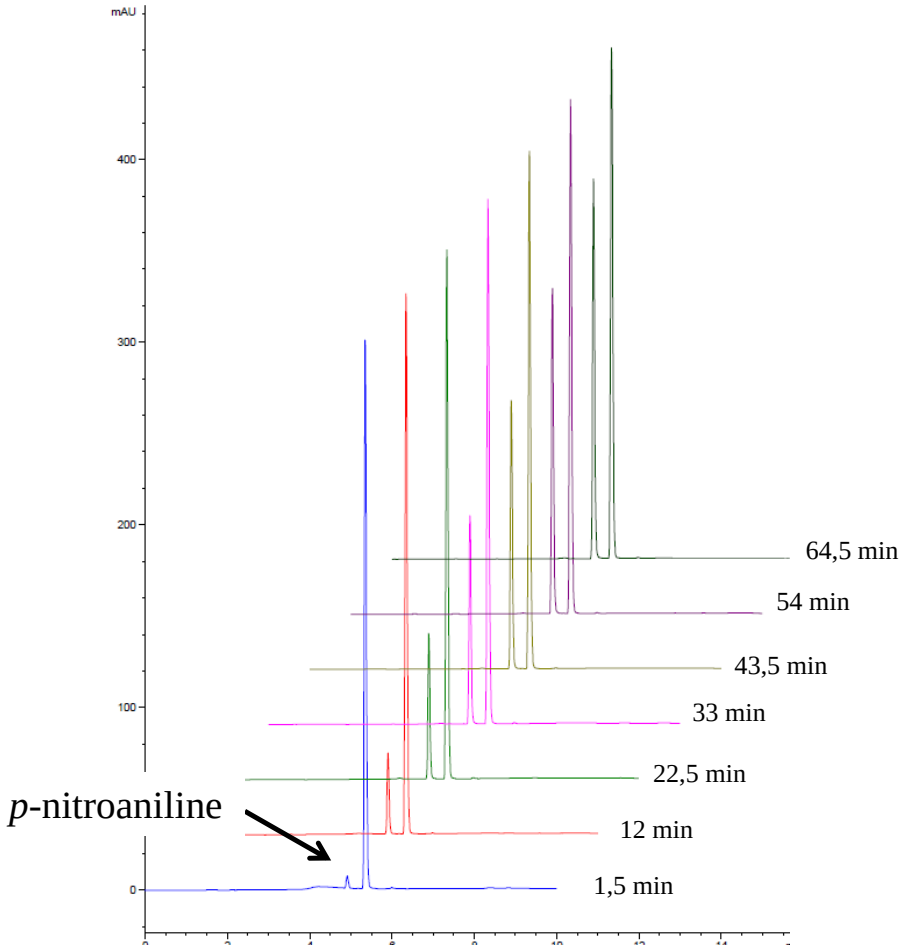

Figure 4.13. Overlay 3D chromatogram of the kinetics (E+S).

4.6.6 Self-selection experiments

Three different solutions (**P_X** + **P_Y**, **P_X** + **P_Y** + Np and **P_X** + **P_Y** + Np + ChT) were prepared and put in three different filtration units. For these experiments the following experimental conditions were used: [TACN-Zn^{2+}] = 50 µM, [$P_{X,Y}$] = 25 µM, [ChT] = 1,5 µM in [HEPES] = 30 mM at pH = 7. The samples were centrifuged at 12000 r.p.m. for 15 seconds. Afterwards, 20 µL of dialysate was injected in the UPLC-MS and the peptides were followed at 280 nm. Zorbax Eclipse Plus C18 column with a length of 150 mm and an internal diameter of 2.1 mm and 1.8-mm fused silica particles at a flow rate of 0.2 mL/min. A solvent gradient from 5% (v/v) ACN+0.1% HCOOH in H_2O+0.1% HCOOH to 95% (v/v) ACN+0.1% HCOOH in H_2O+0.1% HCOOH (8 min) was used. This concentration was kept constant for 9

min after which a gradient to 5% (v/v) ACN+0.1% HCOOH in H_2O+0.1% HCOOH was imposed (10 min). The column temperature was set at 40 ^oC.. The column temperature was 40 ^oC. The presence of peptides was monitored by SIM mode.

4.6.7 MANT-dADP binding assay

Conditions used: [TACN-Zn^{2+}] = 50 µM, [MANT-dADP] = 14,7 µM, [ChT] = 1,5 µM in [HEPES] = 30 mM at pH = 7 and T = 25 ^oC.

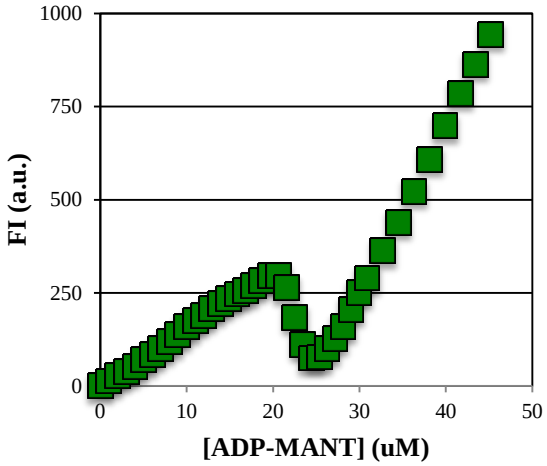

Figure 4.14. Binding assay of the MANT-dADP.

The strange shape (0-25 µM MANT-dADP) is caused by a shift in the emission wavelength[65].

CHAPTER 5: Au NPs as nanozymes for the cleavage on non-activated phosphomonoesters

5.1 Introduction

This project arose from a collaboration with Ulijns' group at the University of Strathclyde within the context of the Marie Curie network.

Ulijn et al. has extensively studied dynamic systems in which the reversibility originates from enzyme-catalyzed peptide bond making and breaking101. Amide hydrolysis reactions are close to equilibrium102 under dilute aqueous conditions (for a typical peptide ΔG0amide hydrolysis = -4.0 kJ/mole at pH = 7.5, 25 oC) and can be shifted towards amide formation by relative stabilization of the amide component. This may occur, for example, when the amides self-assemble into an aggregate. The free energy liberated in this process can compensate the higher free energy associated to formation of the amide bond and, thus, drive the system towards the formation of peptides (Figure 5.1a). In Ulijns' system, the self-assembly of aromatic short peptide fragments into gels provided the energetic driving force to shift the thermodynamic equilibrium.

Hence, *N*-(fluorenyl-9-methoxycarbonyl)-protected (Fmoc-protected) amino acids (Gly, Leu, Phe, Thr) along with four times excesses of nucleophilic fragments (Gly-Gly, Phe-Phe, Leu-Leu or Leu-, Phe-OMe amino acid esters) were used as self-assembly precursors. Thermolysin, a non-specific endoprotease, was used as catalyst(Figure 5.1b).

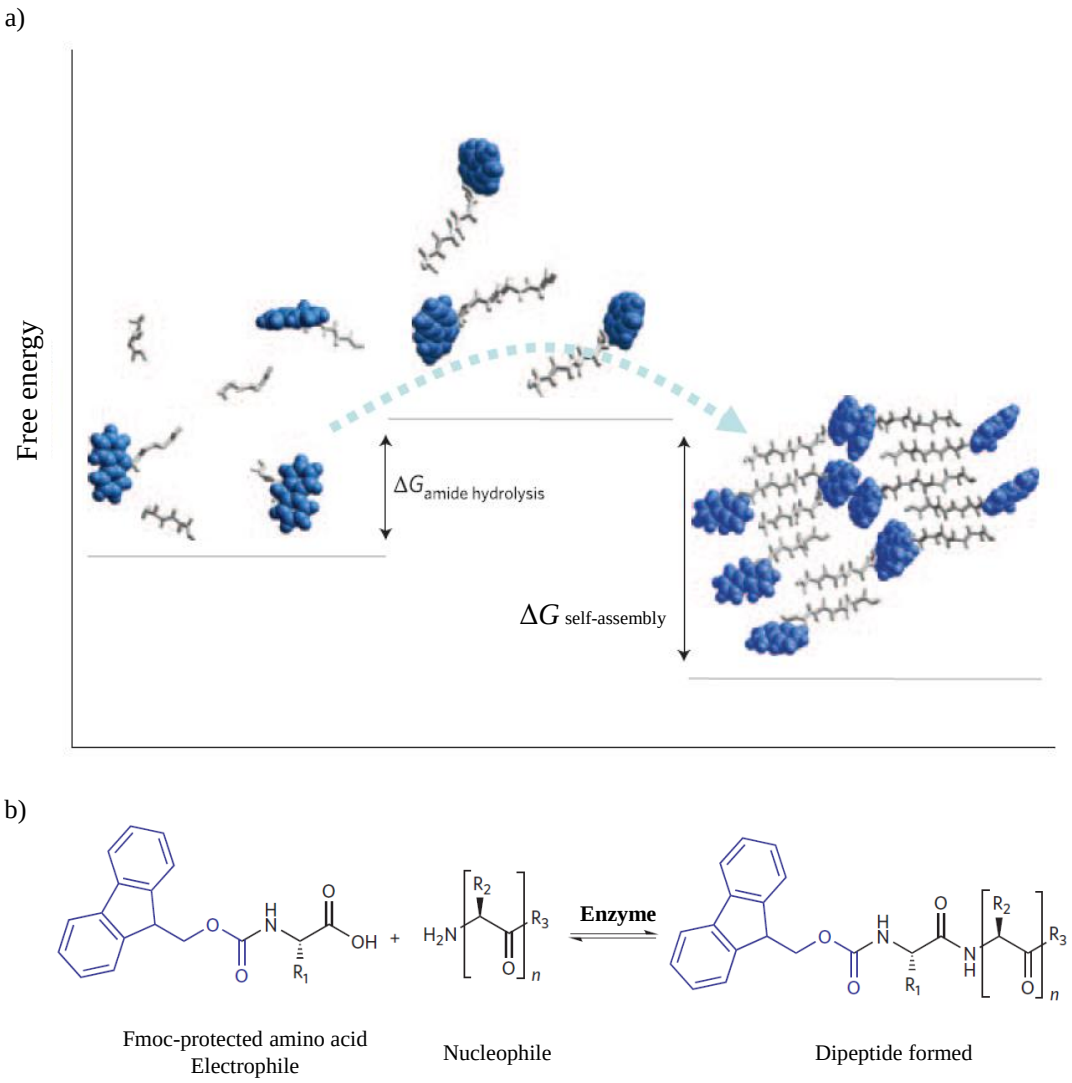

Figure 5.1. (a) Diagram showing the free energy profile of enzyme-assisted self-assembly of peptide derivatives. Peptide derivatives are shown schematically in grey (amino acids) and blue (Fmoc). (b) Reversed hydrolysis reaction.

The time-dependent formation of Fmoc-peptides was analyzed by HPLC. **Fmoc-F_3** was predominant after 3 hours (Figure 5.2a). The peptides composed of the remaining precursors were formed either after much longer times (**Fmoc-L_5**, 65-77 %, > 600 h) or were not formed at all. Structural changes were evaluated by using fluorescence spectroscopy and CD. The formation of Fmoc aggregates was easily followed by a progressive increase of a broad peak at 440 nm[103] (Figure 5.2b). A continuous enhancement of a signal at 307 nm in the CD was proof of increasing chiral ordering of the Fmoc groups (Figure 5.2b).

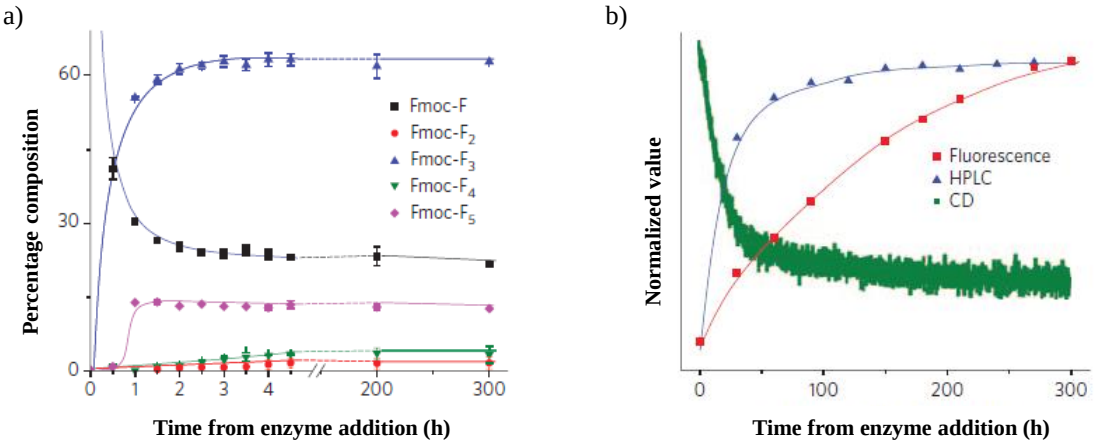

Figure 5.2. (a) HPLC time course for the distribution of Fmoc-Fn derivatives at various times after the addition of enzyme. (b) Comparison of the percentage conversion to the self-assembling Fmoc-F3, by HPLC with structural changes observed by fluorescence spectroscopy and circular dichroism

Hence, the use of fully reversible enzyme reactions to direct self-assembling peptides through changes in the free energy landscape was demonstrated. Structure formation occurred in a spatiotemporally confined manner which adds an extra level of control to early stages of self-assembly.

As seen in this example, peptide bond formation under reversible conditions is possible using enzymes as long as interactions between the formed dipeptides stabilized, *e.g.* by forming self-assembled structures. This led to the hypothesis that the stabilizing interactions between peptides and Au NP **1**, as discussed in previous chapters, could play a similar role in directing the selective formation of peptides under reversible conditions.

5.2 Impact of Au NP 1 on the composition of a dynamic peptide systems

In a recent work by Ulijn *et al*[104] it was shown that different supramolecular structures can be produced (e.g. fibrillar, tubular nanostructure and sheet-like structures) by changing the electronic properties of phenylalanine on Fmoc–Phe–(4-X)–Phe–NH_2, where X is an electron donating or withdrawing group (OH, OPO_3H_2, F, CN, NO_2) (Figure 5.3a). Fibrillar nanostructures were obtained in the case of electron withdrawing groups and neutral phenylalanine, sheet-like structures for the tyrosine derivative and tubular nanostructure for the phosphorylated dipeptide

(Figure 5.3b). This system was used as a starting point for studies aimed at understanding the effect of the presence of Au NP **1**.

a)

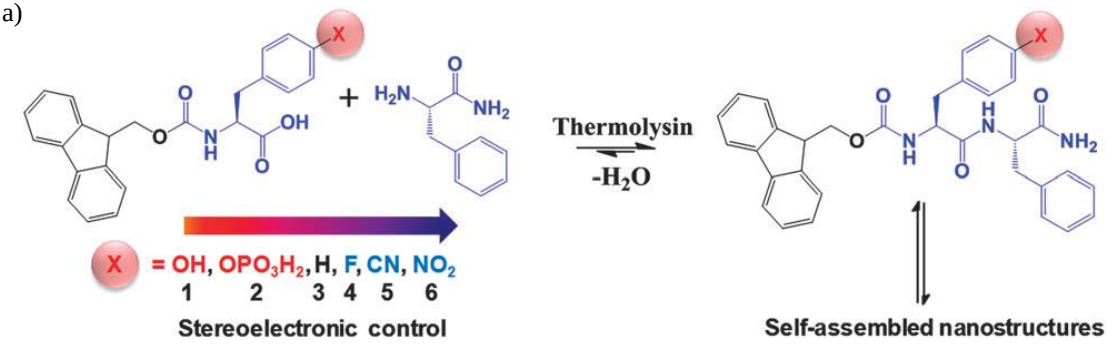

b)

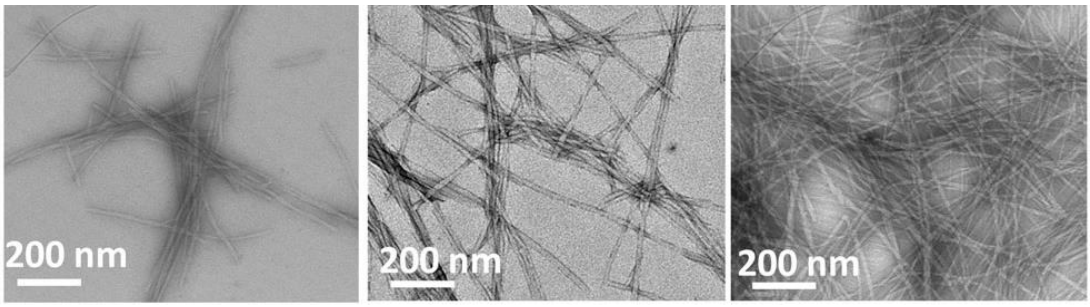

Figure 5.3. (a) Thermolysin catalysed amide bond formation of Fmoc-dipeptide derivatives. (b) TEM images of the different supramolecular structures.

Thermolysin requires an hydrophobic residue in the nucleophilic fragment in order to form the amide bond. Hence, Phe-NH_2, Trp-NH_2, Tyr-NH_2 were used as nucleophiles whereas various negatively charged Fmoc-amino acids were used as electrophiles (Chart 5.1). Initial experiments were aimed at determining how dipeptide formation would be affected by the presence of Au NP **1**.

Fmoc-Yp-OH, Fmoc-D-OH and Fmoc-CA-OH were chosen as the electrophilic fragments, because they have negative charges and could interact electrostatically with the Au NP **1** surface. On the other hand, hydrophobic interactions can take place between the nucleophilic fragments Phe-NH_2, Trp-NH_2 and Tyr-NH_2 and Au NP **1** through insertion of the aromatic unit in the hydrophobic part of the monolayer[65]. Thus, it could be expected that the combination of negative charged and hydrophobic residues in the product would lead to dipeptide with a high affinity for Au NP **1**. In addition, Fmoc-Lys-OH was included as a negative control.

Compared to the original conditions reported by Ulijn (millimolar), lower concentrations were necessary in order to adapt the system to the typical nanoparticles concentrations (micromolar). The concentrations were decreased to the minimum concentrations at which formation of dipeptides could be detected: [Fmoc-X-OH] = 1 mM, [H-X_1-NH_2] = 4 mM (keeping the 1:4 ratio (to favor amide bond formation)).

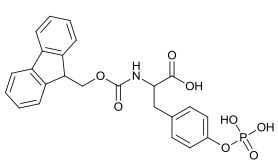

Fmoc-Yp-OH

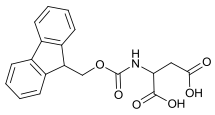

Fmoc-D-OH

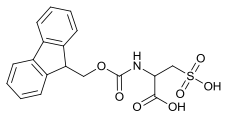

Fmoc-CysteicAcid-OH

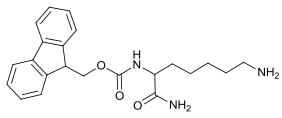

Fmoc-K-OH

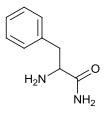

Phe-NH_2

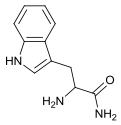

Trp-NH_2

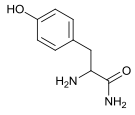

Tyr-NH_2

Chart 5.1.

Thus, an initial set of experiments were performed in which the kinetics of dipeptide formation was followed for a series of combinations of electrophilic and nucleophilic fragments without Au NP **1** present.

Importantly, no conversion was observed for any combination apart from the combination of Fmoc-Yp-OH (**1**) and H-Phe-NH_2 which gave a conversion of 33 % (of dipeptide formed (**2**)) after three days (Figure 5.4a). Encouraged by these results this set of reagents was used to study the effect of Au NP **1**. In the presence of Au NP **1** the conversion was equal after three days (33 % of **2**). Interestingly, however, after four days two new peaks appeared with higher retention times (**3** and **4**) (Figure 5.4b). These peaks were never observed before in the absence of Au NP **1**.

a)

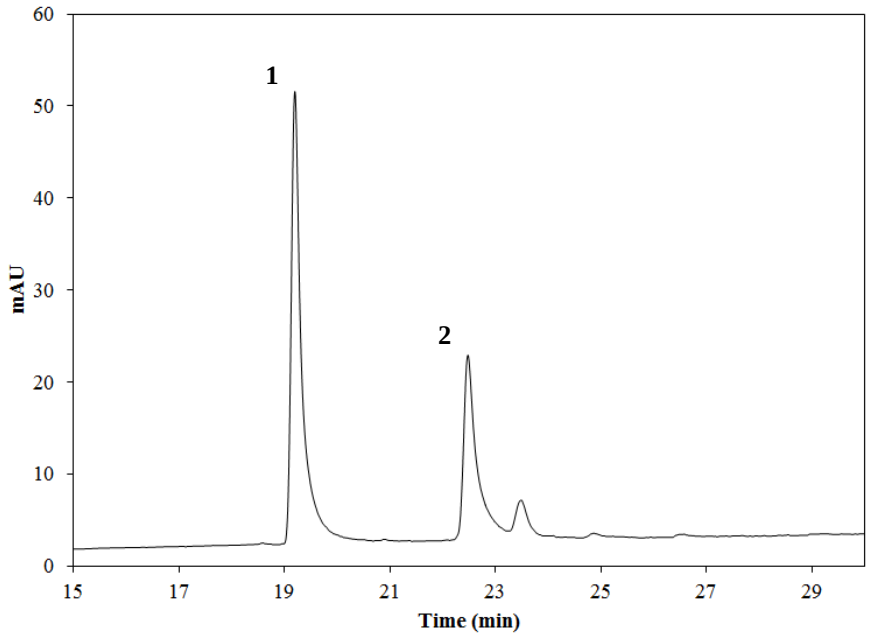
1
2
mAU
Time (min)
0
10
20
30
40
50
60
15
17
19
21
23
25
27
29

b)

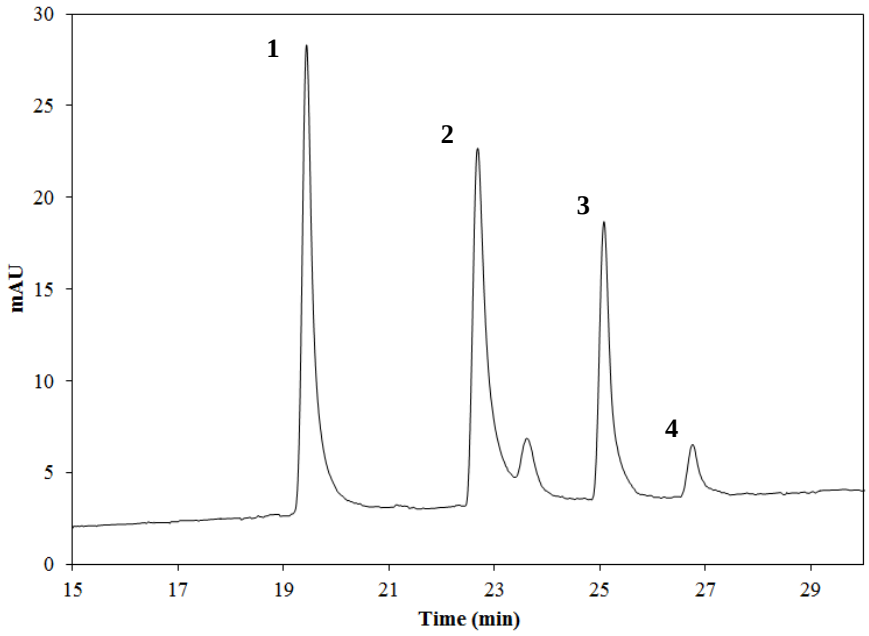
1
2
3
4
mAU
Time (min)
0
5
10
15
20
25
30
15
17
19
21
23
25
27
29

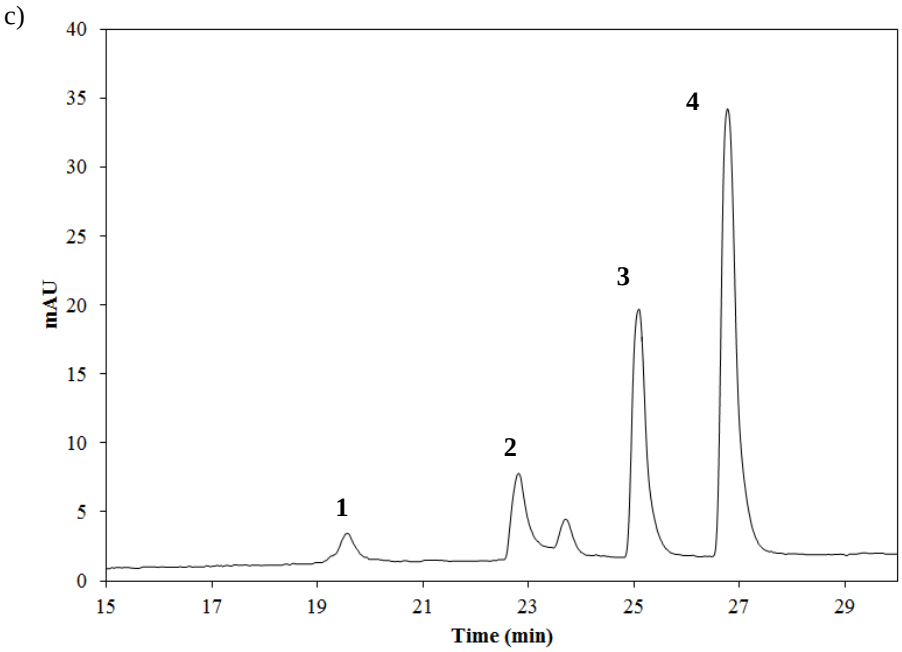

Figure 5.4. HPLC chromatograms of Fmoc-Yp-OH and H-Phe-NH2 after 3-4 days in the absence (a) and in the presence (b) of Au NP **1** (c) after 6 days. Conditions: [Fmoc-Yp-OH] = 1 mM, [H-F-NH_2] = 4 mM, [TACN-Zn^{2+}] = 100 µM only in (b), [Thermolysin] = 1 mg/mL in [HEPES] = 100 mM at pH = 7 and T = 25 ^{o}C. HPLC conditions: 20-80 %B in 30 min, 1 mL/min; A: H_2O+0.1% TFA B: ACN+0.1% TFA at 280 nm.

In the first chromatogram two peaks are observed. The peak **1** (RT = 19,5 min) corresponded to the Fmoc-Yp-OH whereas the peak **2** (RT = 22,7 min) belongs to the formed dipeptide Fmoc-Yp-Phe-NH_2. ESI-MS analysis revealed that that the peaks **3** and **4** (RT = 25,1 min, RT = 26,8 min) observed in the chromatogram in the presence of Au NP **1** corresponded to the Fmoc-Y-OH and Fmoc-Y-Phe-NH_2, that is, the dephosphorylated electrophile and product. Continuation of the kinetics led to a further increase in the intensity of peaks **3** and **4** and decrease in peaks **1** and **2** after 6 day. (Figure 5.4c). A final measurement after twelve days showed the complete disappearance of **1** and **2** and a final 40:60 ratio between **3** and **4** (Figure 5.10). The overall kinetic profiles for each species are depicted in Figure 5.5 as the percentage of the relative areas as a function of time.

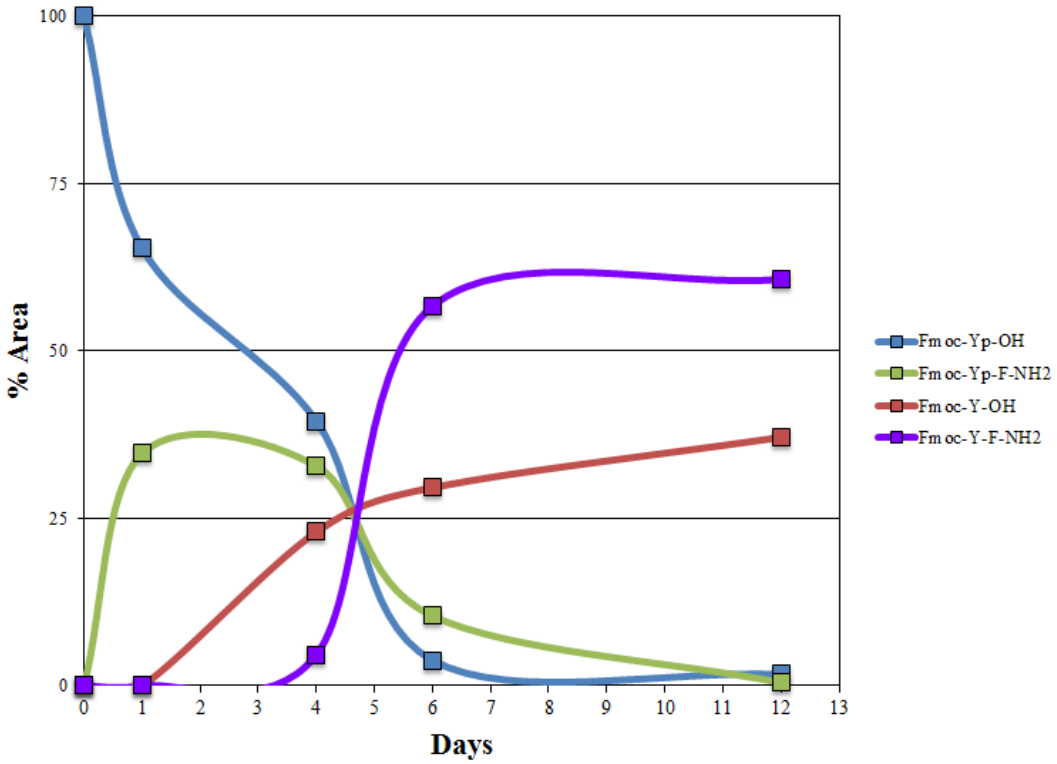

Figure 5.5. Kinetics profile: % relative area as a function of time.

Figure 5.5 shows a remarkable kinetic profile for the dephosphorylation reaction in particular regarding the formation of the dephosphorylated dipeptide Fmoc-YF-NH_2. Despite the fact that the phosphorylated product Fmoc-YpF-NH_2 is already present in significant amounts after 1 day, the formation of the dephosphorylated dipeptide starts only after 3 days exhibiting a sigmoidal increase. This interesting observation prompted a detailed study aimed at identifying the origin of this dephosphorylation activity and at explaining the kinetic profile.

5.3 Mechanistic studies

First, control kinetics were performed to evaluate the reproducibility of the results by monitoring the dephosphorylation Fmoc-Yp-OH in the presence of Au NP **1** and Thermolysin (in the absence of the nucleophilic reagent). Concurrently, other kinetics were also run to figure out which of the components (Au NP **1**, enzyme or Zn^{2+}) were essential for promoting the dephosphorylation reaction. Thus, kinetics combining Au NP **1** and/or Thermolysin and/or Zn^{2+} were performed. The

concentrations of Fmoc-Yp-OH and Fmoc-Y-OH were monitored by UHPLC. The relative area of the peak originating from Fmoc-Y-OH was plotted as a function of time (Figure 5.6).

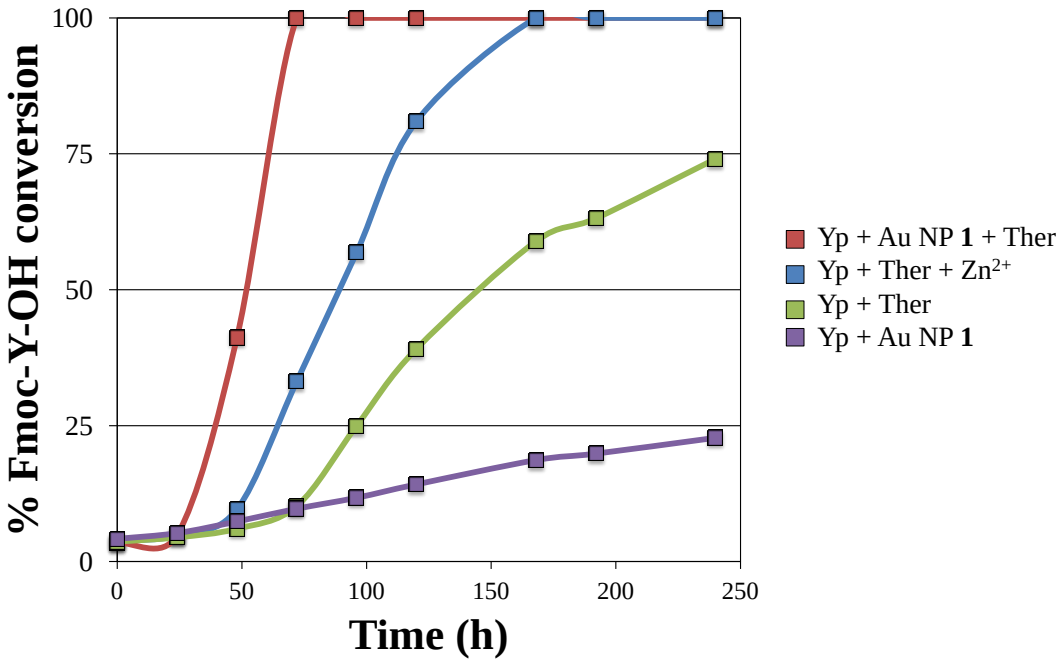

Figure 5.6. Kinetics profiles of the Fmoc-Yp-OH dephosphorylation. Conditions: [Fmoc-Yp-OH] = 1 mM, [TACN-Zn^{2+}] = 100 µM or [Zn^{2+}] = 100 µM, [Thermolysin] = 1 mg/mL in [HEPES] = 30 mM at pH = 7 and T = 25 ^{o}C. UPLC conditions: 20-80 %B in 7 min, 0.2 mL/min; A: H_2O+0.1% HCOOH B: ACN+0.1% HCOOH at 280 nm.

These kinetics confirmed the reproducibility of the dephosphorylation reaction observed before (Figure 5.6, **red**). It was found that thermolysin in the presence of Zn^{2+} (without nanoparticles) was also able to dephosphorylate the substrate (never observed before) (Figure 5.6, **blue**) while removing Zn^{2+} from that mixture caused a decrease in the rate (Figure 5.6, **green**). The same experiment but in the absence of Thermolysin (Figure 5.6, **lilac**) led to a linear increase of the product conversion suggesting just a slight effect of Au NP **1** on the dephosphorylation reaction. Hence, these experiments indicated thermolysin as the main source of dephosphorylation and that the effect is enhanced in the presence of Zn^{2+}, preferably when present in the monolayer of Au NP **1**.

However, follow up experiments showed that the real picture is more complicated than this. During these kinetics a very interesting phenomenon was observed. When diluting the samples (20x) for injecting to the UPLC, the

dephosphorylation of Fmoc-Yp-OH occurred much faster compared to the original kinetics in which such a dilution step was not performed. In other words, injecting a diluted sample and comparing it to the original (non-diluted) one gave a higher rate of dephosphorylation. This led us to reperform some of the kinetics described before at lower concentrations (diluted 20 times). The area relative to Fmoc-Y-OH was plotted as a function of time (Figure 5.7).

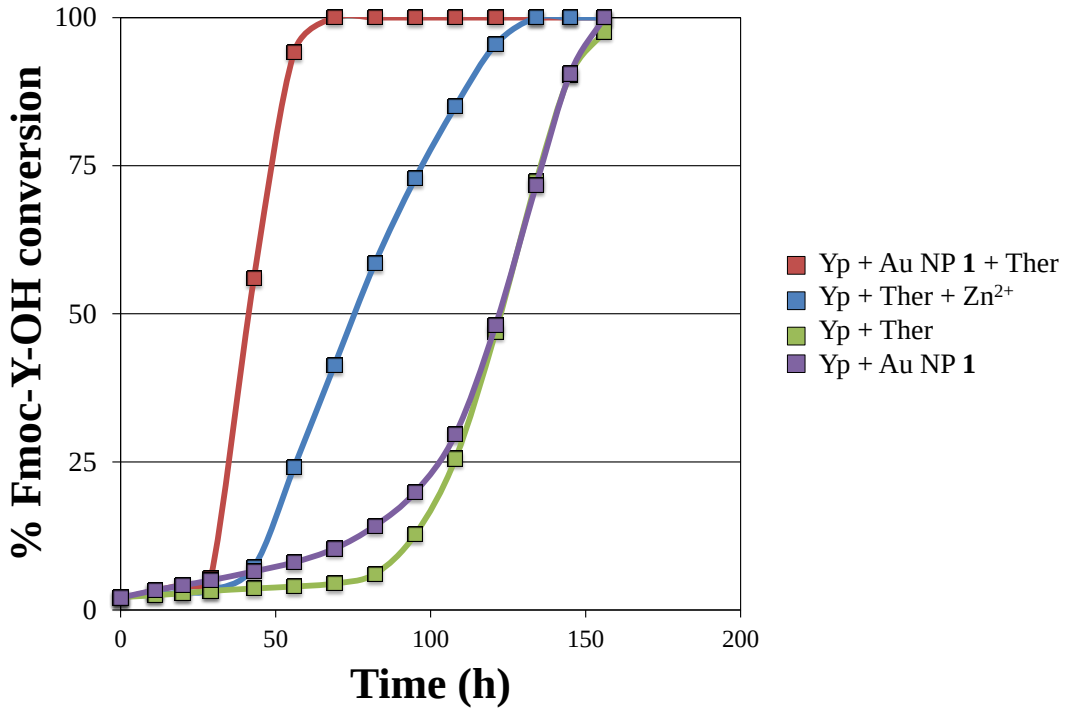

Figure 5.7. Diluted kinetics profiles of the Fmoc-Yp-OH dephosphorylation. Conditions: [Fmoc-Yp-OH] = 50 µM, [TACN-Zn^{2+}] = 5 µM or [Zn^{2+}] = 5 µM, [Thermolysin] = 0,05 mg/mL in [HEPES] = 30 mM at pH = 7 and T = 25 ^{o}C. UPLC Conditions: 20-80 %B in 7 min, 0.2 mL/min; A: H_2O+0.1% HCOOH B: ACN+0.1% HCOOH at 280 nm.

In the presence of Au NP **1** and Thermolysin a 50 % of conversion was reached in 40 hours compared to 48 hours at higher concentrations (Figure 5.7, **red**). Similar increases were observed when just Zn^{2+} was added or just thermolysin (Figure 5.7, **blue** and **green**).

However, the largest difference in rate was observed when only Au NP **1** was present (Figure 5.7, **lilac**). At high concentrations 50 % conversion required more than 10 days (Figure 5.6, **lilac**) whereas under diluted conditions the same conversion was reached just after 125 hours (corresponding to 5 days). Also striking is the strong sigmoidal growth of the product Fmoc-Y-OH. Up till 80 hours hardly

any product formation is observed, after which is takes just 40 hours to reach 50%. These kinetics point to a catalytic role of Au NP **1** that was not at all evident from the kinetics performed at higher concentrations.

In case Au NP **1** plays indeed a role in the transphosphorylation reaction it should be possible to downregulate this activity by adding an inhibitor that competes with the substrate for binding to Au NP **1**. For that purpose, the effect of two anionic competitors, **ATP** and **N1**, on the reaction rate was evaluated (Figure 5.8). **ATP** is known to bind strongly to the Au NP **1** surface as showed in earlier Chapters. The other competitor, **N1**, binds even stronger than ATP thanks to electrostatically and, in addition, through hydrophobic interactions with the aliphatic chain of the monolayer (see Figure 5.11 for a binding assay).

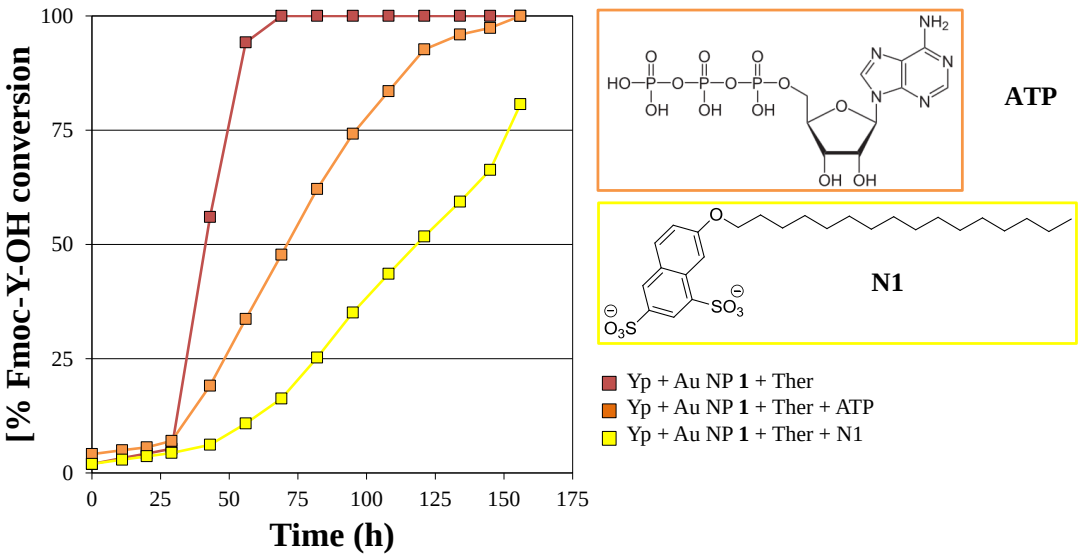

Figure 5.8. Comparison kinetics profiles of the Fmoc-Y-OH in the presence of competitors. . Conditions: [Fmoc-Yp-OH] = 50 µM, [TACN-Zn^{2+}] = 5 µM, [Thermolysin] = 0,05 mg/mL, [Competitor] = 10 µM in [HEPES] = 30 mM at pH = 7 and T = 25 ^{o}C. UPLC conditions: 20-80 %B in 7 min, 0.2 mL/min; A: H_2O+0.1% HCOOH B: ACN+0.1% HCOOH at 280 nm.

The results indeed show a reduced rate when **ATP** or **N1** were present. The 50 % of conversion was reached around 75 hours and 125 hour for **ATP** and **N1** respectively. The profile for N1 was now nearly identical to that of the kinetics with just thermolysin present, indicating that the catalytic effect of Au NP **1** is completely suppressed by **N1**.

One of the striking features of the kinetic profiles is the sigmoidal behavior. The analysis performed so far has shown an important role of Au NP **1** in the catalytic process. On the other hand, from fluorescence titration studies it is known that Fmoc-Yp-OH has a significant affinity for Au NP **1** (Figure 5.12). The combination of these observation led to the following hypothesis on the origin of the sigmoidal curve. As discussed in Chapter 1 a bimetallic catalytic site is needed for the catalysis since, initially, the saturation is so high that bimetallic sites are not available. After at some point (due to slow dephosphorylation by thermolysin) a sufficient amount of substrate is converted this then leads to a liberation of the catalytic surface of Au NP **1** leading toward an increased rate.

To confirm this hypothesis an additional experiment at a lower concentration of Fmoc-Yp-OH was performed (5 μM) keeping the concentrations of Au NP **1** and Thermolysin unvaried. (Figure 5.9). Under these conditions, the amount of substrate was not enough to totally cover the Au NP **1** surface, thus enabling directly catalysis by bimetallic sites.

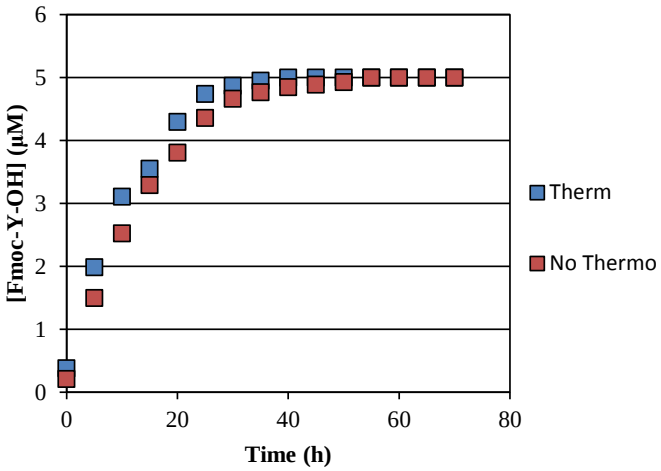

Figure 5.9. Fmoc-Yp-OH dephosphorylation. Conditions: [Fmoc-Yp-OH] = 5 μM, [TACN-Zn^{2+}] = 5 μM, [Thermolysin] = 0,05 mg/mL in [HEPES] = 30 mM at pH = 7 and T = 25 ^{o}C. UPLC conditions: 20-80 %B in 5 min, 0.8 mL/min; A: H_2O+0.1% HCOOH B: ACN+0.1% HCOOH at 280 nm.

The results were very interesting. It can be seen how the rate of conversion extremely increased and, importantly, an induction period was no longer present. Only 10 hours were needed to obtain 50 % of the product. Also, under these conditions no effect of Thermolysin was observed on the reaction rate, indicating that Au NP **1** is the only source of catalysis. Compared to the original studies at high

concentrations at which it appeared that Au NP **1** had no catalytic activity, this is a remarkable conclusion.

Clearly, additional studies are necessary to fully understand the mechanism of this reaction and the role of Au NP **1**. However, the data obtained so far shows that Au NP **1** can catalyze the dephosphorylation of a non-activated monoester. Although, we are far from the catalytic activity of a phosphatase, these promising results are an excellent starting point for further studies. It is reminded that most studies on the catalytic activity of Au NP **1** and analogues have been performed on activated phosphodiesters, which are obviously much easier to cleave.

5.4 Conclusions

In conclusion, a catalytic activity of Au NP **1** has been detected for the catalysis of the dephosphorylation of Fmoc-Yp-OH. Indeed, at conditions, *i.e.* Fmoc-Yp-OH closer to the SSC of Au NP **1**, only 10 hours have been needed to convert 50% of substrate. Although for a precise understanding of the mechanism more studies are required, the fact that Au NP **1** is able to cause the dephosphorylation of a monophosphate is a very exciting result, considering that the catalytic activity of Au NP **1** and related systems has so far mainly been limited to activated phosphodiesters.

5.5 Experimental section

5.5.1 Instrumentation

A Dionex P680 HPLC was used to quantify conversions of the enzymatic reactions reported in Figure 5.4 and 5.5. Remaining studies were performed using UHPLC-MS previous described (section 2.5.1)

5.5.2 Materials

Fmoc-X-OH and H-Y-NH_2 were purchased from Sigma Aldrich. Thermolysin was also purchased from Sigma Aldrich (P1512).

5.5.3 Impact of Au NP 1 on the composition of a dynamic peptide systems

Fmoc-X-OH and H-X_1-NH_2 were separately weighted and then mixed together to prepare 1 mL of an aqueous solution ([HEPES] = 100 mM at pH = 7) with the peptides at a final concentration of10 mM and 40 mM, respectively. Then the solution was diluted either 2 or 10 times to obtain two different solutions at concentrations 5 and 20 mM and 1 and 4 mM, respectively. Au NP **1** was then added to reach a final concentration of 100 uM. Subsequently, 1 mg of Thermolysin was added and the resulting solution was vortexed and sonicated. After 24 hours the samples were analysed by HPLC. A 20 µL sample was injected onto a Macherey-Nagel C18 column with a length of 250 mm and an internal diameter of 4.6 mm and 5-mm fused silica particles at a flow rate of 1 mL/min. The eluting solvent system had a linear gradient of 20% (v/v) ACN in H_2O for 4 min, gradually rising to 80% (v/v) ACN in H_2O at 35 min. This concentration was kept constant until 40 min after which the gradient was decreased to 20% (v/v) acetonitrile in water at 42 min. Sample preparation involved mixing an aliquot of 50 µl of solution with ACN/H_2O (1000 ml, 70:30 mixture) containing 0.1% TFA. The purity of each identified peak was determined by UV detection at 280 nm. The starting materials were also injected separately as controls: Fmoc-Yp-OH, Fmoc-D-OH and Fmoc-Cysteic acid-OH.

5.5.4 Mechanistic studies

Original kinetics

1 mL solution containing [TACN-Zn^{2+}] = 100 µM, [Fmoc-Yp-OH] = 1 mM in [HEPES] = 30 mM at pH = 7 was prepared. Subsequently, 1 mg of Thermolysin was added and the resulting solution was vortexed and sonicated.

For the analysis, an aliquot of 50 µL was taken from the solution (see above) and solved in mQ H_2O. Then, the resulting solution was injected in the UPLC.

A Zorbax Eclipse Plus C18 column with a length of 150 mm and an internal diameter of 2.1 mm and 1.8-mm fused silica particles at a flow rate of 0.4 mL/min. The eluting solvent system started a at 20% (v/v) ACN+0.1% HCOOH in H_2O+0.1% HCOOH gradually rising to 80% (v/v) ACN+0.1% HCOOH in H_2O+0.1% HCOOH in 10 min. This concentration was kept constant until 12 min when the gradient was decreased to 20% (v/v) ACN+0.1% HCOOH in H_2O+0.1% HCOOH at 14 min. The column temperature was 40 ^oC.

Diluted kinetics

1 mL solution containing [TACN-Zn^{2+}] = 5 μM, [Fmoc-Yp-OH] = 50 μM in [HEPES] = 30 mM at pH = 7 was prepared. Subsequently, [Thermolysin] = 0,05 mg/mL was added and the resulting solution was vortexed.

The resulting solution was directly injected in the UPLC, no further dilutions were necessary. Thus, 20 μL wwere injected to a Zorbax Eclipse Plus C18 column with a length of 150 mm and an internal diameter of 2.1 mm and 1.8-mm fused silica particles at a flow rate of 0.4 mL/min. The eluting solvent system started a at 20% (v/v) ACN+0.1% HCOOH in H_2O+0.1% HCOOH gradually rising to 80% (v/v) ACN+0.1% HCOOH in H_2O+0.1% HCOOH in 10 min. This concentration was kept constant until 12 min when the gradient was decreased to 20% (v/v) ACN+0.1% HCOOH in H_2O+0.1% HCOOH at 14 min. The column temperature was 40 ^oC.

5.5.4 Miscellaneous

Impact of Au NP 1 on the composition of a dynamic peptide systems (after 12 days)

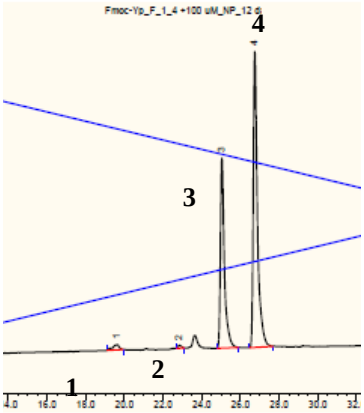

Figure 5.10. HPLC chromatograms of Fmoc-Yp-OH and H-Phe-NH2 after 12 days and in the presence of AuMPC 1. Conditions: 20-80 %B in 30 min, 1 mL/min; A: H2O+0.1% TFA B: ACN+0.1% TFA at 280 nm.

N1 binding assay

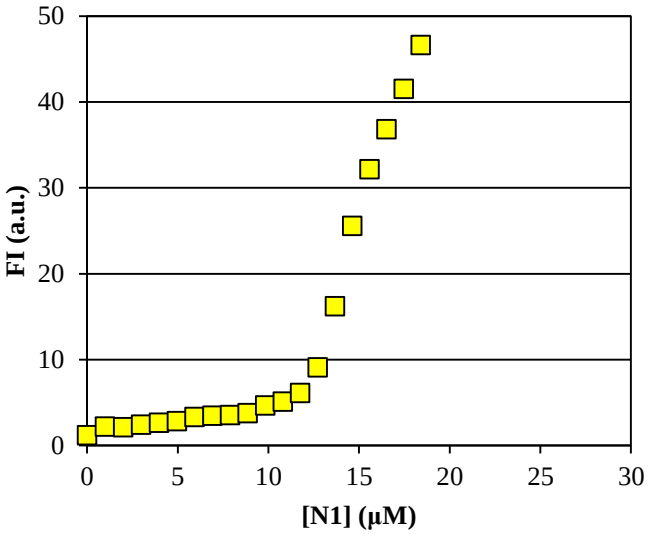

Figure 5.11. Binding assay: fluorescent intensity (a.u.) as a function of N1 concentration (µM) measured at λ_{ex}=335 nm, λ_{em}=490 nm. Conditions: [TACN-Zn^{2+}] = 30 µM, [HEPES] = 10 mM, pH = 7, T = 25 °C.

Fmoc-Yp-OH binding assay

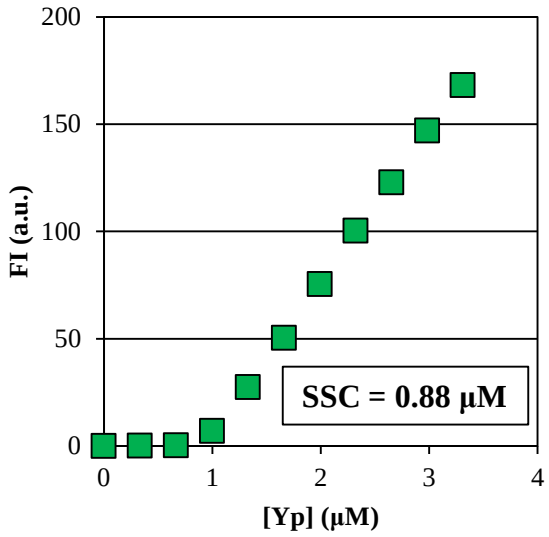

Figure 5.12. Binding assay: fluorescent intensity (a.u.) as a function of Fmoc-Yp-OH concentration (µM) measured at λ_{ex}= 260 nm, λ_{em}= 301 nm (slits: λ_{ex}= 2.5, λ_{em}= 5nm). Conditions: [TACN-Zn^{2+}] = 5 µM, [HEPES] = 30 mM, pH = 7, T = 25 °C.

SUMMARY

Protein-protein interactions mediate a large number of important regulatory pathways in the organism and also play a central role in many pathologies. Protein surface recognition provides a powerful tool for the regulation of those protein-protein interactions. Gold nanoparticles offer a suitable platform for multi-functionalization with a wide range of biological ligands for the selective binding and detection of biological targets such as proteins. In particular, gold nanoparticles functionalized with peptide fragments are very attractive for that purpose, since peptides contain all necessary chemical information to interact with natural proteins. During the past years, self-assembly, *i.e*. the spontaneous organization of molecules into ordered aggregates, has emerged as the most attractive way to develop highly complex nanosized systems. Au NPs containing 1,4,7-triazacyclononane (TACN)·Zn^{2+} head groups (Au NP **1**) have been shown to be attractive scaffolds for the formation of multivalent supramolecular structures.

In this PhD-project the self-assembly of small peptides on monolayer protected gold nanoparticles has been studied as a means to develop dynamic nanoproteins for application in biomolecular recognition and catalysis. The first part has been dedicated to the identification and optimization of small peptides able to bind with high affinity to the surface of Au NP **1**, which are gold nanoparticles ($d \sim$ 2 nm) covered with a monolayer of C9-thiols containing a 1,4,7-triazacyclonane•Zn^{2+} head group. The results showed four potential candidates of which the tripeptide LWS(p) (S(p) = phosphoserine) had the highest affinity. From a series of studies in which the metal-ion in the monolayer was varied, it emerged that Zn^{2+} gave the best results. Using LWS(p) as a lead structure a small peptide library was synthesized successively in which additional amino acid residues were attached to the binding unit. Amino acids containing negatively or positively charged, polar and apolar side chains were chosen in order to create a chemical diverse library. Subsequent binding studies showed that all peptides had a very high affinity for Au NP **1**, apart from the peptides containing positively charged amino acids.

Subsequently, the peptide library was used to self-assembly a dynamic nanoprotein by adding all peptides simultaneously to Au NP **1**. Binding studies revealed that binding occurred under saturation conditions at low micromolar

concentrations in aqueous buffer at pH = 7. The addition of a competitor for binding resulted in a complete displacement of the peptides demonstrating the dynamic nature of the surface. In this way it has been demonstrated that it is possible to build up a complex multivalent system in a straightforward manner.

The dynamic nature of the system was exploited in a series of self-selection experiments, aimed at determining how the surface composition on Au NP **1** would change when an excess of peptides would be present. A new protocol relying on the use of ultracentrifugation filters containing a MW cut-off membrane was developed for the purpose of analyzing the surface composition. The results showed a spontaneous self-selection of the peptides with a higher affinity for Au NP **1** upon increasing the overall concentration of the peptide library.

In the next stage, the ability of the nanoprotein to interact with natural protein surfaces was investigated. A particular attention was paid to exploitation of the dynamic nature of the assembly. The serine protease chymotrypsin (ChT) was chosen as a target, because previous literature reports had already mentioned that peptide-functionalized Au NPs are able to bind ChT. Binding assays confirmed that the presence of ChT did not affect the interaction between the peptide library and Au NP **1**. Apart from peptide **P2**, none of the peptides was hydrolyzed by ChT. Enzyme activity studies in the presence of Au NP **1**-peptide systems did not provide conclusive data. The obtained data showed a slight activation of ChT (1.5 times) in the presence of Au NP, irrespective of whether peptides were present or not. Such an activation of ChT by cationic agents has also been reported in other studies, but a clear explanation is not yet available. Since the measurement of enzyme activity is an indirect method of measuring the interaction between the nanoproteins and ChT, the attention was shifted towards a direct method relying on the ultracentrifugation experiments developed earlier. The aim was to investigate whether the surface composition would be affected by the addition of ChT. Initial data from the ultracentrifugation experiments and additional fluorescence studies seemed to suggest the formation of a ternary multivalent complex with peptide **P1** sandwiched between Au NP **1** and ChT. However, further experiments under different conditions

and including other techniques (such as ITC and DLS) are required to confirm these results.

Finally, a collaboration with the Ulijn group at the University of Strathclyde led to a detailed investigation of the activity of Au NP **1** as artificial phosphatases. The original idea was to exploit the high affinity of peptides for Au NP **1** to shift the equilibrium of a dynamic system of interconverting peptides (catalyzed by thermolysin). However, initial studies immediately revealed that after some days the nanoparticles-enzyme mixture caused the dephosphorylation of Fmoc-Yp-OH. This observation led to an in depth study of the origin of this reaction. Initial experiments performed at high concentrations pointed to thermolysin as the prime responsible for the dephosphorylation reaction assisted by Zn^{2+} or Au NP **1**. Under these conditions hardly any activity by Au NP **1** was observed. However, the picture changed completely when the kinetic studies were repeated at much lower (micro)molar concentrations. Now, a strong catalytic activity of Au NP **1** was detected. Indeed, at conditions, *i.e.* Fmoc-Yp-OH closer to the SSC of Au NP **1**, only 10 hours were needed to convert 50% of substrate. Although for a precise understanding of the mechanism more studies are required, the fact that Au NP **1** is able to cause the dephosphorylation of a monophosphate is a very exciting result, considering that the catalytic activity of Au NP **1** and related systems has so far mainly been limited to activated phosphodiesters.

SOMMARIO

Le interazioni proteina-proteina controllano un gran numero di vie regolatorie all'interno dell'organismo e giocano un ruolo chiave in molte patologie. Il riconoscimento della superficie di una proteina permette di ottenere un potente strumento per la regolazione di queste interazioni. Le nanoparticelle d'oro sono un'adeguata piattaforma per la multi-funzionalizzazione con un'ampia gamma di leganti biologici per l'interazione selettiva e la rivelazione di target biologici come proteine. In particolare le nanoparticelle d'oro funzionalizzate con frammenti peptidici sono molto interessanti per questo scopo, dal momento in cui i peptidi contengono tutte le informazioni chimiche necessarie per interagire con le proteine presenti in natura. In passato l'auto assemblaggio, la spontanea organizzazione di molecole in aggregati ordinati, è emersa come una via molto promettente per lo sviluppo di sistemi altamente complessi di dimensione nanometrica. AuNPs funzionalizzate con tioli che presentano 1,4,7 triazaciclononano $(TACN)^{2+}$ come gruppi di testa possono essere utilizzate come validi sistemi per la formazione di strutture supramolecolari multivalenti.

In questo PhD l'auto-assemblaggio di piccoli peptidi su nanoparticelle d'oro protette da un monostrato costituito da tioli è stato studiato come mezzo per sviluppare nanoproteine dinamiche per applicazioni come il riconoscimento biomolecolare e la catalisi. La prima parte è stata dedicata all'identificazione e ottimizzazione di piccoli peptidi capaci di legarsi con alta affinità alla superficie delle Au NP **1**, che sono nanoparticelle d'oro (d ~ 2 nm) ricoperte da un monostrato di tioli costituiti da una catena alchilica con nove carboni e 1,4,7-triazaciclononano • Zn^{2+} come gruppo di testa. I risultati hanno mostrato quattro potenziali candidati di cui il tripeptide LWS (p) (S (p) = fosfoserina) presenta la più alta affinità. Da una serie di studi in cui è stato variato il metallo-ione coordinato al 1,4,7-triazaciclononano nel monostrato, lo Zn^{2+} ha dato i migliori risultati. Utilizzando LWS (p) come struttura principale, una piccola libreria di peptidi è stata sintetizzata in cui ulteriori residui amminoacidici sono stati attaccati all'unità vincolante. Gli amminoacidi contenenti cariche negative o positive, catene laterali polari o apolari sono stati scelti in modo di creare una libreria chimica con ampia diversità.

Successivi studi di interazione hanno mostrato che tutti i peptidi avevano un'affinità molto elevata per le Au NP **1**, tranne i peptidi contenenti amminoacidi carichi positivamente.

Successivamente, aggiungendo tutti i peptidi contemporaneamente sulle Au NP **1**, si è cercato di promuovere l'autoassemblaggio di una nano-proteina dinamica. Studi di affinità hanno rivelato che l'interazione avviene in condizioni di saturazione a concentrazioni in scala micromolare (tampone acquoso, pH = 7). L'aggiunta di un composto che compete con i peptidi per la superficie delle Au NP **1** provoca uno spiazzamento completo dei peptidi mostrando la natura dinamica della superficie. In questo modo è stato dimostrato che è possibile costruire in modo semplice un sistema multivalente complesso.

La natura dinamica del sistema è stata sfruttata in una serie di esperimenti di auto-selezione, volti a determinare come la composizione della superficie peptidica sulle Au NP **1** cambi dopo l'aggiunta di un eccesso di peptidi. È stato sviluppato un nuovo protocollo basato sull'impiego di filtri da ultracentrifugazione contenenti una membrana con un determinato limite di PM allo scopo di analizzare la composizione dei peptidi sulla superficie. I risultati hanno mostrato una spontanea selezione dei peptidi con una maggiore affinità per Au NP **1** all'aumentare della concentrazione complessiva della libreria peptidica.

Nella fase successiva, è stata studiata la capacità delle nano-proteine di interagire con superfici proteiche naturali. La chimotripsina serina proteasi (ChT) è stata scelta come target. Era già riportato in letteratura, infatti, che le Au NP funzionalizzate con peptidi sono in grado di interagire con la ChT. Esperimenti di binding hanno confermato che la presenza della proteina non influenza l'interazione tra la libreria peptidica e le Au NP **1**. Nessuno dei peptidi è stato idrolizzato dalla ChT, a parte il peptide **P2**. Gli studi sull'attività enzimatica in presenza di Au NP **1**-peptide non hanno fornito dati conclusivi. I dati ottenuti hanno mostrato una lieve attivazione della ChT (1,5 volte) in presenza di Au NP, indipendentemente dalla presenza dei peptidi. Una tale attivazione della ChT dovuta agenti cationici è stata riportata anche in altri studi, ma una spiegazione chiara non è ancora disponibile. L'attenzione, quindi, si è spostata verso un metodo diretto per misurare l'interazione

tra i nano-proteine e ChT basandosi sugli esperimenti di ultracentrifugazione sviluppati in precedenza, considerando che la misurazione dell'attività enzimatica è un metodo indiretto. L'obiettivo era quello di verificare se la composizione della superficie risentisse dell'aggiunta della proteina. I dati iniziali degli esperimenti di ultracentrifugazione e studi di fluorescenza supplementari sembravano suggerire la formazione di un complesso ternario multivalente tra le Au NP **1** e la ChT e il peptide **P1**. Tuttavia, ulteriori esperimenti con diverse condizioni sperimentali e l'utilizzo di altre tecniche di analisi (come la ITC e DLS) sono necessari per confermare questi risultati.

Infine, una collaborazione con il Prof. Ulijn presso l'Università di Strathclyde ha portato ad un esame approfondito dell'attività fosfatasi delle Au NP **1**. L'idea originale era quella di sfruttare l'alta affinità dei peptidi per Au NP **1** per spostare l'equilibrio di un sistema dinamico di inter-conversione degli stessi (catalizzata dalla termolisina). Tuttavia, gli studi iniziali hanno rivelato che, dopo alcuni giorni, la miscela composta da nanoparticelle ed enzima ha causato la defosforilazione dell' Fmoc-Yp-OH. Questa osservazione ha portato ad uno studio più approfondito sull'origine di questa reazione. I primi esperimenti effettuati ad alte concentrazioni hanno indicato che la termolisina assistita dallo Zn^{2+} o dalle Au NP **1** è la prima responsabile della reazione di defosforilazione. In queste condizioni non è stata osservata nessuna attività da parte delle Au NP **1.** Il quadro è cambiato completamente nel momento in cui gli studi cinetici sono stati ripetuti a più basse concentrazioni (micromolare). È stato rilevata una forte attività catalitica dalle Au NP **1**. In condizioni in cui la concentrazione dell'Fmoc-Yp-OH è vicina alla SSC sulle Au NP **1**, sono state necessarie soltanto 10 ore per convertire il 50% del substrato. Tuttavia, per una precisa comprensione del meccanismo sono necessari ulteriori studi, il fatto che le Au NP **1** siano in grado di provocare la defosforilazione di un monofosfato è un risultato molto interessante, considerando che l'attività catalitica delle Au NP **1** e sistemi relativi sono limitati, finora, principalmente a fosfodiesteri attivati.

ACKNOWLEDGEMENTS

Firstly, I would like to express my sincere gratitude to my advisor Prof. Leonard Prins for the continuous support of my PhD study and related research, for his patience, motivation, and immense knowledge. I would like also to thank Marie Curie ITN for the financial support (289723).

I wish to thank Prof. Rein Ulijn from University of Strathclyde for giving the opportunity to visit his labs and collaborate together.

I also gratefully acknowledge all my labmates: Gregory Pieters, Davide Zaramella for the music lessons, Christian Franceschini for tarallini from Puglia, and Cristian Pezzato, Subhabrata Maiti and Jack Chen for these incredible last months (dinners, football&cricket matches, beers, birthdays,…). It has been amazing guys!

Very specials thanks go to the people of the second floor, particularly, Giovanni Salassa for the assists, pick ‘n’ rolls and the showtime! (also for the cover, many thanks). I have also to thank the Spanish committee in Padova and my basketball team that make this experience even greater. Thanks also the group of the Marie Curie Network, PIs, PostDocs, PhD students for organizing such a wonderful congress and meetings.

Final but not least, I wish to thank my family, specially, my father and mother for supporting me in everything and encourage me to realize my dreams. Also, I will be eternally grateful to my mother- and grandmother-in-law. They greeted me as a son, I will never forget it. Lastly, the greatest of the thanks is for Simona Neri for supporting me, for cheering me up in frustrated moments, for the passionate conversations about culture, art, science, sport...for teaching me all of these things and, specially, for sharing your life with me.

(1) Wells, J. A.; McClendon, C. L. *Nature* **2007**, *450* (7172), 1001.

(2) Yin, H.; Hamilton, A. D. *Angew. Chem. Int. Ed.* **2005**, *44* (27), 4130.

(3) Babine, R. E.; Bender, S. L. *Chem. Rev.* **1997**, *97* (5), 1359.

(4) J Wilson, A. *Chem. Soc. Rev.* **2009**, *38* (12), 3289.

(5) Keskin, O.; Gursoy, A.; Ma, B.; Nussinov, R. *Chem. Rev.* **2008**, *108* (4), 1225.

(6) Clackson, T.; Wells, J. *Science* **1995**, *267* (5196), 383.

(7) Pelletier, H.; Kraut, J. *Science* **1992**, *258* (5089), 1748.

(8) Kresheck, G. C.; Vitello, L. B.; Erman, J. E. *Biochemistry* **1995**, *34* (26), 8398.

(9) Kussie, P. H.; Gorina, S.; Marechal, V.; Elenbaas, B.; Moreau, J.; Levine, a J.; Pavletich, N. P. *Science* **1996**, *274* (5289), 948.

(10) Lai, Z.; Auger, K. R.; Manubay, C. M.; Copeland, R. *Arch. Biochem. Biophys.* **2000**, *381* (2), 278.

(11) Walensky, L. D.; Kung, A. L.; Escher, I.; Malia, T. J.; Barbuto, S.; Wright, R. D.; Wagner, G.; Verdine, G. L.; Korsmeyer, S. J. *Science* **2004**, *305* (5689), 1466.

(12) Wang, D.; Liao, W.; Arora, P. S. *Angew. Chem. Int. Ed.* **2005**, *44* (40), 6525.

(13) Hirschmann, R.; Nicolaou, K.; Pietranico, S.; Salvino, J.; Leahy, E. M.; Sprengeler, P. a.; Furst, G.; Smith, a. B.; Strader, C. D.; Cascieri, M.; Candelore, M. R.; Donaldson, C.; Vale, W.; Maechler, L. *J. Am. Chem. Soc.* **1992**, *114* (23), 9217.

(14) Saraogi, I.; Hamilton, A. D. *Biochem. Soc. Trans.* **2008**, *36* (Pt 6), 1414.

(15) Vidal, M.; Cusick, M. E.; Barabási, A.L. *Cell* **2011**, *144* (6), 986.

(16) Daniel, M.-C.; Astruc, D. *Chem. Rev.* **2004**, *104*, 293.

(17) Saha, K.; Agasti, S. S.; Kim, C.; Li, X.; Rotello, V. M. *Chem. Rev.* **2012**, *112* (5), 2739.

(18) Alvarez, M. M.; Khoury, J. T.; Schaaff, T. G.; Shafigullin, M. N.; Whetten, R. L.; Vezmar, I. *J. Phys. Chem. B* **1997**, *101* (19), 3706.

(19) Yamada, M.; Nishihara, H. *Chem. Comm.* **2002**, No. 21, 2578.

(20) Rosi, N. L.; Mirkin, C. *Chem. Rev.* **2005**, *105* (4), 1547.

(21) Boisselier, E.; Astruc, D. *Chem. Soc. Rev.* **2009**, *38* (6), 1759.

(22) Dubertret, B.; Calame, M.; Libchaber, J. *Nat. Biotechnol.* **2001**, *19* (4), 365.

(23) Dulkeith, E.; Morteani, C.; Niedereichholz, T.; Klar, T.; Feldmann, J.; Levi, S.; van Veggel, F. C. J. M.; Reinhoudt, D. N.; Möller, M.; Gittins, D. I. *Phys. Rev. Lett.* **2002**, *89* (20), 203002.

(24) Brust, M.; Walker, M.; Bethell, D.; Schiffrin, D. J.; Whyman, R. *J. Chem. Soc., Chem. Comm.* **1994**, 801.

(25) Manea, F.; Bindoli, C.; Polizzi, S.; Lay, L.; Scrimin, P. *Langmuir* **2008**, *24* (8), 4120.

(26) Whaley, S. R.; English, D. S.; Hu, E. L.; Barbara, P. F.; Belcher, M. *Nature* **2000**, *405* (6787), 665.

(27) Prins, L. J.; Scrimin, P. *Functional Synthetic Receptors. Artif icial (Pseudo) peptides for Molecular Recognition and Catalysis*, 2005 WILEY.; T. Schrader, A. D. H., Ed.; 2005.

(28) Tkachenko, A. G.; Xie, H.; Coleman, D.; Glomm, W.; Ryan, J.; Anderson, M. F.; Franzen, S.; Feldheim, D. L. *J. Am. Chem. Soc.* **2003**, *125* (16), 4700.

(29) De La Fuente, J. M.; Berry, C. C. *Bioconjug. Chem.* **2005**, *16* (5), 1176.

(30) Mammen, M.; Choi, S.-K.; Whitesides, G. M. *Angew. Chem. Int. Ed.* **1998**, *37* (20), 2754.

(31) Manea, F.; Houillon, F. B.; Pasquato, L.; Scrimin, P. *Angew. Chem. Int. Ed.* **2004**, *43* (45), 6165.

(32) Pengo, P.; Broxterman, Q. B.; Kaptein, B.; Pasquato, L.; Scrimin, P. *Langmuir* **2003**, *19* (6), 2521.

(33) Pengo, P.; Polizzi, S.; Pasquato, L.; Scrimin, P. *J. Am. Chem. Soc.* **2005**, *127* (6), 1616.

(34) Mancin, F.; Prins, L. J.; Scrimin, P. *Curr. Op. Col. Int. Sci.* **2013**, *18* (1), 61.

(35) Pieters, G.; Prins, L. J. *New J. Chem.* **2012**, *36* (10), 1931.

(36) Pengo, P.; Baltzer, L.; Pasquato, L.; Scrimin, P. *Angew. Chemie - Int. Ed.* **2007**, *46* (3), 400.

(37) Malkov, A. V; Figlus, M.; Cooke, G.; Caldwell, S. T.; Rabani, G.; Prestly, M. R.; Kocovský, P. *Org. Biomol. Chem.* **2009**, *7* (9), 1878.

(38) Gadek, T. R.; Nicholas, J. B. *Biochem. Pharmacol.* **2003**, *65* (1), 1.

(39) Toogood, P. L. *J. Med. Chem.* **2002**, *45* (8), 1543.

(40) Apostolovic, B.; Danial, M.; Klok, H.A. *Chem. Soc. Rev.* **2010**, *39* (9), 3541.

(41) Lévy, R. *Chem. Biochem.* **2006**, *7* (8), 1141.

(42) Kim, B.; Choi, S.; Han, S.; Choi, K.Y.; Lim, Y. *Chem. Comm.* **2013**, *49* (69), 7617.

(43) Battiste, J. L.; Mao, H.; Rao, N. S.; Tan, R.; Muhandiram, D. R.; Kay, L. E.; Frankel, D.; Williamson, J. R. *Science* **1996**, *273* (5281), 1547.

(44) Chang-Cheng You, Mrinmoy De, Gang Han, and Rotello, V. M. *J. Am. Chem. Soc.* **2005**, *127*, 12873.

(45) Bayraktar, H.; Ghosh, P. S.; Rotello, V. M.; Knapp, M. J. *Chem. Comm.* **2006**, No. 13, 1390.

(46) Miller, M. *Biochemistry* **1996**, *35* (49), 15791.

(47) Engineering, S.; Miller, M. a; Geren, L.; Han, G. W.; Saunders, A.; Beasley, J.; Pielak, G. J.; Durham, B.; Millett, F.; Kraut, J. *Biochemistry* **1996**, *35* (3), 667.

(48) Marini, M. A.; Marti, G. E.; Biochemistry, P. *Biopolymers* **1980**, *19*, 885.

(49) Yonetani, T. *J. Biol. Chem.* **1967**, *242* (21), 5008.

(50) Whitesides, G. M.; Mathias, J. P.; Seto, C. T. *Science* **1991**, *254* (5036), 1312.

(51) Soc, J. A. C.; Whitesides, G. M.; Grzybowski, B. *Science* **2002**, *295* (March), 2418.

(52) Stupp, S. I.; Palmer, L. C. *Chem. Mater.* **2014**, *26* (1), 507.

(53) Mattia, E.; Otto, S. *Nat. Nanotechnol.* **2015**, *10* (2), 111.

(54) Porter, M. D.; Bright, T. B.; Allara, D. L.; Chidsey, C. E. D. *J. Am. Chem. Soc.* **1987**, *109* (6), 3559.

(55) Gentilini, C.; Pasquato, L. *J. Mater. Chem.* **2010**, *20* (8), 1403.

(56) Verma, A.; Nakade, H.; Simard, J. M.; Rotello, V. M. *J. Am. Chem. Soc.* **2004**, *126*, 10806.

(57) Prins, L. J. *Acc. Chem. Res.* **2015**, 150622152535007.

(58) Zaupa, G.; Mora, C.; Bonomi, R.; Prins, L. J.; Scrimin, P. *Chem. Eur. J.* **2011**, *17* (17), 4879.

(59) Pieters, G.; Cazzolaro, A.; Bonomi, R.; Prins, L. J. *Chem. Comm.* **2012**, *48* (13), 1916.

(60) Pezzato, C.; Scrimin, P.; Prins, L. J. *Angew. Chem. Int. Ed.* **2014**, *53* (8), 2104.

(61) Sapsford, K. E.; Berti, L.; Medintz, I. L. *Angew. Chem. Int. Ed.* **2006**, *45* (28), 4562.

(62) Franceschini, C.; Scrimin, P.; Prins, L. J. *Langmuir* **2014**, *30*, 13831.

(63) Bonomi, R.; Cazzolaro, A.; Prins, L. J. *Chem. Comm.* **2010**, *47* (1), 445.

(64) Spreti, N.; Mancini, M. V.; Germani, R.; Di Profio, P.; Savelli, G. *J. Mol. Catal. B Enzym.* **2008**, *50* (1), 1.

(65) Pieters, G.; Pezzato, C.; Prins, L. J. *Langmuir* **2013**, *29* (24), 7180.

(66) Hostetler, M. J.; Wingate, J. E.; Zhong, C.-J.; Harris, J. E.; Vachet, R. W.; Clark, M. R.; Londono, J. D.; Green, S. J.; Stokes, J. J.; Wignall, G. D.; Glish, G. L.; Porter, M. D.; Evans, N. D.; Murray, R. W. *Langmuir* **1998**, *14*, 17.

(67) Gottlieb, H. E.; Kotlyar, V.; Nudelman, A. *J. Org. Chem.* **1997**, *62* (3), 7512.

(68) Wu, D. H.; Chen, a. D.; Johnson, C. S. An Improved Diffusion-Ordered Spectroscopy Experiment Incorporating Bipolar-Gradient Pulses. *J. Magn. Reson., Series A*, 1995, *115*, 260–264.

(69) Bonomi, R.; Cazzolaro, A.; Sansone, A.; Scrimin, P.; Prins, L. J. *Angew. Chem. Int. Ed.* **2011**, *50* (10), 2307.

(70) Lehn, J.-M. *Chem. Eur. J.* **1999**, *5* (9), 2455.

(71) Corbett, P. T.; Leclaire, J.; Vial, L.; West, K. R.; Wietor, J.-L.; Sanders, J. K. M.; Otto, S. *Chem. Rev.* **2006**, *106* (9), 3652.

(72) Ludlow, R. F.; Otto, S. *Chem. Soc. Rev.* **2008**, *37* (1), 101.

(73) Giuseppone, N.; Lehn, J.-M. *Chem. Eur. J.* **2006**, *12* (6), 1715.

(74) Hioki, H.; Still, W. C. *J. Org. Chem.* **1998**, *63* (4), 904.

(75) Huc, I.; Krische, M. J.; Funeriu, D. P.; Lehn, J.-M. *Eur. J. Inorg. Chem.* **1999**, *1999* (9), 1415.

(76) Vial, L.; Sanders, J. K. M.; Otto, S. *New J. Chem.* **2005**, *29*, 1001.

(77) Brisig, B.; Sanders, J. K. M.; Otto, S. *Angew. Chem. Int. Ed.* **2003**, *42* (11), 1270.

(78) Ramström, O.; Lehn, J.-M. *Nat. Rev. Drug Discov.* **2002**, *1* (1), 26.

(79) Buryak, A.; Severin, K. *Angew. Chem. Int. Ed.* **2005**, *44* (48), 7935.

(80) Sala, F.; Kay, E. R. *Angew. Chem. Int. Ed.* **2015**, *54*, 4187.

(81) Cordes, E. H.; Jencks, W. P. *J. Am. Chem. Soc.* **1962**, *84* (2), 826.

(82) Cordes, E. H.; Jencks, W. P. *J. Am. Chem. Soc.* **1962**, *84*, 4319.

(83) Dirksen, A.; Dirksen, S.; Hackeng, T. M.; Dawson, P. E. *J. Am. Chem. Soc.* **2006**, *128* (49), 15602.

(84) Nowak, P.; Saggiomo, V.; Salehian, F.; Colomb-Delsuc, M.; Han, Y.; Otto, S. *Angew. Chemie Int. Ed.* **2015**, n/a.

(85) Maiti, S.; Prins, L. J. *Chem. Comm.* **2015**, *51*, 5714.

(86) Maiti, S.; Pezzato, C.; Garcia Martin, S.; Prins, L. J. *J. Am. Chem. Soc.* **2014**, *136* (32), 11288.

(87) Ono, A.; Togashi, H. *Angew. Chem.Int. Ed.* **2004**, *43* (33), 4300.

(88) Ono, A.; Cao, S.; Togashi, H.; Tashiro, M.; Fujimoto, T.; Machinami, T.; Oda, S.; Miyake, Y.; Okamoto, I.; Tanaka, Y. *Chem. Comm.* **2008**, No. 39, 4825.

(89) Rauschenberg, M.; Bomke, S.; Karst, U.; Ravoo, B. J. *Angew. Chem. Int. Ed.* **2010**, *49* (40), 7340.

(90) Park, H. S.; Lin, Q.; Hamilton, A. D. *J. Am. Chem. Soc.* **1999**, *121* (10), 8.

(91) Stites, W. *Chem. Rev.* **1997**, *97*, 1233.

(92) Ripka, W. C.; Vlasuk, G. P. *Ann. Rep. Med. Chem.* **1997**, *32*, 71.

(93) Ui, N. *Biochim. Biophys. Acta* **1971**, *229* (3), 567.

(94) Capasso, C.; Rizzi, M.; Menegatti, E.; Ascenzi, P.; Bolognesi, M. *J. Mol. Recognit.* **1997**, *10* (1), 26.

(95) Blevins, R. a; Tulinsky, a. *J. Biol. Chem.* **1985**, *260* (7), 4264.

(96) Fersht, A.; Julet, M. R.; Britch, J. *Structure and Mechanicsm in Protein Science - A guide to enzyme catalysis and protein folding*, W. H. Free.; 1999.

(97) Fischer, N. O.; McIntosh, C. M.; Simard, J. M.; Rotello, V. M. *PNAS* **2002**, 1.

(98) Fischer, N. O.; Verma, A.; Goodman, C. M.; Simard, J. M.; Rotello, V. M. *J. Am. Chem. Soc.* **2003**, *125* (44), 13387.

(99) Hong, R.; Fischer, N. O.; Verma, A.; Goodman, C. M.; Emrick, T.; Rotello, V. M. *J. Am. Chem. Soc.* **2004**, *126* (3), 739.

(100) Spreti, N.; Profio, P. Di; Marte, L.; Bufali, S.; Brinchi, L.; Savelli, G. *Eur. J. Biochem.* **2001**, *268* (24), 6491.

(101) Williams, R. J.; Smith, A. M.; Collins, R.; Hodson, N.; Das, A. K.; Ulijn, R. V. *Nat. Nanotechnol.* **2009**, *4* (1), 19.

(102) Frederick H. Carpenter. *J. Am. Chem. Soc.* **1959**, *I* (6), 1111.

(103) Smith, A. M.; Williams, R. J.; Tang, C.; Coppo, P.; Collins, R. F.; Turner, M. L.; Saiani, A.; Ulijn, R. V. *Adv. Mater.* **2008**, *20* (1), 37.

(104) Pappas, C. G.; Abul-Haija, Y. M.; Flack, A.; Frederix, P. W. J. M.; Ulijn, R. V. *Chem. Commun.* **2014**, *50* (73), 10630.